Moderate High Temperature is Beneficial or Detrimental Depending on Carbon Availability in the Green Alga *Chlamydomonas reinhardtii*

Ningning Zhang[1,#], Benedikt Venn[2,#], Catherine E. Bailey[1], Ming Xia[1], Erin M. Mattoon[1,3], Timo Mühlhaus[2], Ru Zhang[1,*]

[1]Donald Danforth Plant Science Center, St. Louis, Missouri 63132, USA;
[2]Computational Systems Biology, RPTU Kaiserslautern, Kaiserslautern, 67663, Germany;
[3]Plant and Microbial Biosciences Program, Division of Biology and Biomedical Sciences, Washington University in Saint Louis, St. Louis, MO 63130, USA;
[4]Bioinformatics and Computational Biology, Saint Louis University, St. Louis, Missouri 63103, USA.

Ningning Zhang: lucy.nnzhang@gmail.com, co-first-author[#]
Benedikt Venn: venn@rptu.de, co-first-author[#]
Ming Xia: celine.xia@wustl.edu, present address[3]
Catherine E. Bailey: cady.e.bailey@gmail.com, present address[4]
Erin M. Mattoon: emattoon@danforthcenter.org
Timo Mühlhaus: timo.muehlhaus@rptu.de
Ru Zhang: rzhang@danforthcenter.org, corresponding author*

Running title: Algal heat responses interact with carbon availability.

Highlight

We revealed the overlooked, dynamic effects of moderate high temperature in algae depending on carbon availability and demonstrated the importance of carbon metabolism in thermotolerance of photosynthetic cells.

Abstract

High temperatures impair plant and algal growth and reduce food and biofuel production, but the underlying mechanisms remain elusive. The unicellular green alga *Chlamydomonas reinhardtii* is a superior model to study heat responses in photosynthetic cells due to its fast growth rate, many similarities in cellular processes to land plants, simple and sequenced genome, and ample genetic and genomics resources. Chlamydomonas grows in light by photosynthesis and/or with the externally supplied organic carbon source, acetate. Most of the published research about Chlamydomonas heat responses used acetate-containing medium. Understanding how organic carbon sources affect heat responses is important for the algal industry but understudied. We cultivated Chlamydomonas wild-type cultures under highly controlled conditions in photobioreactors at control of 25°C, moderate high temperature of 35°C, or acute high temperature of 40°C with and without constant acetate supply for 1- or 4-days. Our results showed that 35°C increased algal growth with constant acetate supply but reduced algal growth without sufficient acetate. The overlooked and dynamic effects of 35°C could be explained by induced carbon metabolism, including acetate uptake and assimilation, glyoxylate cycle, gluconeogenesis pathways, and glycolysis. Acute high temperature at 40°C for more than 2 days was lethal to algal cultures with and without constant acetate supply. Our research provides insights to understand algal heat responses and help improve thermotolerance in photosynthetic cells.

Key words: moderate high temperature, acute high temperature, heat responses, *Chlamydomonas reinhardtii*, acetate, glyoxylate cycle, gluconeogenesis, glycolysis, photobioreactors

Abbreviations:

Photobioreactors (PBRs), Tris-acetate-phosphate (TAP) medium, Tris-phosphate (TP) medium

Introduction

Many biological processes in photosynthetic cells are sensitive to high temperatures (Mittler *et al.*, 2012; Schroda *et al.*, 2015; Mishra *et al.*, 2021; Guihur *et al.*, 2022). Global

62 warming increases the intensity, duration, and frequency of high temperatures in the field,
63 reducing plant growth and food production (Janni *et al.*, 2020). A recent model revealed
64 high temperature as the primary climatic driver for yield loss in crops from 1981-2017 in
65 the U.S. (Ortiz-Bobea *et al.*, 2019). Considering the increasing global temperature and
66 human population, it is imperative to understand how photosynthetic cells respond to high
67 temperatures and improve plant thermotolerance.
68
69 High temperatures in the field have different intensities and durations. For many land
70 plants and algae grown in temperate regions, moderate high temperatures refer to heat
71 slightly above the optimal temperature for growth (at or around 35°C), while acute high
72 temperatures refer to heat at or above 40°C, which significantly reduces or completely
73 halts growth (Zhang *et al.*, 2022*a*). Moderate high temperatures are often long-lasting and
74 frequent in nature with mild effects on photosynthetic cells, while acute high temperatures
75 are often short-term but severely damaging. Most previous heat-stress experiments in
76 plants and algae used acute high temperatures at or above 40°C (Hemme *et al.*, 2014;
77 Rütgers *et al.*, 2017; Balfagón *et al.*, 2019; Kim *et al.*, 2020; Ji *et al.*, 2021), likely due to
78 the rapid onset and easily quantifiable phenotypes as compared to moderate high
79 temperatures. Although the impact of moderate high temperatures in photosynthetic cells
80 can be difficult to investigate due to comparatively mild phenotypes, moderate high
81 temperatures are physiologically relevant stresses in field conditions. Additionally, global
82 warming can further increase the frequency and duration of moderate high temperatures
83 in nature. The frequent and long-lasting features of moderate high temperatures could
84 reduce agricultural yield significantly (Delorge *et al.*, 2014; Anderson *et al.*, 2021).
85 Arabidopsis seedlings treated with 5-day heat at 35°C had reduced growth and viability
86 (Song *et al.*, 2021). Furthermore, long-term (4-6 days) moderate high temperatures
87 resulted in coral bleaching by causing cell death in endosymbiotic algae and their coral
88 hosts (Dunn *et al.*, 2004) and destabilizing the symbiotic nutrient cycling relationship
89 between these two organisms (Rädecker *et al.*, 2021). However, the effects of moderate
90 high temperatures in photosynthetic cells and the interaction of moderate high
91 temperatures with nutrient status especially carbon availability are underexplored. Algae
92 have great potential for production of biofuels and bioproducts (Scranton *et al.*, 2015;

93 Mathimani and Pugazhendhi, 2019). However, how algal cells respond to high
94 temperatures is under-investigated as compared to land plants (Schroda *et al.*, 2015). To
95 study the effects of carbon status, heat intensities and duration on heat responses in
96 photosynthetic cells, we utilized the unicellular green alga *Chlamydomonas reinhardtii*
97 (Chlamydomonas throughout).
98
99 Chlamydomonas is a superior model to study heat responses in photosynthetic cells
100 (Schroda *et al.*, 2015). Chlamydomonas can grow in light under photoautotrophic
101 conditions using photosynthesis (Minagawa and Tokutsu, 2015). It can also grow with
102 supplied organic carbon source (acetate) in light (mixotrophic) or dark (heterotrophic)
103 conditions (Sasso *et al.*, 2018), providing a platform to study heat responses under
104 different light and carbon conditions. Additionally, it has a haploid, sequenced, annotated,
105 small genome (111 Mb, 17,741 protein-encoding genes) with simpler gene families and
106 fewer gene duplications than land plants (Merchant *et al.*, 2007; Karpowicz *et al.*, 2011).
107 Furthermore, several well-established gene editing, cloning, high-throughput, and
108 functional genomic tools are available in Chlamydomonas (Shimogawara *et al.*, 1998; Li
109 *et al.*, 2016, 2019; Greiner *et al.*, 2017; Crozet *et al.*, 2018; Wang *et al.*, 2019; Dhokane
110 *et al.*, 2020; Emrich-Mills *et al.*, 2021).
111
112 Outdoor algal ponds frequently experience moderate high temperatures around 35°C
113 during the summer (Mata *et al.*, 2010; Krishnan *et al.*, 2021), but the effects of moderate
114 high temperatures on algal growth have been overlooked. Previously published algal heat
115 treatments were often conducted in flasks in pre-warmed water baths at or above 42°C
116 with sharp temperature switches (Hemme *et al.*, 2014; Rütgers *et al.*, 2017). While
117 previous research was highly valuable to understanding algal heat responses, high
118 temperatures in the field or outdoor ponds often increase gradually. Rapid increases to
119 high temperatures largely reduce algal viability (Zhang *et al.*, 2022*a*); similar effects have
120 also been reported in land plants (Mittler *et al.*, 2012). Acute high temperatures at or
121 above 40°C inhibit algal cell division (Mühlhaus *et al.*, 2011*b*; Hemme *et al.*, 2014;
122 Zachleder *et al.*, 2019; Ivanov *et al.*, 2021), while moderate high temperature at 35°C only
123 transiently inhibits cell division during the first 4-8 hour (h) heat (Zhang *et al.*, 2022*a*).

124 Thus, conducting long-term experiments at moderate high temperatures in flasks can
125 result in overgrown cultures, nutrient depletion, and light limitation, complicating data
126 interpretation.
127
128 Consequently, it is advantageous to investigate algal heat responses under highly-
129 controlled conditions in photobioreactors (PBRs) (Zhang *et al.*, 2022*a*; Mattoon *et al.*,
130 2022*a*), which have several evident strengths: (1) precise temperature regulation with a
131 sterile temperature probe inside each algal culture; (2) controlled heating to mimic the
132 heating speed in nature; (3) precisely controlled cultivation conditions, including
133 temperature, light, nutrient, and air agitation, allowing for reproducible experiments; (4)
134 automatic recording of culture status every minute, including growth conditions and
135 optical densities, enabling quantitative growth rate measurements; (5) the availability of
136 turbidostatic control based on defined parameters (e.g., chlorophyll contents) to enable
137 frequent culture dilutions with constant medium supply; (6) being able to simulate nutrient
138 depletion by turning off the turbidostatic control to investigate how nutrient availability
139 affects algal heat responses. Utilization of PBRs for algal cultivation and heat treatments
140 can largely reduce compounding effects during high temperature treatments and improve
141 our understanding of algal heat responses.
142
143 Recently, we conducted systems-wide analyses in wild-type (WT) Chlamydomonas
144 cultures during and after 24-h heat of 35°C and 40°C in PBRs under light in acetate-
145 containing medium (mixotrophic condition) with turbidostatic control and constant nutrient
146 supply (Zhang *et al.*, 2022*a*). We chose moderate high temperature of 35°C and acute
147 high temperature of 40°C based on the algal growth rates under different temperatures
148 and their relevance to physiologically high temperatures experienced in nature (Krishnan
149 *et al.*, 2021). The 24-h heat duration allowed us to balance time-course sample collection
150 over a sufficient duration while maintaining culture viability (heat at 40°C for longer time
151 killed algal cells); our experimental conditions enabled us to investigate algal heat
152 responses during and after physiologically relevant high temperatures (Zhang *et al.*,
153 2022*a*). Our results showed that 40°C inhibited algal growth while 35°C increased algal
154 growth with constant acetate supply. The growth inhibition at 40°C could be explained by

155 reduced photosynthesis, impaired respiration, and arrested cell cycle, while these cell
156 parameters had minor changes in algal cultures treated by 35ºC. Our proteomics data
157 indicated that several proteins involved in acetate uptake and assimilation, glyoxylate
158 cycle, and gluconeogenesis were up-regulated during 35ºC (Zhang *et al.*, 2022*a*).
159 Chlamydomonas uptakes acetate and feeds it into the glyoxylate cycle and
160 gluconeogenesis for starch biosynthesis (Johnson and Alric, 2012, 2013). The main
161 function of glyoxylate cycle is assimilation of 2-carbon compounds (e.g., acetate) into
162 organic acids that can be metabolized by the cell; the glyoxylate cycle is a shunt of the
163 tricarboxylic acid (TCA) cycle in mitochondria without releasing CO_2, which allows for the
164 anabolism of simple carbon compounds in gluconeogenesis, a process to make sugars,
165 e.g., glucose (Johnson and Alric, 2012; Chew *et al.*, 2019; Walker *et al.*, 2021).
166
167 We hypothesized that the increased growth in Chlamydomonas at 35ºC with constant
168 acetate supply was attributable to up-regulated acetate metabolism. In our previous
169 papers, we found out that 35ºC increased the growth rates of Chlamydomonas cultures
170 with constant acetate supply (Zhang *et al.*, 2022*a*), but not in cultures without acetate
171 (Mattoon *et al.*, 2022*b*), as compared to the control at 25ºC with the same medium type.
172 Therefore, we hypothesized that the effects of moderate high temperature at 35ºC was
173 dynamic depending on the availability of acetate, e.g., constant-acetate, acetate-
174 depleting, or no-acetate conditions. The majority of published high temperature research
175 in Chlamydomonas has been conducted in acetate-containing medium (Voß *et al.*, 2010;
176 Mühlhaus *et al.*, 2011*a*; Hemme *et al.*, 2014; Rütgers *et al.*, 2017; Zhang *et al.*, 2022*a*),
177 but the interface between acetate supply and Chlamydomonas heat responses is
178 understudied. To validate our hypothesis and address these unknown questions, we
179 cultivated the same Chlamydomonas WT strain in PBRs as before but heated the cultures
180 at 35ºC or 40ºC with and without constant acetate supply for 1 or 4 days. Our previous
181 work was conducted at 35ºC and 40ºC for 24 h with constant acetate supply (Zhang *et*
182 *al.*, 2022*a*). In this paper, to investigate the effects of carbon availability on algal
183 thermotolerance, we included 3 new different heat treatments at 35ºC and 40ºC: (1)
184 acetate-depleting condition for 24 h, (2) constant-acetate condition for 4 days, and (3) no-
185 acetate condition for 4 days. The last two conditions utilized turbidostatic control with

186 constant nutrient supply. Our new results confirmed our hypothesis about the role of
187 acetate metabolism in algal thermotolerance and revealed the overlooked effects of
188 moderate high temperature of 35°C on algal growth. Heat of 35°C was beneficial or
189 detrimental to Chlamydomonas cultures depending on acetate availability. Acute high
190 temperature of 40°C was lethal to Chlamydomonas cultures, with and without constant
191 acetate supply. Our research helps fill the knowledge gaps about how external carbon
192 supply affects algal heat responses, provides new insights to understand algal heat
193 responses, has potential applications in production of algal biofuel and bioproducts, and
194 contributes to improved thermotolerance in photosynthetic cells.
195
196 **Materials and methods**
197
198 **Algal cultivation**
199 The *Chlamydomonas reinhardtii* wild-type strain CC-1690 (also called *21gr*, mating type
200 plus) (Sager, 1955; Pröschold *et al.*, 2005; Zhang *et al.*, 2022*b*) was purchased from the
201 Chlamydomonas resource center and used in all experiments. Algal cultures were grown
202 in Tris-acetate-phosphate (TAP, with acetate) or Tris-phosphate (TP, without acetate)
203 medium with revised trace elements (Kropat *et al.*, 2011) in 400 mL photobioreactors
204 (PBRs) (Photon System Instruments, FMT 150/400-RB) as described previously (Zhang
205 *et al.*, 2022*a*). Each medium type was used in individual PBRs for independent
206 experiments. Cultures were illuminated with constant 100 μmol photons m^{-2} s^{-1} light (red:
207 blue, 1:1 ratio), and agitated by bubbling with filtered air at a flow rate of 1 L min^{-1}. Algal
208 cultures with targeted cell density around 1-2 x10^6 cells mL^{-1} (~4-6 μg mL^{-1} chlorophyll
209 content) were maintained at 25°C for 4 days with constant nutrient supply through
210 turbidostatic control before different temperature treatments. The turbidostatic mode was
211 controlled by OD_{680} (optical density at 680 nm), which is proportional to chlorophyll
212 contents (μg mL^{-1}) and was monitored once per min automatically. When OD_{680} increased
213 to a maximum value slightly above the target value (for target cell density) due to algal
214 growth, OD_{680} signaled the control computer to turn on a turbidostatic pump to add fresh
215 medium to dilute the culture until a minimum OD_{680} slightly below the target value was
216 reached, then the turbidostatic pump was turned off automatically. Because of the small

217 OD range we used, the PBR cultures had exponential growth between dilution events
218 through the turbidostatic control with constant nutrient supply (Fig. 1A). The OD_{680} data
219 during exponential growth phases in between dilution events was log_2 transformed, and
220 the relative growth rate was calculated using the slope of $log_2(OD_{680})$. The relative growth
221 rate is the inverse of the algal culture doubling time. For the treatments without constant
222 nutrient supply (acetate-depleting condition), the turbidostatic pumps were turned off after
223 PBR cultures reached steady growth and at the start of different temperature treatments
224 (Fig. 1B).
225
226 **High temperature treatments in PBRs**
227 After algal cultures in PBRs reached steady growth with turbidostatic control at 25°C for
228 4 days, PBR temperatures were increased to moderate (35°C) or acute (40°C) high
229 temperatures in different PBRs for the indicated duration with indicated nutrient
230 conditions. PBR temperatures were increased from 25°C to 35°C or 40°C gradually over
231 the course of 30 min with controlled heating speeds. PBR cultures grown under constant
232 25°C with the same nutrient status and treatment duration served as controls. Algal
233 cultures were harvested from PBRs at different time points during different treatments for
234 various measurements.
235
236 **Algal biomass quantification**
237 Algal cultures (90 mL) were harvested from PBRs, centrifuged to remove supernatant,
238 flash frozen in liquid nitrogen, then stored in a -80°C freezer until analysis. Algal cell
239 pellets were freeze dried for 24 h over liquid nitrogen. The remaining algal dry biomass
240 were weighed and quantified.
241
242 **Acetate quantification assay**
243 Algal cultures were harvested from PBRs (2 mL) and centrifuged to collect 500 μL top
244 clear supernatant to a new tube. The supernatant was stored in a -80°C freezer until
245 analysis. The acetate content in the supernatant was quantified using the Acetate
246 Colorimetric Assay Kit (Sigma, Cat No. MAK086) according to manufacture instructions.
247

248 **Cell imaging using light microscopy**

249 Chlamydomonas cultures harvested at select time points with different temperature
250 treatments were fixed with 0.2% glutaraldehyde (VWR, Cat No. 76177-346). Algal cells
251 were imaged with a Leica DMI6000 B microscope and a 63x (NA1.4) oil-immersion
252 objective.

253

254 **Chlorophyll quantification**

255 Chlorophyll contents in algal cells were quantified as previously described (Zhang *et al.*,
256 2022*a*). PBR cultures of 1 mL were harvested in 1.5-mL tubes with 2.5 µL 2% Tween20
257 (Sigma, P9416-100ML, to help cell pelleting), and centrifuged at 18,407 g at 4°C. After
258 removing supernatant, cell pellets were stored in a -80°C freezer until quantification.
259 Later, cell pellets were thawed, resuspended in 1 mL of HPLC grade methanol (100%,
260 Sigma, 34860-4L-R), vortexed for 1 min, incubated in the dark at 4°C for 5 min, and
261 centrifuged at 15,000 g at 4°C for 5 min. Supernatant was pipetted out to a two-sided
262 disposable plastic cuvettes (VWR, 97000-586) for chlorophyll (Chl) quantification at 652
263 nm and 665 nm in a spectrophotometer (IMPLEN Nonophotometer P300) using the
264 following equations: Chl a + Chl b = $22.12*A_{652} + 2.71*A_{665}$ (in µg mL^{-1} algal cultures)
265 (Zhang *et al.*, 2022*a*). Chlorophyll concentrations were also normalized to cell densities
266 (Chl pg cell^{-1}) or mean cell volume (Chl pg µm^{-3}). Cell density and mean cell volume were
267 measured using a Coulter Counter (Multisizer 3, Beckman Counter, Brea, CA). For 35°C
268 with photoautotrophic medium, algal cells formed palmelloids, clumps of non-motile cells,
269 thus the size of palmelloids instead of cell size was measured by the Coulter Counter.

270

271 **RNA extraction**

272 PBR cultures of 2 mL were pelleted with Tween-20 (0.005%, v/v) by centrifugation at
273 11,363 x g and 4°C for 2 min, followed by supernatant removal. The cell pellet was flash
274 frozen in liquid nitrogen and then stored in a -80°C freezer until processing. RNA
275 extraction and RT-qPCR analysis were performed as previously described with minor
276 modifications (Zhang *et al.*, 2022*a*). Total RNA was extracted with TRIzol reagent
277 (Thermo Fisher Scientific, Cat No. 15596026), digested on-column with RNase-free

278 DNase (Qiagen, Cat No. 79256), purified by RNeasy mini-column (Qiagen, Cat No.
279 74106), and quantified with Qubit™ RNA BR Assay Kit, (Life technology, Cat No.
280 Q10210).

281

282 **RT-qPCR analysis**

283 Total 0.4 µg RNA was reverse transcribed with oligo dT primers using SuperScript® III
284 First-Strand Synthesis System (Life technology, Cat No. 18080-051) following
285 manufacturer instructions. Quantitative real-time PCR (RT-qPCR) analysis was
286 performed using a CFX384 Real-Time System (C 1000 Touch Thermal Cycler, Bio-Rad,
287 Hercules, California) using SensiFAST SYBR No-ROS kit (Bioline, BIO-98020) following
288 this program: (1) 95ºC (2 min); (2) 40 cycles of 95ºC (5 s), 60ºC (10 s), and 72ºC (15 s);
289 (3) final melt curve at 60°C (5 s), followed by continuous temperature ramping from 60°C
290 to 99°C at a rate of 0.5°C s^{-1}. Melting curves and qPCR products were tested to ensure
291 there were no primer dimers or unspecific PCR products. All RT-qPCR products were
292 sequenced for confirmation. Primers and gene IDs for RT-qPCR can be found in
293 Supplementary Table 1. *CBLP* (*β-subunit-like polypeptide*, Cre06.g278222) (Schloss,
294 1990; Xie *et al.*, 2013) and *EIF1A* (*Eukaryotic translation initiation factor 1A,*
295 Cre02.g103550) (Strenkert *et al.*, 2019) had stable expression among all time points, and
296 were used as reference genes for RT-qPCR normalization. The relative gene expressions
297 were calculated relative to the pre-heat time point by using the $2^{-\Delta\Delta CT}$ method (Livak and
298 Schmittgen, 2001; Hellemans *et al.*, 2007; Remans *et al.*, 2014). Three biological
299 replicates were included for each time point and treatment. RT-qPCR was used to verify
300 some selected transcripts and compared with the results of RNA-seq for samples
301 harvested under the acetate-depleting conditions (Supplemental Fig. 2). RNA-seq for
302 samples harvested under the constant-acetate conditions were verified by RT-qPCR
303 previously (Zhang *et al.*, 2022*a*).

304

305 **RNA-seq analysis**

306 Raw sequencing data for the constant-acetate experiments at 35°C and 40°C were
307 obtained from Zhang *et al.*, 2022*a*. Raw sequencing data for the constant-acetate

experiment at 25°C and acetate-depleting experiments at 25°C, 35°C, and 40°C were collected in this study. All raw sequencing data were processed using the same pipeline as described below.

RNA libraries were prepared and sequenced by the Joint Genome Institute (JGI, Community Science Program) using the NovaSeq platform generating 151-nt paired-end reads. Plate-based RNA sample preparation was performed on the PerkinElmer Sciclone NGS robotic liquid handling system using Illumina's TruSeq Stranded mRNA HT sample prep kit utilizing poly-A selection of mRNA following the protocol outlined by Illumina in their user guide, with the following conditions: total RNA starting material was 1 µg per sample and 8 cycles of PCR was used for library amplification. The prepared libraries were quantified using KAPA Biosystems' next-generation sequencing library qPCR kit and ran on a Roche LightCycler 480 real-time PCR instrument. Sequencing of the flowcell was performed on the Illumina NovaSeq sequencer using NovaSeq XP V1.5 reagent kits, S4 flowcell, following a 2x151 indexed run recipe.

Samples were quality control filtered using the JGI BBDuk and BBMap pipelines (BBDuk, 2022). Samples were quality assessed using FastQC (Andrews) and mapped to the *Chlamydomonas reinhardtii* v5.6 genome (Merchant *et al.*, 2007) using HISAT2 version 2.2.0 (Kim *et al.*, 2015). Reads per feature were counted via featureCounts (Liao *et al.*, 2014). The count matrix was combined with existing data (Zhang *et al.*, 2022*a*), resulting in a 16,403x101 count matrix (Supplemental Dataset 4, 5). The normalization of the count matrix was conducted using the median of ratios method (Liao *et al.*, 2014). Prior to imputation of two missing time points in the constant-acetate-25°C condition (see details below), transcripts were filtered to have nonzero counts in at least 90% of the samples.

Under constant 25°C, acetate, and light with turbidostatic control (constant-acetate-25°C), the algal growth rate and cell physiology stays constant (Fig. 5). We had RNA-seq data for 8 time points (pre-heat, 0, 0.5, 1, 2, 24, 26, and 48 h) under constant-acetate-25°C and these samples were highly correlated with each other (with Pearson correlation ≥ 0.993) (Supplemental Fig. 1). RNA samples for the time points of 4 and 8 h under the

339 constant-acetate-25ºC condition were unavailable; thus RNA-seq data for the 4 and 8 h
340 under the constant-acetate-25ºC condition were imputed from other extra time points (0,
341 0.5, 1, 26, 48 h) of the same condition. For the time points of 4 and 8 h under the constant-
342 acetate-25ºC condition, each transcript triplicates were sampled randomly using the 5
343 extra time points under the same condition mentioned above. It was ensured that both
344 missing time points were not imputed with the same count data. The final count matrix
345 consists of 14,893 transcripts in 90 samples (5 time points measured at 6 conditions as
346 triplicates). The natural logarithm was determined for all normalized counts before
347 averaging triplicates. Pearson correlation coefficients were calculated for all sample pairs.
348
349 The count data were tested for differential expression using DESeq2 v1.38.3 (Love *et al.*,
350 2014). DESeq2 applies a Benjamini Hochberg correction for multiple testing. The design
351 matrix was constructed to test for global kinetic differences between the three different
352 temperatures and both growth media over time. The following tests were performed
353 (Supplemental Dataset 1, 3, 5, Supplemental Fig. 5): (A) acetate-depleting 25°C vs
354 acetate-depleting 35°C; (B) acetate-depleting 25°C vs acetate-depleting 40°C; (C)
355 constant-acetate 25°C vs constant-acetate 35°C; (D) constant-acetate 25°C vs constant-
356 acetate 40°C; (E) temperature effect: (constant-acetate 35°C and acetate-depleting 35°C)
357 vs (constant-acetate 40°C and acetate-depleting 40°C); (F) medium effect: (constant-
358 acetate 35°C and constant-acetate 40°C) vs (acetate-depleting 35°C and acetate-
359 depleting 40°C); (G) acetate-depleting 25°C vs constant-acetate 25°C.
360
361 Functional descriptions were determined for each transcript (Merchant *et al.*, 2007;
362 Usadel *et al.*, 2009; Venn and Mühlhaus, 2022). Transcripts were grouped according to
363 their functional description. Time courses of normalized transcript counts were visualized
364 as $\log_2$(fold change). An ANOVA was performed for each transcript at each treatment to
365 elucidate whether a transcript underwent a relevant change during its time course (Venn
366 et al., 2022a). Heatmaps (Supplemental Dataset 1) and functional sets figures
367 (Supplemental Dataset 2) were created using Plotly.NETv4.0.0 (Schneider *et al.*, 2022).
368

369 Ontology enrichment was performed using extended MapMan annotations (for example
370 "PS.lightreaction.LHC" became "PS.Lightreaction.LHC", "PS.Lightreaction" and "PS")
371 (Supplemental Dataset 3). The measured and filtered transcripts served as background.
372 If a transcript showed significant differential expression in the respective comparison
373 (FDR < 0.05), it was considered as significant for its annotation. Enrichment p values
374 were determined using hypergeometric tests. Multiple testing correction was performed
375 using the Benjamini-Hochberg method (Benjamini and Hochberg, 1995; Venn *et al.*,
376 2022). Additional ontology enrichment was performed using ChlamyCyc annotations
377 (v2023-01-04). This pathway ontology combines KEGG, MapMan, and JGI pathway
378 information (May *et al.*, 2009). The enrichment procedure and statistical analysis were
379 the same as above.
380
381 **Results**
382 To investigate how the availability of an organic carbon source, acetate, affected algal
383 heat responses, we first cultivated WT Chlamydomonas cells (CC-1690, *21gr*) in PBRs
384 in Tris-acetate-phosphate (TAP, acetate as an organic carbon source) medium at 25°C
385 with constant nutrient supply through turbidostatic control (providing frequent fresh
386 medium for culture dilution) (Fig. 1A). After algal cultures reached steady growth rates in
387 PBRs, the turbidostatic control was turned off and the temperatures of algal cultures were
388 increased to 35°C or 40°C or stayed at 25°C for 24 h without constant acetate supply,
389 defined as the acetate-depleting condition. This experiment allowed us to quantify acetate
390 consumption under different temperatures, which could not be performed in cultures with
391 turbidostatic control and frequent medium dilution. It also enabled us to investigate algal
392 heat responses under the acetate-depleting condition, like shaker cultures, which were
393 used by most previous algal heat experiments in published literatures (Hemme *et al.*,
394 2014; Rütgers *et al.*, 2017). Under the acetate-depleting condition, algal cultures were
395 harvested at different time points to analyze cell physiology, biomass, and transcriptome
396 (Fig. 1B). Algal dry biomass quantification showed that cultures treated with 35°C had
397 increased biomass at 8-h heat but decreased biomass at 24-h heat as compared to 25°C
398 (Fig. 1C). Acetate quantification in the supernatant of algal cultures showed that 35°C-

399 treated cultures had increased acetate consumption and depleted acetate faster than
400 25°C or 40°C (Fig. 1D).
401
402 We hypothesized the transiently increased and then decreased algal biomass in 35°C-
403 treated cultures was due to increased acetate uptake and usage which led to acetate
404 starvation at 24 h of the acetate-depleting condition (Fig. 1). Chlamydomonas uptakes
405 acetate and feeds it into the glyoxylate and gluconeogenesis cycles to produce starch,
406 which can be used in glycolysis to generate ATP (Johnson and Alric, 2012, 2013) (Fig.
407 2A). To verify this hypothesis, we performed RNA-seq analysis and investigated key
408 transcripts involved in acetate uptake and assimilation, glyoxylate, gluconeogenesis, and
409 glycolysis cycles under the acetate-depleting condition by comparing with the constant-
410 acetate condition (Fig. 2B-P). Under the acetate-depleting condition, almost all these
411 transcripts related to acetate uptake and metabolism were up-regulated under 35°C as
412 compared to 25°C, especially the early heat time points of 2 and 4 h at 35°C. Similar 35°C
413 effects on these transcripts were held under the constant-acetate condition, although the
414 up-regulation of these transcripts were often stronger and lasted longer at 35°C under the
415 constant-acetate condition than the acetate-depleting condition. In contrast, these
416 transcripts related to acetate uptake and metabolism were down-regulated under 40°C
417 as compared to 25°C under both the acetate-depleting and constant-acetate conditions,
418 especially the 2-h heat time point at 40°C. Our RT-qPCR results of selected transcripts
419 showed similar trends as our RNA-seq data (Supplemental Fig. 2). These results showed
420 that 35°C promoted acetate metabolism, from acetate uptake and assimilation to
421 glyoxylate, gluconeogenesis, and glycolysis cycles; however, these acetate metabolism
422 pathways were reduced under 40°C.
423
424 In addition to the acetate metabolism pathways mentioned above, we investigated
425 transcripts related to other processes that are often affected by high temperatures
426 (Supplemental Fig. 3, 4). Chlamydomonas has two heat shock transcription factors, HSF1
427 and HSF2; HSF1 is the master heat regulator but the function of HSF2 is unclear (Schulz-
428 Raffelt *et al.*, 2007). The transcripts of both *HSF*s were induced by heat, with higher
429 induction at 40°C than 35°C under the same acetate condition and higher induction under

430 the acetate-depleting than constant-acetate condition under the same high temperature
431 (Supplemental Fig. 3A, B). Heat shock proteins (HSPs) are the hallmarks of heat
432 responses and function as chaperones to help refold denatured proteins, fold nascent
433 polypeptides, and prevent denatured protein aggregates (Altschuler and Mascarenhas,
434 1982; Schroda *et al.*, 2015; Haq *et al.*, 2019). Based on molecular mass, HSPs are
435 grouped into large HSPs (HSP100/90/70/60, >50 kDa) and small HSPs (10-43 kDa) (Jee,
436 2016; Bourgine and Guihur, 2021). Under the acetate-depleting condition, many
437 transcripts related to large HSPs, *HSP60/70/90s*, were down-regulated at 24 h of 25°C
438 and 35°C; such down-regulation of *HSP60/70/90s* was absent at 24 h of 25°C and 35°C
439 under the constant-acetate condition or 24 h of 40°C under both acetate conditions
440 (Supplemental Fig. 4A-C). Additionally, transcripts of *HSP100* and most of the small
441 *HSPs* did not have such down-regulation at 24 h of 25°C and 35°C under the acetate-
442 depleting condition (Supplemental Fig. 4D, E). Almost all transcripts related to the *HSPs*
443 we examined, including *HSP60/70/90/100s* and small *HSPs*, were up-regulated at 2 h of
444 40°C, with similar induction fold change under either the acetate-depleting or constant-
445 acetate condition (Supplemental Fig. 4A-E). This suggested the early induction of these
446 *HSPs* under 40°C was temperature-dependent (present at 40°C while much less so under
447 35°C) but acetate-availability-independent. Alternatively, the acetate-availability might not
448 differ significantly at 2 h of the acetate-depleting and constant-acetate condition (Fig. 1D).
449 However, the absence of down-regulated *HSP* transcripts at 24 h of 40°C under the
450 acetate-depleting condition supported that the induced *HSP* transcripts at 40°C was
451 independent of acetate.
452
453 The global transcriptome changes related to light reaction and Calvin-Benson cycle of
454 photosynthesis suggested more disturbance of these transcripts under the acetate-
455 depleting than the constant-acetate conditions at the same temperatures, and more
456 disturbance of these transcripts at 40°C than 35°C under the same acetate conditions
457 (Supplemental Fig. 4F-M). These photosynthesis-related transcripts behaved similarly at
458 40°C under both the acetate-depleting and constant-acetate conditions, suggesting 40°C
459 heat effects were more dominant than the changes of acetate availability.
460 Chlamydomonas employs a cellular structure, pyrenoid, to concentrate CO_2 for improved

461 carbon fixation efficiency, called carbon concentrating mechanisms (CCM) (Meyer *et al.*,
462 2017; Hennacy and Jonikas, 2020). The CCM is especially important under high
463 temperature conditions, where the solubility of CO_2 decreases in water by approximately
464 30% from 25°C to 40°C (Dodds *et al.*, 1956). Under the acetate-depleting conditions,
465 several transcripts related to CCM were up-regulated at 24 h under 25°C and 35°C, but
466 not under the same temperature of the constant-acetate condition (Supplemental Fig.
467 4N). This suggested that as acetate became depleted in the medium and cell density
468 increased, cells relied more on the photosynthetic carbon fixation by up-regulating CCM.
469 Such induction of the CCM transcripts was much less at 40°C under the acetate-depleting
470 condition, which may correlate with the compromised pyrenoid structures with decreased
471 appearance of thylakoid tubules at 40°C in our previous publication (Zhang *et al.*, 2022*a*).
472 Thylakoid tubules deliver concentrated CO_2 to the pyrenoid and also serve as the diffusion
473 path of Calvin-Benson Cycle metabolites (Hennacy and Jonikas, 2020). Transcripts
474 related to photoprotection had larger induction at 24 h under all three temperatures of the
475 acetate-depleting than the constant-acetate conditions at the same temperature,
476 indicating compromised photosynthesis and the need for photoprotection when acetate
477 was depleted (Supplemental Fig. 4O).
478
479 The compromised photosynthesis under high temperatures lead to increased
480 accumulation of reactive oxygen species (ROS) (Pospíšil, 2016; Janni *et al.*, 2020;
481 Niemeyer *et al.*, 2021). Some transcripts related to ROS scavenging were down-regulated
482 at 24 h of 25°C and 35°C under the acetate-depleting condition but much less so under
483 the constant-acetate condition at the same temperatures (Supplemental Fig. 4R-V). This
484 may be related to the increased cell density and reduced light and oxidative stress at 24
485 h of 25°C and 35°C under the acetate-depleting condition. Such down-regulation of
486 transcripts related to ROS scavenging was not present at 24 h of 40°C under the acetate-
487 depleting condition. This may suggest relatively increased ROS accumulation and ROS
488 scavenging activity at 40°C than 25°C and 35°C under the acetate-depleting conditions.
489 Additionally, transcripts related to ROS scavenging had very similar transcriptional
490 changes at 40°C under either the acetate-depleting or constant-acetate condition,

491 suggesting 40°C had more dominant effects on the ROS accumulation and ROS
492 scavenging activities than acetate.
493
494 Transcripts related to cell cycle and cell wall had similar transcriptional patterns under
495 each of the six conditions (Supplemental Fig. 4W, X). Under diurnal cycles, cell wall genes
496 were up-regulated following the up-regulation of cell cycle genes and cell walls form
497 around daughter cells during cell division (Zones *et al.*, 2015). These transcripts were
498 down-regulated at 24 h of 25°C under the acetate-depleting condition, suggesting the
499 transition to reduced cell division due to the acetate-depletion. The reduction of these
500 transcripts was larger and more prolonged under 40°C than 35°C, consistent with
501 complete and transient inhibition of cell cycle under 40°C and 35°C, respectively (Hemme
502 *et al.*, 2014; Zhang *et al.*, 2022*a*). At 24 h of 40°C and 35°C, these transcripts were more
503 reduced under the acetate-depleting condition than the constant-acetate condition. It is
504 worthwhile to note that the changes during 24 h of the acetate-depletion condition were
505 dynamic and here we just mentioned the changes at 24 h in the end when acetate was
506 depleted.
507
508 Almost all transcripts mentioned above had little changes at 25°C during all time points
509 of the constant-acetate condition, validating the steady growth and constant cell status
510 under the turbidostatic control with constant nutrient and light but without heat treatments
511 in our algal cultures grown in PBRs (Supplemental Fig. 4).
512
513 We performed statistical analysis to investigate global transcript kinetic differences
514 between different conditions (Supplemental Dataset 1, 3). We then applied ontology
515 enrichments analysis for transcripts that were significantly expressed in a defined
516 comparison to identify differentially regulated biological processes (Supplemental Fig. 5,
517 Supplemental Dataset 3). The top enriched function group that differed at 25°C and 35°C
518 under both acetate-depleting and constant-acetate condition was the nuclear-encoded
519 ribosomal proteins that are involved in chloroplast protein synthesis (Supplemental Fig.
520 5A, C). More than half of the ribosomal related transcripts were down-regulated at 4 h
521 heat of 35°C as compared to 25°C under both acetate conditions (Supplemental Fig. 4Y,

522 Z), suggesting 35ºC may inhibit chloroplast protein synthesis. The down-regulation of
523 ribosomal related transcripts at 35ºC could recover partially under the constant-acetate
524 condition, but much less so under the acetate-depleting condition. The top enriched
525 function group that differs between 25ºC and 40ºC under the acetate-depleting condition
526 was the mitochondrial electron transport (Supplemental Fig. 5B). Many transcripts related
527 to mitochondrial electron transport were down-regulated at 2 h heat of 40ºC as compared
528 to 25ºC under the acetate-depleting condition, especially these related to ATP synthesis
529 (Supplemental Fig. 4AA, AB). When comparing 35ºC and 40ºC conditions independent
530 of the acetate availability, the top enriched function group was also the mitochondrial
531 electron transport (Supplemental Fig. 5E). The results suggested that mitochondrial
532 electron transport was more sensitive to 40ºC than 25ºC and 35ºC. Under the constant-
533 acetate condition, 40ºC affected transcripts related to RNA processing the most as
534 compared to 25ºC (Supplemental Fig. 5D, 4AC, AD). When comparing the acetate-
535 depleting and constant-acetate conditions independent of temperatures, the top two
536 enriched groups were phosphate transport and mitogen-activated protein kinase (MAP
537 kinase) cascades signaling (Supplemental Fig. 5F). MAP kinase signaling pathways have
538 important roles in plant growth and stress responses and involve protein phosphorylation
539 and dephosphorylation (Bigeard and Hirt, 2018; Jagodzik *et al.*, 2018; Zhang and Zhang,
540 2022). The biggest differences in transcripts related to the MAP kinase signaling
541 pathways between the acetate-depleting and constant-acetate conditions were at the 24
542 h time point at 25ºC and 35ºC when the acetate was depleted (Supplemental Fig. 4AF),
543 suggesting potential roles of the MAP kinase signaling pathways in nutrient sensing and
544 growth regulation. When comparing the acetate-depleting and constant-acetate
545 conditions at 25ºC, the top enriched functional groups are dominantly related to cell
546 motility (Supplemental Fig. 5G). More than half of the transcripts related to cell motility at
547 25ºC were down-regulated at 24 h under the acetate-depleting condition but not the
548 constant-acetate condition (Supplemental Fig. 4AG, AH). Microscopic images showed
549 that cells had cilia at 24 h of 25ºC under the acetate-depleting condition (Supplemental
550 Fig. 6). Cell motility needs energy and ciliary beating frequency corelates with the
551 cytosolic ATP concentration in Chlamydomonas (Takano *et al.*, 2021). Thus, the down-
552 regulation of transcripts related to cell motility may suggest the reduced cellular ATP level

553 and the transition from motile to non-motile phase when the acetate was depleted at 24
554 h of the acetate-depleting condition.
555
556 Besides MapMan ontology enrichment, we performed ChlamyCyc pathway enrichment
557 analysis of differentially regulated transcripts compared between two conditions
558 (Supplemental Dataset 6). The ChlamyCyc annotations (v2023-01-04) and pathway
559 ontology combine KEGG, MapMan, and JGI pathway information (May et al. 2009). The
560 KEGG pathway annotation for Chlamydomonas is sparse, therefore it was difficult to
561 determine significances. As comparison, for the MapMan functional ontology we got
562 23,500 annotations in the RNA-seq data, for KEGG pathways we only got 803. Both
563 analyses showed the mitochondrial activity was the top enrichment for the comparisons
564 of 25°C versus 40°C under the acetate-depleting condition and 35°C versus 40°C under
565 either acetate condition (temperature effects) (Supplemental Fig. 5B, E, Supplemental
566 Dataset 6).
567
568 To further understand our transcriptome data and the effects of acetate, we compared
569 cell physiology at different temperatures between the acetate-depleting and constant-
570 acetate conditions (Fig. 3). Under the acetate-depleting condition without medium dilution,
571 cell density increased over time at 25°C and 35°C but no changes at 40°C because of
572 cell cycle arrest at 40°C (Fig. 3A). Cell density was lower at 35°C than 25°C at 8 h and 24
573 h time points, suggesting reduced growth rates at 35°C at the end of the acetate-depleting
574 condition. Algal cells treated at 35°C had transiently increased then decreased cell size
575 while 40°C-treated algal cells had steadily increased cell size due to heat-inhibited cell
576 division (Fig. 3B). Under the acetate-depleting condition, chlorophyll content per culture
577 volume (mL) had no significant differences between 25°C and 40°C but was significantly
578 higher at 8-h of 35°C than 25°C (Fig. 3C), consistent with the increased biomass at the
579 8-h of 35°C (Fig. 1C). Chlorophyll content normalized to cell density revealed constant
580 chlorophyll per cell during 25°C, but transiently and constantly increased cellular
581 chlorophyll during 35°C and 40°C, respectively (Fig. 3D). Chlorophyll content normalized
582 to cell volume showed the increased cellular chlorophyll during 40°C and 35°C could not
583 be completely explained by increased cell volume (Fig. 3E).

584

585 Based on our previously published data, we summarized cell parameters in algal cultures
586 grown in the same PBRs but under the 24-h constant-acetate condition through
587 turbidostatic control (Zhang *et al.*, 2022*a*) (Fig. 3F-J). Cell parameters at different time
588 points during 25°C had little or no changes as compared to the pre-heat time points,
589 demonstrating the steady algal growth and effectiveness of the turbidostatic control with
590 constant acetate supply. Under the constant acetate condition, the smaller changes of
591 cell density and chlorophyll per mL culture as compared to the acetate-depleting
592 conditions were due to the turbidostatic control and frequent dilution of the culture (Fig.
593 3F and 3H). The changes of cell volume and chlorophyll content per cell during 35°C and
594 40°C had similar trends under both the acetate-depleting and constant-acetate condition,
595 but the increase of these parameters was larger under 40°C in cultures with the constant-
596 acetate than the acetate-depleting condition (Fig. 3B, D, G, I). This was supported by the
597 fold changes of cell parameters by comparing the data under the acetate-depleting and
598 constant-acetate conditions (Fig. 3K-O).

599

600 In addition to the cellular parameters mentioned above using time-course harvesting, we
601 next utilized non-disruptive and automatic methods to quantify algal growth under
602 different temperatures. The acetate-depleting condition without turbidostatic control
603 allowed us to have a large range of cell densities under different temperature treatments
604 to investigate the optical density (OD) vs cell density relationship and validate automatic
605 culture monitoring under different temperature treatments. OD_{680} (optical density at 680
606 nm) monitors chlorophyll content per mL culture (Chapman *et al.*, 2015; Xiao *et al.*, 2015;
607 Young *et al.*, 2022). OD_{750} (optical density at 750 nm) monitors light scattering and is
608 thought to be proportional to cell density or cell volume (Chioccioli *et al.*, 2014; Young *et*
609 *al.*, 2022). Our PBRs can measure OD_{680} and OD_{720}, but not OD_{750}. However, OD_{720}
610 serves as a proxy for OD_{750} for light scattering. Thus, we investigated the dynamic
611 changes of OD_{680} and OD_{720} relative to chlorophyll content, cell density, and cell volume
612 before and during heat treatments under the acetate-depleting condition (Fig. 4). The
613 change of OD_{680} and OD_{720} mimicked the change of chlorophyll content per mL algal
614 culture for all three temperature treatments (Fig. 4A, B, 3C). But the change of OD_{720}

615 (Fig. 4B) mimicked the change of cell density for 25°C and 35°C but not 40°C (Fig. 3A).
616 Combining all data from different temperature treatments and time points, both OD_{680} and
617 OD_{720} were linearly proportional to chlorophyll content per mL algal culture (Fig. 4C, D),
618 but they were much less proportional to cell volume or cell density (Fig. 4E-H). Our results
619 showed that OD_{680} and OD_{720} can be used to accurately estimate chlorophyll content in
620 algal cultures with different heat treatments under a wide range of cell densities. Thus,
621 OD_{680} and OD_{720} can be used to estimate algal relative growth rates based on chlorophyll
622 accumulation during an exponential growth phase between two dilution events under the
623 turbidostatic control in PBRs (Zhang *et al.*, 2022*a*) (See methods for details). The relative
624 growth rates calculated from both OD_{680} and OD_{720} yielded similar results. Because OD_{680}
625 had larger values and higher signal/noise ratios than OD_{720}, we used OD_{680} to estimate
626 relative growth rates of PBR cultures over several days under the turbidostatic controls
627 with and without acetate supply to investigate how acetate affected algal heat responses
628 at 35°C and 40°C in long-term (Fig. 5-8). This research goal could not be achieved without
629 turbidostatic control because our acetate-depleting experiment revealed that acetate was
630 fully depleted in 24 h during all three temperature treatments of 25°C, 35°C and 40°C
631 without constant acetate supply (Fig. 1D).
632
633 To investigate the effects of acetate on long-term heating, after algal cultures reached
634 steady growth at 25°C in PBRs with turbidostatic control, we conducted all three
635 temperature treatments with continuous turbidostatic control and constant acetate supply
636 for 4 days (Fig. 5). Without heat treatments, algal growth rates and cell parameters stayed
637 constant at 25°C, demonstrating the effectiveness of our turbidostatic control for steady
638 algal growth (Fig. 5A). At 35°C with constant acetate supply, the relative growth rates
639 increased first, but the increase was smaller after 2-day heating at 35°C and stabilized
640 thereafter. At 40°C, the relative growth rates decreased steadily, and the cultures died
641 after 2-day heating at 40°C, suggesting algal cells could not acclimate to long-term
642 constant heat at 40°C, even with constant acetate supply. Cells treated with 40°C had
643 more than 4-fold increase of cell volume as compared to the pre-heat condition, followed
644 by reduced cellular chlorophyll and cell death (Fig. 5C-F). The turbidostatic mode by
645 OD_{680} tightly controlled the chlorophyll contents in unit of ug per mL culture in PBRs during

646 the treatments of 25°C and 35°C (Fig. 5D), but not 40°C due to the cell cycle arrest and
647 overwhelmingly increased chlorophyll per cell, and eventually cell death under 40°C (Fig.
648 5B and E).
649
650 To further test the effects of acetate on algal heat responses, we conducted experiments
651 using algal cultures grown in PBRs under the turbidostatic control with constant nutrient
652 supply of photoautotrophic medium (no acetate) and different temperature treatments for
653 4 days (Fig. 6, 7). Our microscopic images showed that 35°C-treated cells in
654 photoautotrophic medium formed palmelloids (Fig. 6). Palmelloids are clumps of non-
655 motile cells, which often result from a failure of hatching or release from the mother cell
656 wall under stressful conditions (Harris, 2009). It was reported that Chlamydomonas cells
657 aggregated to form palmelloids after 3 min acute heat shock at 50°C in acetate-containing
658 medium (de Carpentier *et al.*, 2022). The formation of palmelloids did not occur in our
659 constant-acetate-35°C condition (Zhang *et al.*, 2022*a*), suggesting 35°C was more
660 stressful without acetate than with acetate. Without heat treatments, algal growth rates
661 and cell parameters stayed constant at 25°C, demonstrating the effectiveness of our
662 turbidostatic control for steady algal growth under photoautotrophic conditions (Fig. 7A).
663 Without acetate but with constant medium supply, algal growth had gradually decreased
664 growth rates during 35°C (Fig. 7A), unlike the increased growth rates during 35°C with
665 constant acetate supply (Fig. 5A), strongly supporting the role of acetate in algal heat
666 tolerance. Without acetate, algal cells with 35°C treatment had increased palmelloid
667 volume (or size) and chlorophyll contents (Fig. 7B-F). The reduction of growth rates during
668 40°C was comparable with and without acetate (Fig. 5A and 7A).
669
670 Our PBRs could also monitor photosystem II (PSII) operating efficiency using chlorophyll
671 fluorescence measurement automatically (Fig. 8). Heat at 40°C reduces PSII operating
672 efficiency dramatically, with more reduction without acetate than with acetate during the
673 first two days of heating (Fig. 8B, C, D). The acetate effects on PSII operating efficiency
674 disappeared in algal cells treated with 40°C for more than 2 days (Fig. 8D). The reduction
675 of PSII operating efficiency during 35°C was much smaller than during 40°C, with higher

676 PSII operating efficiency in 35°C-treated algal cells with acetate than without acetate (Fig.
677 8D).
678
679 **Discussion**
680 By performing algal cultivation under highly controlled conditions in PBRs with and without
681 the constant organic carbon source, acetate, we investigated how acetate availability
682 affected the growth of Chlamydomonas under moderate (35°C) and acute high
683 temperatures (40°C) (Fig. 9). The moderate high temperature of 35°C is frequently
684 experienced by outdoor, open algal ponds in summertime and enclosed outdoor algal
685 ponds can often heat up to 40°C or above (Krishnan *et al.*, 2021). Thus, both high
686 temperatures we chose were physiologically relevant for algae in nature. Additionally,
687 global warming increases the duration of moderate and acute high temperatures in the
688 field conditions. By using highly controlled turbidostatic conditions in PBRs, our research
689 not only investigated the short-term (within 24 h) but also long-term (up to 4-days) heat
690 effects on algal growth with and without acetate supply or under the acetate-depleting
691 conditions. Our research advanced the understanding of algal heat responses under
692 different heat intensities, heat durations, and carbon availability.
693
694 **Heat of 35°C was beneficial or detrimental depending on carbon availability**
695 Under the turbidostatic control with frequent medium dilutions, moderate high
696 temperature of 35°C increased algal growth rates with constant acetate supply (Fig. 5A)
697 but decreased algal growth rates without acetate in photoautotrophic medium (Fig. 7A),
698 confirming the important role of acetate in heat tolerance. The increased heat tolerance
699 at 35°C with acetate is not strain-dependent because the acetate effects were similar in
700 two different algal strains: CC-1690 (this study) and CC-5325 (Mattoon *et al.*, 2022*a*). In
701 medium starting with acetate but without constant acetate supply (the acetate-depleting
702 condition), algal biomass increased first but then decreased at 35°C compared to 25°C,
703 which can be explained by increased acetate uptake and usage initially followed by
704 acetate depletion and starvation by the end of the 24-h 35°C treatments (Fig. 1C, D).
705

706 Under the acetate-depleting condition without medium dilution, besides acetate, other
707 nutrients may also be depleted gradually during 24 h. We checked known transcription
708 factors and regulators responding to starvation of other nutrients, including *nitrogen*
709 *starvation responsive regulator 1 (NRR1)* (Boyle *et al.*, 2012), *sulfur starvation responsive*
710 *regulator 2.1 (SNRK2.1)* (González-Ballester *et al.*, 2010), *phosphorus starvation*
711 *response 1 (PSR1)* (Bajhaiya *et al.*, 2016), *copper deficiency response regulator 1*
712 *(CRR1)* (Sommer *et al.*, 2010), and *iron deficiency response regulator (Mitogen-Activated*
713 *Protein Kinase 3, MAPK3)* (Fei *et al.*, 2017). If these nutrients were depleted, the
714 corresponding transcription factors and regulators would be up-regulated. Most of these
715 nutrient-deficiency transcription factors and regulators had minimal or no induction at 24
716 h of the acetate-depleting condition (Supplemental Fig. 3C-G). One exception is the
717 *NRR1*, which was up-regulated at 25°C or 35°C but was down-regulated under 40°C at
718 24 h of the acetate-depleting condition (Supplemental Fig. 3C). The results suggested
719 minimal or no limitation of sulfur, phosphorus, copper, and iron during the acetate-
720 depleting condition, but possibly some nitrogen deficiency at 24 h of the acetate-depleting
721 condition at 25°C and 35°C but not 40°C. One of the responses to nitrogen deficiency is
722 the reduction of chlorophyll (Schmollinger *et al.*, 2014). During our acetate-depleting
723 condition, most transcripts involved in chlorophyll biosynthesis were stable (Supplemental
724 Fig. 4Q). Additionally, there was no change of the chlorophyll per cell or per cell volume
725 at 24 h of 25°C as compared to the pre-heat time point which did not have acetate-
726 limitation; these parameters were higher under 35°C and 40°C than 25°C at 24 h of the
727 acetate-depleting condition (Fig. 3D, E). Collectively, the results indicated that the
728 nitrogen limitation may have just started at 24 h of the acetate-depleting condition, thus
729 would not majorly impact cell physiology. Finally, our results from the 4-day constant-
730 acetate and no-acetate conditions under the turbidostatic control strongly pointed to the
731 specific effects of acetate on algal heat tolerance but not other nutrients (Fig. 5, 7). Thus,
732 the acetate effects are the focus of this paper.
733
734 Chlamydomonas uptakes acetate and feeds it into the glyoxylate cycle and
735 gluconeogenesis for starch biosynthesis and starch is broken down through glycolysis to
736 make cellular energy (Johnson and Alric, 2012, 2013) (Fig. 2A). The dynamic effects of

737 35°C on algal growth under different acetate conditions can be explained by the 35°C-
738 induced acetate metabolism, supported by increased acetate consumption and up-
739 regulated transcripts related to acetate metabolism pathway at 35°C (Fig. 1, 2). Energy
740 produced from glycolysis can be used for energy-requiring cellular activities to increase
741 thermotolerance (Olas *et al.*, 2021), e.g., repair pathways related to photosynthesis
742 (Murata and Nishiyama, 2018). Pyruvate kinase catalyzes the final step of glycolysis by
743 converting phosphoenolpyruvate and one ADP to pyruvate and one ATP (Baud *et al.*,
744 2007; Wulfert *et al.*, 2020). Chlamydomonas mutants deficient in pyruvate kinase were
745 heat-sensitive under 35°C in acetate-containing medium (Mattoon *et al.*, 2022*a*),
746 supporting the important roles of glycolysis in thermotolerance of 35°C. Although ATP is
747 primarily produced through mitochondrial oxidative respiration, the ATP production from
748 glycolysis can be important under stressful conditions where energy availability is limited
749 (van Dongen *et al.*, 2011). Under low oxygen conditions, plants increase activity of
750 pyruvate kinases to produce more ATP (van Dongen *et al.*, 2011). Heat-treated barley
751 leaves utilized glycolysis as an alternative energy source for thermotolerance based on
752 proteomics analysis (Rollins *et al.*, 2013).
753
754 Additionally, acetate may protect photosynthesis from heat-induced photoinhibition.
755 Acetate is proposed to protect PSII against photoinhibition by replacing the bicarbonate
756 associated to the non-heme iron at the acceptor side of PSII, changing the environment
757 of plastoquinone and affecting PSII charge recombination (Roach *et al.*, 2013). Our PSII
758 efficiency data supported this report because PSII efficiency was higher with acetate than
759 without acetate during 25°C, 35°C or 40°C treatments (Fig. 8D). Furthermore,
760 experimental and modeling analysis suggested that acetate promoted cyclic electron flow
761 (CEF) around photosystem I (PSI); reducing equivalents produced during the acetate
762 metabolism reduce plastoquinone pools and increase CEF activity (Johnson and Alric,
763 2012; Lucker and Kramer, 2013; Chapman *et al.*, 2015). CEF cycles photosynthetic
764 electrons around PSI, producing only ATP but no NADPH and providing extra ATP
765 needed for photosynthesis and other cellular activities (Munekage *et al.*, 2004; Baker *et*
766 *al.*, 2007). CEF balances the ATP/NADPH ratio, contributes to the generation of
767 transthylakoid proton motive force, and protects both PSI and PSII from photo-oxidative

768 damage (Johnson, 2011; Yamori and Shikanai, 2016). The increased acetate uptake
769 under 35°C (Fig. 1D) was coupled with induced CEF activity in Chlamydomonas under
770 the constant-acetate condition (Zhang *et al.*, 2022*a*). Our transcriptome analysis also
771 showed up-regulation of transcripts related to PSI and CEF at 2 h of 35°C treatments
772 under either the constant-acetate or acetate-depleting condition (little acetate depletion
773 at 2 h), consistent with heat-induced CEF in the presence of acetate (Supplemental Fig.
774 4J, P).
775
776 The effects of acetate on the improved heat tolerance under the moderate high
777 temperature may also be related to the accumulation of thermoprotective metabolites
778 (osmolytes, including amino acids, sugars, and sugar alcohols) (Guihur *et al.*, 2022) or
779 compatible solutes (Hemme *et al.*, 2014; Schroda *et al.*, 2015). Compatible solutes
780 accumulate from the catabolism of large molecules upon the onset of heat to stabilize
781 membranes and prevent protein unfolding and aggregation (Schroda *et al.*, 2015). In
782 Chlamydomonas, these compatible solutes include glycerophos-phoglycerol (GPG),
783 trehalose, alanine, isoleucine, asparagine, glutamine, and guanosine (Hemme *et al.*,
784 2014). The elevated acetate metabolism at 35°C with constant acetate supply may
785 increase the accumulation of these thermoprotective compatible solutes. This is an
786 understudied but exciting area. Future metabolite analysis may provide more information
787 about this.
788
789 With constant acetate supply, 35°C is beneficial, increasing carbon metabolism and
790 improving thermotolerance for enhanced growth (Fig. 5). If algal cells can be cultivated
791 under sterile conditions with constant organic carbon supply, 35°C could be used to
792 promote algal growth and increase biofuel and bioproduct generation under mixotrophic
793 conditions in light. Culture temperature of 35°C in closed, outdoor algal ponds may not
794 be difficult to reach with natural sunlight heating in the summertime of the moderate
795 climate regions and year-round in the tropical regions. If photoautotrophic medium is used
796 for enclosed outdoor algal cultivation, acetate could be added to improve algal
797 thermotolerance before the occurrence of moderate high temperature around 35°C. The
798 improved algal thermotolerance and growth may outweigh the cost of added acetate.

799

800 Without constant acetate supply, 35°C is detrimental. Under the acetate-depleting
801 condition, the 35°C-elevated carbon metabolism without sufficient carbon input may
802 deplete cellular carbon reserves. This was not sustainable in the long-term and eventually
803 reduced biomass accumulation (Fig. 1C). With constant acetate supply, heat at 35°C
804 transiently arrested the cell cycle, which recovered after 8 h at 35°C (Fig. 3G). In
805 photoautotrophic medium without acetate, 35°C reduced algal growth rates and resulted
806 in stressed cells aggregated to form palmelloids (Fig. 6, 7). Such effects of 35°C can
807 particularly compromise the yields of outdoor algal ponds because they usually do not
808 contain carbon sources but frequently experience moderate high temperatures (Mata *et*
809 *al.*, 2010; El-Sheekh *et al.*, 2019).
810

811 It is reported that the growth rate of another Chlamydomonas WT strain (CC-125) at 35°C
812 was about 50% of that at 28°C (0.083 vs 0.166) in photoautotrophic medium under
813 constant light and continuous dilution but with 2% CO_2 (Vítová *et al.*, 2011). The 50%
814 growth reduction is comparable to the reduced growth of our data at 35°C without acetate
815 (Fig. 7A). We used air level CO_2, which is 400 ppm or 0.04% CO_2 to mimic the nature
816 condition (1/50th of 2% CO_2 as in Vítová *et al.*, 2011). CO_2 provides the inorganic carbon
817 source for algal growth. However, the equivalent 50% growth reduction at 35°C as
818 compared to the control temperature with (Vítová *et al.*, 2011) and without (this study)
819 high CO_2 suggests CO_2 (inorganic carbon source) is not as effective as acetate (organic
820 carbon source) to improve thermotolerance in algal cells. Furthermore, different algal
821 strains with changes in cultivation conditions may have varying moderate high
822 temperature ranges. For example, another Chlamydomonas WT strain (CC-137) had
823 optimal growth at 35°C in photoautotrophic medium with 2% CO_2 in day/night cycle with
824 semi-dilution (one dilution per day at the end of dark phase) (Lien and Knutsen, 1979).
825 Such semi-dilution may result in a large range of cell densities, which may affect the light
826 perceived by each cell. Additionally, the day/night cycle may also alleviate photooxidative
827 stress as photosynthesis only occurs in light. However, the author mentioned that
828 cytokinesis and sporulation became inhibited at temperature above 36°C (Lien and
829 Knutsen, 1979), indicating 35°C may be close to the moderate high temperature range

830 that would reduce algal growth in this strain without acetate under their cultivation
831 condition. Additionally, the fast-growing marine alga *Picochlorum celery*, which is tolerant
832 to high salt, high light, and high temperature, had maximal growth rates around 35°C
833 which was reduced at temperatures around 40°C, with photoautotrophic medium and
834 unlimited CO_2 supply in outdoor open ponds under semi-continuous, drain and fill mode
835 of operation (cells were harvested and fresh medium was added every 2-3 days)
836 (Krishnan *et al.*, 2021), suggesting the moderate high temperature range is strain-specific
837 and depending on the cultivation condition.
838
839 Furthermore, some tissues in land plants are either mixotrophic or heterotrophic, such as
840 reproductive tissues (e.g., developing green seeds) (Koley *et al.*, 2022) or sink tissues
841 (e.g., roots). Reproductive tissues are often considered the most heat sensitive in land
842 plants (Barnabás *et al.*, 2008; Ullah *et al.*, 2022) and are the main harvest of grain crops
843 such as soybean, wheat, barley, sorghum, and maize. The up-regulated carbon
844 metabolism under moderate high temperatures may also occur in land plants, especially
845 in reproductive or sink tissues. Heat-induced glyoxylate cycle, gluconeogenesis, and
846 glycolysis have been reported in plants (Rollins *et al.*, 2013; Zhang *et al.*, 2013; Aprile *et*
847 *al.*, 2013). Carbon metabolism and sugar availability were shown to be essential for heat
848 tolerance in Arabidopsis (Olas *et al.*, 2021). The thermotolerant wheat cultivar had
849 increased carbohydrate molecules in sink tissues (Mishra *et al.*, 2021). It is also reported
850 that heat stress impaired sucrose metabolism in leaves and anthers, which were
851 associated with heat-induced reproductive failures in chickpea (Kaushal *et al.*, 2013). A
852 better understanding of the interaction between carbon availability and heat tolerance
853 could be leveraged to protect sink and/or reproductive tissues from heat stresses.
854
855 **Heat of 40°C was detrimental to algal cells with and without constant acetate supply**
856 Acute high temperatures at or above 40°C inhibit the algal cell cycle (Fig. 3, 5-7)
857 (Mühlhaus *et al.*, 2011*b*; Hemme *et al.*, 2014; Zachleder *et al.*, 2019; Ivanov *et al.*, 2021),
858 alter thylakoid membranes, reduce photosynthesis, and damage respiration (Zhang *et al.*,
859 2022*a*). These cellular damages took place quickly, mostly within 4 h of heat at 40°C with
860 constant acetate supply (Zhang *et al.*, 2022*a*). Although 40°C-treated cells grew bigger

861 and had more chlorophyll per cell under the constant-acetate condition than the acetate-
862 depleting condition in the short-term (24-h heat) (Fig. 3B, G, D, I, L, N), the constant
863 acetate supply could not prevent ultimate cell death with 40ºC-heat longer than 2 days
864 (Fig. 5). Without acetate, Chlamydomonas cells also died after 2-day heat at 40ºC (Fig
865 7). The death of Chlamydomonas cultures was also reported at 39ºC for 33 h in
866 photoautotrophic medium without acetate using the same WT strain *21gr* (Zachleder *et*
867 *al.*, 2019; Ivanov *et al.*, 2021). In conclusion, constant heating at 40ºC is lethal for
868 Chlamydomonas cells independent of acetate availability.
869
870 At 24-h of the acetate-depleting condition, algal cells exposed to 40ºC had very little
871 division (only 30% increase of cell density, thus 1.3 X) but they still grew and accumulated
872 biomass by increasing cell volume (3 X) as compared to the pre-heat condition (Fig. 3B).
873 In comparison, algal cells exposed to 25ºC at 24 h of the acetate-depleting condition had
874 5.5 X increased cell density but reduced cell volume (55% of the pre-heat values, due to
875 acetate starvation). If we use fold change of cell density multiplied by fold change of cell
876 volume to estimate biomass, it could explain the comparable amount of dry biomass in
877 cultures treated with 40ºC and 25ºC by the end of 24-h treatment under the acetate-
878 depleting condition (Fig. 1C). However, the inefficient system with reduced carbon input
879 and little cell division at 40ºC was not sustainable, eventually killing all the algal cells by
880 the end of 2-day heat of 40ºC, even with constant acetate supply (Fig. 5). Our results
881 suggested that the increased thermotolerance by acetate did not apply to long-term heat
882 at 40ºC.
883
884 Acetate had very limited effects on the tolerance to 40ºC in Chlamydomonas possibly
885 because 40ºC damaged mitochondrial activities, which are important for acetate
886 metabolism. Most of the reducing power from acetate assimilation is used in mitochondrial
887 respiration to produce ATP (Johnson and Alric, 2012, 2013). Our previous results showed
888 that 40ºC reduced mitochondrial activities significantly under the 24-h constant-acetate
889 condition (Zhang *et al.*, 2022*a*). When comparing 40ºC vs 25ºC under the acetate-
890 depleting condition and 40ºC vs 35ºC independent of the acetate condition, the top
891 enriched function group was related to mitochondrial electron transport (Supplemental

892 Fig. 5B, E), suggesting mitochondria were particularly sensitive to 40ºC. This was also
893 supported by the down-regulation of transcripts related to mitochondrial electron
894 transport, especially those related to F1-ATPase at 2 h of 40ºC (Supplemental Fig. 4AA,
895 AB, Supplemental Dataset 2). The compromised mitochondrial activities may restrict
896 acetate uptake and assimilation during 40ºC heat treatment. Although there were no
897 significant differences in acetate consumption between 40ºC and 25ºC under the 24-h
898 acetate-depleting conditions (Fig. 1D), the differences may be underestimated and
899 masked by the acetate depletion. Transcripts of many genes involved in carbon
900 metabolism, e.g., acetate uptake and assimilation, glyoxylate cycle and gluconeogenesis
901 pathways, and glycolysis were significantly down-regulated during 40ºC under either the
902 acetate-depleting or constant-acetate condition, especially at 2 h heat (Fig. 2), consistent
903 with the down-regulated transcripts related to mitochondrial electron transport. Heat at
904 40ºC for longer than 1 day would eventually slow down mitochondrial activities and reduce
905 acetate-uptake. The decreased acetate uptake and assimilation, in addition to reduced
906 photosynthesis and arrested cell cycle, may result in the ultimate death of the algal culture
907 with 2-day heat at 40ºC (Fig. 3, 5-8).
908
909 Under the acetate-depleting condition, without frequent medium dilution, cell densities
910 increased at 25ºC and 35ºC during the 24-h experiments (Fig. 3A). With the constant light
911 source, the increased cell densities resulted in light shading. However, the amount of
912 chlorophyll per mL culture was comparable at 24 h of 25ºC, 35ºC, and 40ºC under the
913 acetate-depleting condition, suggesting comparable level of light shading under all three
914 temperatures (Fig. 3C). Thus, we could cross off the effects of light shading when
915 comparing the results at the 24 h of 25ºC, 35ºC, and 40ºC under the acetate-depleting
916 condition. Additionally, the up-regulated transcripts related to photoprotection at 24 h of
917 all three temperatures under the acetate-depleting condition when light shading was
918 present indicated compromised or inefficient photosynthesis that was not due to high light
919 stress (Supplemental Fig. 4O). The up-regulation of transcripts related to photoprotection
920 at 24 h of 25ºC and 35ºC was only present under the acetate-depleting condition but not
921 the constant-acetate condition, which may be due to reduced CO_2 concentrations with
922 increased cell density without frequent culture dilution, supported by a recent report that

923 low CO_2 induced photoprotection independent of light (Ruiz-Sola *et al.*, 2023). The up-
924 regulation of transcripts related to photoprotection at 24 h of 40°C was similar under either
925 acetate condition, just with higher induction under the acetate-depleting than the
926 constant-acetate condition, suggesting it was mainly caused by damaged photosynthesis
927 at 40°C.
928
929 At 24-h of the acetate-depleting condition, the transcripts related to large *HSP*s,
930 *HSP60/70/90s*, were down-regulated at 25°C and 35°C, but not under 40°C
931 (Supplemental Fig. 4A-C). The down-regulation of large *HSP*s may be related to the
932 increased cell density and light shading, thus reduced light stress at 24 h of 25°C and
933 35°C under the acetate-depleting condition (Fig. 3A). Besides heat stress, transcripts of
934 large *HSPs* also responded to light and were also up-regulated under high light stresses
935 (Anderson et al. 2021). Additionally, the down regulation of large *HSP*s at 25°C and 35°C
936 but not 40°C at 24 h of the acetate-depleting condition may suggest the energy distribution
937 between growth and heat tolerance. Most large HSPs are ATP-dependent chaperones,
938 especially HSP90s (Al-Whaibi, 2011; Xu *et al.*, 2012; Guihur *et al.*, 2022). Down-
939 regulation of these large HSPs when acetate was depleted may be helpful to reserve
940 energy for cell growth when the temperature stress was none (25°C) or moderate (35°C).
941 However, under the acute heat of 40°C, thermotolerance has higher priority than growth,
942 thus the expression of these large *HSPs* were maintained while cell cycle was arrested
943 to preserve energy (Supplemental Fig. 4A-C,W, X).
944
945 As compared to 40°C, the induction of *HSP*s at 35°C was minimal or none under either
946 acetate condition (Supplemental Fig. 4A-C), suggesting the 35°C-induced
947 thermotolerance by acetate may not be related to the accumulation of HSPs. This may
948 suggest some none-overlapping heat sensing and signaling pathways between 35°C and
949 40°C, because HSPs have important roles in the classical heat shock responses (Guihur
950 *et al.*, 2022). Several heat sensors have been proposed (Vu *et al.*, 2019), including
951 membrane fluidity (Martinière *et al.*, 2011), Ca^{2+} channels in the plasma membrane (Gao
952 *et al.*, 2012; Finka *et al.*, 2012), unfolded proteins (Rütgers *et al.*, 2017; Li *et al.*, 2020),
953 and phytochromes (Jung *et al.*, 2016; Legris *et al.*, 2016), and some circadian clock

954 components (e.g. EARLY FLOWERING 3, ELF3) (Jung *et al.*, 2020). Among these, the
955 heat effects on phytochromes and ELF3 have been reported around the temperature
956 ranges of 30°C-35°C (Jung *et al.*, 2016, 2020; Legris *et al.*, 2016), providing potential heat
957 sensor candidates for moderate high temperatures. Future research to investigate the
958 shared and unique heat sensors under moderate and acuate high temperatures may
959 provide more information about how plants sense and adapt to different high
960 temperatures.
961
962 High temperatures affect Chlamydomonas lipid metabolism (Schroda *et al.*, 2015). To
963 overcome heat-induced membrane fluidity and leakiness, Chlamydomonas reduced
964 unsaturated membrane lipids and increased the production of saturated lipids to restore
965 normal membrane viscosity (Schroda *et al.*, 2015; Légeret *et al.*, 2016). Saturated fatty
966 acids are more stable than unsaturated fatty acids under high temperatures. It was
967 proposed that the diacylglycerols (DAGs) acyltransferase, DGTT1, converted the
968 chloroplast unsaturated membrane lipids monogalactosyldiacylglycerols (MGDG) to
969 DAGs then triacylglycerols (TAGs) in Chlamydomonas with 1 h heat at 42°C (Légeret *et*
970 *al.*, 2016). Our RNA-seq data showed that the transcripts of *DGTT1* were quickly and
971 largely up-regulated at 40°C independent of acetate availability (Supplemental Figure
972 3H), consistent with a strategy to reduce unsaturated membrane lipids during high
973 temperatures. The transcripts of *DGTT1* were also up-regulated at 35°C, but with a
974 smaller induction than at 40°C. Additionally, a long chain fatty acid CoA ligase, LCS2,
975 involves in de novo synthesis of saturated fatty acids by incorporating newly synthesized
976 fatty acids exported from the plastid into saturated TAGs in lipid droplets (Li *et al.*, 2016;
977 Li-Beisson *et al.*, 2023). Our RNA-seq data showed that the transcripts of *LCS2* were
978 quickly and significantly up-regulated at 40°C independent of acetate availability
979 (Supplemental Figure 3I), suggesting increased de novo synthesis of saturated fatty acids
980 at 40°C. The de novo fatty acids biosynthesis is the only option for increasing the fraction
981 of lipids with saturated fatty acids (Hemme *et al.*, 2014). Heat at 40°C reduced
982 photosynthetic activities within 4 h, which increased chloroplast redox pressure and
983 oxidative stress under high temperatures (Zhang *et al.*, 2022*a*). Biosynthesis of lipids with
984 saturated fatty acids via the de novo pathway requires reducing power NADPH and

985 energy ATP (Ohlrogge and Browse, 1995), which may serve as an electron sink and
986 alleviate heat-induced redox stresses (Hemme *et al.*, 2014). The transcripts of *LCS2* were
987 also up-regulated at 24 h of 25°C and 35°C under the acetate-depleting condition
988 (Supplemental Figure 3I), which may be related to the protective role of the de novo lipid
989 biosynthesis pathway as an electron sink when acetate was depleted and photosynthesis
990 was inefficient, consistent with the induced transcripts involved in photoprotection under
991 the same conditions (Supplemental Figure 4O). Furthermore, our MapMan ontology
992 enrichment analysis showed that the functional group of lipid metabolism and lipid
993 degradation was significantly enriched in differentially regulated transcripts between 25°C
994 and 35°C under the acetate-depleting conditions but not under the constant-acetate
995 condition, suggesting acetate depletion may make the moderate high temperature more
996 stressful (Supplemental Figure 5A, C). Our work provides rich datasets for researchers
997 with interest and expertise in lipid metabolism to further investigate how changes of lipids
998 affect algal heat responses.
999
1000 Most previous heat treatments in Chlamydomonas used cultures grown with acetate-
1001 containing medium in flasks without turbidostatic control (Hemme *et al.*, 2014; Rütgers *et*
1002 *al.*, 2017). Our results showed that such heat treatment could not last more than 8 h at
1003 35°C or 24 h of 40°C due to acetate-depletion (Fig. 1D). In fact, many previous heat
1004 experiments were conducted for a short-term, e.g., 1 h (Légeret *et al.*, 2016; Rütgers *et*
1005 *al.*, 2017). Using our highly controlled PBR systems, we could not only conduct heat
1006 experiments under the 24-h acetate-depleting condition but also during 4-day heating with
1007 and without acetate under the turbidostatic control with constant nutrient supply to
1008 uniquely reveal the effects of carbon availability, heat duration and intensity on algal heat
1009 responses. Additionally, we used constant light in our experimental conditions to focus
1010 specifically on the effects of high temperatures. In nature, high temperatures are
1011 accompanied by day and night cycles. The interaction among high temperatures, carbon
1012 status, and diurnal cycles will be an exciting area in future research.
1013
1014 In summary, by using the model green alga Chlamydomonas and highly controlled
1015 cultivation systems in PBRs, we revealed how the availability of an organic carbon source,

1016 acetate, interacted with different intensities and durations of high temperatures in
1017 photosynthetic cells. Our research revealed the overlooked effects of moderate high
1018 temperature of 35°C, which was beneficial with constant carbon supply or detrimental with
1019 insufficient or no carbon supply. We also showed that the damaging effects of acute high
1020 temperature of 40°C was dominant and independent of carbon availability. Our research
1021 not only helped us understand heat responses in photosynthetic cells but also provided
1022 insights for high temperature effects on the production of algal biofuels and bioproducts.
1023 Our results will also be useful to study how carbon availability affects heat responses in
1024 mixotrophic and heterotrophic (reproductive or sink) tissues in land plants.
1025
1026 **Supplementary data**
1027 **Supplemental Table 1**: Gene IDs and primers for RT-qPCR analysis in Fig. 2 and
1028 Supplemental Fig. 2 and 3.
1029
1030 **Supplemental Dataset 1**. RNA-seq data and plots of each transcript detected, including
1031 mean normalized read count plots, mean normalized read count heat map, log_2(fold
1032 change) of mean normalized read counts relative to the pre-heat time point under the
1033 same condition, and statistical analysis using False Discovery Rate (FDR).
1034
1035 **Supplemental Dataset 2**. Log_2(fold change, FC) of mean normalized read counts of
1036 groups of transcripts based on MapMan function annotation (MapMan folder) or manual
1037 curation (Manual_curation folder). Manual curation was based on the gene lists from this
1038 paper Zhang *et al.*, 2022*a*). Each line in the plots represent one unique transcript in that
1039 function category under one of six conditions. RNA-seq data with normalized read counts
1040 were used for this analysis. Log_2FC is relative to the pre-heat time point under the same
1041 condition. Black vertical lines indicated the start of heat treatments under 35°C or 40°C
1042 or the equivalent time point at 25°C. ANOVA test was applied to the time course (five time
1043 points) of one transcript for each condition. If a transcript differed significantly during the
1044 time course (or underwent a global significant change) of one condition, it is colored
1045 purple (ANOVA significant); blue lines had no significant changes during the time course.
1046 Different intensities of purple and blue colors were used to distinguish different transcripts.

1047 Each file opens as a web page. Please use the interactive feature of the figures to see
1048 the gene IDs for each panel.
1049
1050 **Supplemental Dataset 3**. MapMan ontology enrichment. Ontology enrichment was
1051 performed for transcripts with significantly differential expression in the indicated
1052 comparisons using the extended MapMan ontology. The p values were calculated using
1053 a hypergeometric test and corrected for multiple testing using the Benjamini-Hochberg
1054 method.
1055
1056 **Supplemental Dataset 4**. Normalized RNA-seq read counts.
1057
1058 **Supplemental Dataset 5**. RNA-seq data summary, including gene IDs, MapMan function
1059 groups, annotation, adjusted False Discovery Rate (FDR) values for comparisons of
1060 different conditions, mean and standard deviation (sd) of normalized read counts.
1061
1062 **Supplemental Dataset 6**. ChlamyCyc Pathway enrichment analysis of differentially
1063 regulated transcripts compared between two conditions. The ChlamyCyc annotations
1064 (v2023-01-04) and pathway ontology combine KEGG, MapMan, and JGI pathway
1065 information (May *et al.*, 2009). The p values were calculated using a hypergeometric test
1066 (BioFSharp.Stats) and corrected for multiple testing using the Benjamini-Hochberg
1067 method (FSharp.Stats).
1068
1069 **Supplemental Figures 1-6** (see figure file)
1070
1071 **Acknowledgements**
1072 We would like to thank Dr. Michael Schroda for discussing the initial experimental idea
1073 under the acetate-depleting conditions, Dr. Trent Northen for recommending the acetate
1074 quantification assay, and Dr. Jaruswan Warakanont for discussion about
1075 Chlamydomonas lipid metabolism. We also want to thank the team of the Department of
1076 Energy (DOE) Joint Genome Institute (JGI) Community Science Program (Anna Lipzen,

Christa Pennacchio, Kerrie Barry, Dr. Jeremy Schmutz, and others) for managing and sequencing our RNA samples.

Author contributions

RZ designed the experiments. CB and MX operated and maintained the algal growth in photobioreactors. NZ, CB, and MX harvested algal samples at different time points and quantified biomass. NZ and MX performed acetate quantification assay. NZ performed RT-qPCR analysis and extracted RNA for RNA-seq. CB and NZ performed light microscope imaging. CB, MX, and NZ quantified cell density, cell size, and chlorophyll contents, and recorded OD_{608}/OD_{720} readings. CB and MX performed 4-day heating experiments and quantified growth rates as well as cell parameters. CB analyzed PSII data. BV, TM, RZ did RNA-seq analysis. EMM did initial analysis of the acetate pathways. NZ, BV, CB, RZ, MX, and EMM prepared the figures. BV wrote the RNA-seq method and related figure legends. RZ wrote the rest of the manuscript. RZ, EMM, BV, and CB revised the manuscript.

Conflict of interest

No conflict of interest declared.

Funding statement

This work was supported by the start-up funding from the Donald Danforth Plant Science Center (DDPSC) and the DOE Biological & Environmental Research (BER) grant (DE-SC0020400) to RZ. EMM was supported by the William H. Danforth Fellowship in Plant Sciences and the DDPSC start-up funding (to RZ). BV and TM were supported by the Germany funding TRR 175 D02 (Project No: 270050988). The RNA-seq service support was from the Department of Energy (DOE) Joint Genome Institute (JGI) Community Science Program (CSP, 503414) to RZ. The NovaSeq for RNA-seq (proposal: 10.46936/10.25585/60001126) was conducted by the U.S. Department of Energy Joint Genome Institute (https://ror.org/04xm1d337), a DOE Office of Science User Facility, is supported by the Office of Science of the U.S. Department of Energy operated under Contract No. DE-AC02-05CH11231.

1108

1109 **Data availability**

1110 All data supporting the findings of this study are available within the paper and within its
1111 supplementary materials published online. Raw RNA-seq data was deposited to
1112 Sequence Read Archive (SRA) following the Data Policy of the Joint Genome Institute
1113 (JGI) with Sequencing Project ID: 1377265.

1114

References

Altschuler M, Mascarenhas JP. 1982. Heat shock proteins and effects of heat shock in plants. Plant molecular biology **1**, 103–115.

Al-Whaibi MH. 2011. Plant heat-shock proteins: A mini review. Journal of King Saud University - Science **23**, 139–150.

Anderson CM, Mattoon EM, Zhang N, *et al.* 2021. High light and temperature reduce photosynthetic efficiency through different mechanisms in the C4 model Setaria viridis. Communications Biology **4**, 1092.

Aprile A, Havlickova L, Panna R, *et al.* 2013. Different stress responsive strategies to drought and heat in two durum wheat cultivars with contrasting water use efficiency. BMC genomics **14**, 821.

Bajhaiya AK, Dean AP, Zeef LAH, Webster RE, Pittman JK. 2016. PSR1 Is a Global Transcriptional Regulator of Phosphorus Deficiency Responses and Carbon Storage Metabolism in Chlamydomonas reinhardtii. Plant physiology **170**, 1216–1234.

Baker NR, Harbinson J, Kramer DM. 2007. Determining the limitations and regulation of photosynthetic energy transduction in leaves. Plant, cell & environment **30**, 1107–1125.

Balfagón D, Sengupta S, Gómez-Cadenas A, Fritschi FB, Azad RK, Mittler R, Zandalinas SI. 2019. Jasmonic acid Is required for plant acclimation to a combination of high light and heat stress. Plant physiology **181**, 1668–1682.

Barnabás B, Jäger K, Fehér A. 2008. The effect of drought and heat stress on reproductive processes in cereals. Plant, cell & environment **31**, 11–38.

Baud S, Wuillème S, Dubreucq B, de Almeida A, Vuagnat C, Lepiniec L, Miquel M, Rochat C. 2007. Function of plastidial pyruvate kinases in seeds of Arabidopsis thaliana. The Plant journal: for cell and molecular biology **52**, 405–419.

BBDuk. 2022. BBMap short read aligner, and other bioinformatic tools.

Benjamini Y, Hochberg Y. 1995. Controlling the false discovery rate: a practical and powerful approach to multiple testing. Journal of the Royal Statistical Society. Series B, Statistical methodology **57**, 289–300.

Bigeard J, Hirt H. 2018. Nuclear Signaling of Plant MAPKs. Frontiers in plant science **9**, 469.

Bourgine B, Guihur A. 2021. Heat Shock Signaling in Land Plants: From Plasma Membrane Sensing to the Transcription of Small Heat Shock Proteins. Frontiers in plant science **12**, 710801.

Boyle NR, Page MD, Liu B, *et al.* 2012. Three acyltransferases and nitrogen-responsive regulator are implicated in nitrogen starvation-induced triacylglycerol accumulation in Chlamydomonas. The Journal of biological chemistry **287**, 15811–15825.

de Carpentier F, Maes A, Marchand CH, Chung C, Durand C, Crozet P, Lemaire SD, Danon A. 2022. How abiotic stress-induced socialization leads to the formation of massive aggregates in Chlamydomonas. Plant physiology **190**, 1927–1940.

Chapman S, Paget C, Johnson G, Schwartz J-M. 2015. Flux balance analysis reveals acetate metabolism modulates cyclic electron flow and alternative glycolytic pathways in Chlamydomonas reinhardtii. Frontiers in plant science **6**.

Chew SY, Chee WJY, Than LTL. 2019. The glyoxylate cycle and alternative carbon metabolism as metabolic adaptation strategies of Candida glabrata: perspectives from Candida albicans and Saccharomyces cerevisiae. Journal of Biomedical Science **26**.

Chioccioli M, Hankamer B, Ross IL. 2014. Flow Cytometry Pulse Width Data Enables Rapid and Sensitive Estimation of Biomass Dry Weight in the Microalgae Chlamydomonas reinhardtii and Chlorella vulgaris. PLoS ONE **9**, e97269.

Crozet P, Navarro FJ, Willmund F, *et al.* 2018. Birth of a photosynthetic chassis: A MoClo toolkit enabling synthetic biology in the microalga *Chlamydomonas reinhardtii*. ACS synthetic biology **7**, 2074–2086.

Delorge I, Janiak M, Carpentier S, Van Dijck P. 2014. Fine tuning of trehalose biosynthesis and hydrolysis as novel tools for the generation of abiotic stress tolerant plants. Frontiers in plant science **5**.

Dhokane D, Bhadra B, Dasgupta S. 2020. CRISPR based targeted genome editing of *Chlamydomonas reinhardtii* using programmed Cas9-gRNA ribonucleoprotein. Molecular biology reports **47**, 8747–8755.

Dodds WS, Stutzman LF, Sollami BJ. 1956. Carbon Dioxide Solubility in Water. Industrial & Engineering Chemistry Chemical & Engineering Data Series **1**, 92–95.

van Dongen JT, Gupta KJ, Ramírez-Aguilar SJ, Araújo WL, Nunes-Nesi A, Fernie AR. 2011. Regulation of respiration in plants: a role for alternative metabolic pathways. Journal of plant physiology **168**, 1434–1443.

Dunn SR, Thomason JC, Le Tissier MDA, Bythell JC. 2004. Heat stress induces different forms of cell death in sea anemones and their endosymbiotic algae depending on temperature and duration. Cell death and differentiation **11**, 1213–1222.

El-Sheekh MM, Gheda SF, El-Sayed AE-KB, Abo Shady AM, El-Sheikh ME, Schagerl M. 2019. Outdoor cultivation of the green microalga Chlorella vulgaris under stress conditions as a feedstock for biofuel. Environmental science and pollution research international **26**, 18520–18532.

Emrich-Mills TZ, Yates G, Barrett J, *et al.* 2021. A recombineering pipeline to clone large and complex genes in Chlamydomonas. The Plant Cell **33**, 1161–1181.

Fei X, Yu J, Li Y, Deng X. 2017. CrMAPK3 regulates the expression of iron-deficiency-responsive genes in Chlamydomonas reinhardtii. BMC biochemistry **18**, 6.

Finka A, Cuendet AFH, Maathuis FJM, Saidi Y, Goloubinoff P. 2012. Plasma membrane cyclic nucleotide gated calcium channels control land plant thermal sensing and acquired thermotolerance. The Plant cell **24**, 3333–3348.

Gao F, Han X, Wu J, Zheng S, Shang Z, Sun D, Zhou R, Li B. 2012. A heat-activated calcium-permeable channel - Arabidopsis cyclic nucleotide-gated ion channel 6 - is involved in heat shock responses. The Plant Journal **70**, 1056–1069.

González-Ballester D, Casero D, Cokus S, Pellegrini M, Merchant SS, Grossman AR. 2010. RNA-seq analysis of sulfur-deprived Chlamydomonas cells reveals aspects of acclimation critical for cell survival. The Plant cell **22**, 2058–2084.

Greiner A, Kelterborn S, Evers H, Kreimer G, Sizova I, Hegemann P. 2017. Targeting of photoreceptor genes in *Chlamydomonas reinhardtii* via zinc-finger nucleases and CRISPR/Cas9. The Plant cell **29**, 2498–2518.

Guihur A, Rebeaud ME, Goloubinoff P. 2022. How do plants feel the heat and survive? Trends in biochemical sciences **47**, 824–838.

Haq S, Khan A, Ali M, Khattak AM, Gai W-X, Zhang H-X, Wei A-M, Gong Z-H. 2019. Heat Shock Proteins: Dynamic Biomolecules to Counter Plant Biotic and Abiotic Stresses. International journal of molecular sciences **20**, 5321.

Hellemans J, Mortier G, De Paepe A, Speleman F, Vandesompele J. 2007. QBase relative quantification framework and software for management and automated analysis of real-time quantitative PCR data. Genome biology **8**, R19.

Hemme D, Veyel D, Mühlhaus T, *et al.* 2014. Systems-wide analysis of acclimation responses to long-term heat stress and recovery in the photosynthetic model organism *Chlamydomonas reinhardtii*. The Plant cell **26**, 4270–4297.

Hennacy JH, Jonikas MC. 2020. Prospects for engineering biophysical CO2 concentrating mechanisms into land Plants to enhance yields. Annual review of plant biology **71**, 461–485.

Ivanov IN, Zachleder V, Vítová M, Barbosa MJ, Bišová K. 2021. Starch production in *Chlamydomonas reinhardtii* through supraoptimal temperature in a pilot-scale photobioreactor. Cells **10**, 1084.

Jagodzik P, Tajdel-Zielinska M, Ciesla A, Marczak M, Ludwikow A. 2018. Mitogen-Activated Protein Kinase Cascades in Plant Hormone Signaling. Frontiers in plant science **9**, 1387.

Janni M, Gullì M, Maestri E, Marmiroli M, Valliyodan B, Nguyen HT, Marmiroli N. 2020. Molecular and genetic bases of heat stress responses in crop plants and breeding for increased resilience and productivity. Journal of experimental botany **71**, 3780–3802.

Jee H. 2016. Size dependent classification of heat shock proteins: a mini-review. Journal of exercise rehabilitation **12**, 255–259.

Ji S, Siegel A, Shan S-O, Grimm B, Wang P. 2021. Chloroplast SRP43 autonomously protects chlorophyll biosynthesis proteins against heat shock. Nature plants **7**, 1420–1432.

Johnson GN. 2011. Physiology of PSI cyclic electron transport in higher plants. Biochimica et Biophysica Acta (BBA) - Bioenergetics **1807**, 384–389.

Johnson X, Alric J. 2012. Interaction between starch breakdown, acetate assimilation, and photosynthetic cyclic electron flow in *Chlamydomonas reinhardtii*. The Journal of biological chemistry **287**, 26445–26452.

Johnson X, Alric J. 2013. Central carbon metabolism and electron transport in *Chlamydomonas reinhardtii*: metabolic constraints for carbon partitioning between oil and starch. Eukaryotic cell **12**, 776–793.

Jung J-H, Barbosa AD, Hutin S, *et al.* 2020. A prion-like domain in ELF3 functions as a thermosensor in Arabidopsis. Nature **585**, 256–260.

Jung J-H, Domijan M, Klose C, *et al.* 2016. Phytochromes function as thermosensors in Arabidopsis. Science **354**, 886–889.

Karpowicz SJ, Prochnik SE, Grossman AR, Merchant SS. 2011. The GreenCut2 resource, a phylogenomically derived inventory of proteins specific to the plant lineage. The Journal of biological chemistry **286**, 21427–21439.

Kaushal N, Awasthi R, Gupta K, Gaur P, Siddique KHM, Nayyar H. 2013. Heat-stress-induced reproductive failures in chickpea (Cicer arietinum) are associated with impaired sucrose metabolism in leaves and anthers. Functional plant biology: FPB **40**, 1334–1349.

Kim S-C, Guo L, Wang X. 2020. Nuclear moonlighting of cytosolic glyceraldehyde-3-phosphate dehydrogenase regulates Arabidopsis response to heat stress. Nature communications **11**, 3439.

Kim D, Langmead B, Salzberg SL. 2015. HISAT: a fast spliced aligner with low memory requirements. Nature methods **12**, 357–360.

Koley S, Chu KL, Mukherjee T, Morley SA, Klebanovych A, Czymmek KJ, Allen DK. 2022. Metabolic synergy in Camelina reproductive tissues for seed development. Science advances **8**, eabo7683.

Krishnan A, Likhogrud M, Cano M, Edmundson S, Melanson JB, Huesemann M, McGowen J, Weissman JC, Posewitz MC. 2021. Picochlorum celeri as a model system for robust outdoor algal growth in seawater. Scientific reports **11**, 11649.

Kropat J, Hong-Hermesdorf A, Casero D, Ent P, Castruita M, Pellegrini M, Merchant SS, Malasarn D. 2011. A revised mineral nutrient supplement increases biomass and growth rate in Chlamydomonas reinhardtii. The Plant journal: for cell and molecular biology **66**, 770–780.

Légeret B, Schulz-Raffelt M, Nguyen HM, Auroy P, Beisson F, Peltier G, Blanc G, Li-Beisson Y. 2016. Lipidomic and transcriptomic analyses of *Chlamydomonas reinhardtii* under heat stress unveil a direct route for the conversion of membrane lipids into storage lipids. Plant, cell & environment **39**, 834–847.

Legris M, Klose C, Burgie ES, Rojas CCR, Neme M, Hiltbrunner A, Wigge PA, Schäfer E, Vierstra RD, Casal JJ. 2016. Phytochrome B integrates light and temperature signals in Arabidopsis. Science **354**, 897–900.

Li X, Fauser F, Jinkerson RE, *et al.* 2019. A genome-wide algal mutant library and functional screen identifies genes required for eukaryotic photosynthesis. Nature genetics **51**, 627–635.

Li Z, Tang J, Srivastava R, Bassham DC, Howell SH. 2020. The transcription factor bZIP60 links the unfolded protein response to the heat stress response in maize. The Plant cell **32**, 3559–3575.

Li X, Zhang R, Patena W, *et al.* 2016. An indexed, mapped mutant library enables reverse genetics studies of biological processes in *Chlamydomonas reinhardtii*. The Plant cell **28**, 367–387.

Liao Y, Smyth GK, Shi W. 2014. featureCounts: an efficient general purpose program for assigning sequence reads to genomic features. Bioinformatics **30**, 923–930.

Li-Beisson Y, Warakanont J, Riekhof W, Benning C. 2023. Chapter 2 - Chlamydomonas glycerolipid metabolism. In: Grossman AR,, In: Wollman F-A, eds. The Chlamydomonas Sourcebook (Third Edition). London: Academic Press, 51–97.

Lien T, Knutsen G. 1979. Synchronous growth of *Chlamydomonas reinhardtii*(chlorophyceae): a review of optimal conditions. Journal of phycology **15**, 191–200.

Livak KJ, Schmittgen TD. 2001. Analysis of relative gene expression data using real-time quantitative PCR and the 2(-Delta Delta C(T)) Method. Methods **25**, 402–408.

Love MI, Huber W, Anders S. 2014. Moderated estimation of fold change and dispersion for RNA-seq data with DESeq2. Genome biology **15**, 550.

Lucker B, Kramer DM. 2013. Regulation of cyclic electron flow in *Chlamydomonas reinhardtii* under fluctuating carbon availability. Photosynthesis research **117**, 449–459.

Martinière A, Shvedunova M, Thomson AJW, Evans NH, Penfield S, Runions J, McWatters HG. 2011. Homeostasis of plasma membrane viscosity in fluctuating temperatures. The New phytologist **192**, 328–337.

Mata TM, Martins AA, Caetano NS. 2010. Microalgae for biodiesel production and other applications: A review. Renewable and Sustainable Energy Reviews **14**, 217–232.

Mathimani T, Pugazhendhi A. 2019. Utilization of algae for biofuel, bio-products and bio-remediation. Biocatalysis and agricultural biotechnology **17**, 326–330.

Mattoon EM, McHargue W, Bailey CE, *et al.* 2022*a*. High-throughput Identification of Novel Heat Tolerance Genes via Genome-wide Pooled Mutant Screens in the Model Green Alga Chlamydomonas reinhardtii. bioRxiv, 2022.07.13.499508.

Mattoon EM, McHargue W, Bailey CE, *et al.* 2022*b*. High-throughput identification of novel heat tolerance genes via genome-wide pooled mutant screens in the model green alga Chlamydomonas reinhardtii. Plant, cell & environment.

May P, Christian J-O, Kempa S, Walther D. 2009. ChlamyCyc: an integrative systems biology database and web-portal for Chlamydomonas reinhardtii. BMC genomics **10**, 209.

Merchant SS, Prochnik SE, Vallon O, *et al.* 2007. The *Chlamydomonas* genome reveals the evolution of key animal and plant functions. Science **318**, 245–250.

Meyer MT, Whittaker C, Griffiths H. 2017. The algal pyrenoid: key unanswered questions. Journal of experimental botany **68**, 3739–3749.

Minagawa J, Tokutsu R. 2015. Dynamic regulation of photosynthesis in *Chlamydomonas reinhardtii*. The Plant journal: for cell and molecular biology **82**, 413–428.

Mishra D, Shekhar S, Chakraborty S, Chakraborty N. 2021. High temperature stress responses and wheat: Impacts and alleviation strategies. Environmental and experimental botany **190**, 104589.

Mittler R, Finka A, Goloubinoff P. 2012. How do plants feel the heat? Trends in biochemical sciences **37**, 118–125.

Mühlhaus T, Weiss J, Hemme D, Sommer F, Schroda M. 2011*a*. Quantitative Shotgun Proteomics Using a Uniform 15N-Labeled Standard to Monitor Proteome Dynamics in Time Course Experiments Reveals New Insights into the Heat Stress Response of Chlamydomonas reinhardtii. Molecular & Cellular Proteomics **10**, M110.004739.

Mühlhaus T, Weiss J, Hemme D, Sommer F, Schroda M. 2011*b*. Quantitative shotgun proteomics using a uniform ^{15}N-labeled standard to monitor proteome dynamics in time course experiments reveals new insights into the heat stress response of *Chlamydomonas reinhardtii*. Molecular & cellular proteomics: MCP **10**, M110.004739.

Munekage Y, Hashimoto M, Miyake C, Tomizawa K-I, Endo T, Tasaka M, Shikanai T. 2004. Cyclic electron flow around photosystem I is essential for photosynthesis. Nature **429**, 579–582.

Murata N, Nishiyama Y. 2018. ATP is a driving force in the repair of photosystem II during photoinhibition. Plant, cell & environment **41**, 285–299.

Niemeyer J, Scheuring D, Oestreicher J, Morgan B, Schroda M. 2021. Real-time monitoring of subcellular H2O2 distribution in *Chlamydomonas reinhardtii*. The Plant cell.

Ohlrogge J, Browse J. 1995. Lipid biosynthesis. The Plant cell **7**, 957–970.

Olas JJ, Apelt F, Annunziata MG, John S, Richard SI, Gupta S, Kragler F, Balazadeh S, Mueller-Roeber B. 2021. Primary carbohydrate metabolism genes participate in heat-stress memory at the shoot apical meristem of Arabidopsis thaliana. Molecular plant **14**, 1508–1524.

Ortiz-Bobea A, Wang H, Carrillo CM, Ault TR. 2019. Unpacking the climatic drivers of US agricultural yields. Environmental research letters: ERL [Web site] **14**, 064003.

Pospíšil P. 2016. Production of reactive oxygen species by photosystem II as a response to light and temperature stress. Frontiers in plant science **7**, 1950.

Pröschold T, Harris EH, Coleman AW. 2005. Portrait of a species: *Chlamydomonas reinhardtii*. Genetics **170**, 1601–1610.

Rädecker N, Pogoreutz C, Gegner HM, *et al.* 2021. Heat stress destabilizes symbiotic nutrient cycling in corals. Proceedings of the National Academy of Sciences of the United States of America **118**.

Remans T, Keunen E, Bex GJ, Smeets K, Vangronsveld J, Cuypers A. 2014. Reliable gene expression analysis by reverse transcription-quantitative PCR: reporting and minimizing the uncertainty in data accuracy. The Plant cell **26**, 3829–3837.

Roach T, Sedoud A, Krieger-Liszkay A. 2013. Acetate in mixotrophic growth medium affects photosystem II in Chlamydomonas reinhardtii and protects against photoinhibition. Biochimica et Biophysica Acta (BBA) - Bioenergetics **1827**, 1183–1190.

Rollins JA, Habte E, Templer SE, Colby T, Schmidt J, von Korff M. 2013. Leaf proteome alterations in the context of physiological and morphological responses to drought and heat stress in barley (Hordeum vulgare L.). Journal of experimental botany **64**, 3201–3212.

Ruiz-Sola MÁ, Flori S, Yuan Y, *et al.* 2023. Light-independent regulation of algal photoprotection by CO2 availability. Nature communications **14**, 1–12.

Rütgers M, Muranaka LS, Schulz-Raffelt M, Thoms S, Schurig J, Willmund F, Schroda M. 2017. Not changes in membrane fluidity but proteotoxic stress triggers heat shock protein expression in *Chlamydomonas reinhardtii*. Plant, cell & environment **40**, 2987–3001.

Sager R. 1955. Inheritance in the green alga *Chlamydomonas reinhardtii*. Genetics **40**, 476–489.

Sasso S, Stibor H, Mittag M, Grossman AR. 2018. From molecular manipulation of domesticated Chlamydomonas reinhardtii to survival in nature. eLife **7**, e39233.

Schloss JA. 1990. A *Chlamydomonas* gene encodes a G protein β subunit-like polypeptide. Molecular & general genetics: MGG **221**, 443–452.

Schmollinger S, Mühlhaus T, Boyle NR, *et al.* 2014. Nitrogen-sparing mechanisms in *Chlamydomonas* affect the transcriptome, the proteome, and photosynthetic metabolism. The Plant cell **26**, 1410–1435.

Schneider K, Venn B, Mühlhaus T. 2022. Plotly.net: A fully featured charting library for .NET programming languages. F1000Research **11**, 1094.

Schroda M, Hemme D, Mühlhaus T. 2015. The *Chlamydomonas* heat stress response. The Plant journal: for cell and molecular biology **82**, 466–480.

Schulz-Raffelt M, Lodha M, Schroda M. 2007. Heat shock factor 1 is a key regulator of the stress response in *Chlamydomonas*. The Plant journal: for cell and molecular biology **52**, 286–295.

Scranton MA, Ostrand JT, Fields FJ, Mayfield SP. 2015. *Chlamydomonas* as a model for biofuels and bio-products production. The Plant journal: for cell and molecular biology **82**, 523–531.

Shimogawara K, Fujiwara S, Grossman A, Usuda H. 1998. High-efficiency transformation of *Chlamydomonas reinhardtii* by electroporation. Genetics **148**, 1821–1828.

Sommer F, Kropat J, Malasarn D, Grossoehme NE, Chen X, Giedroc DP, Merchant SS. 2010. The CRR1 nutritional copper sensor in Chlamydomonas contains two distinct metal-responsive domains. The Plant cell **22**, 4098–4113.

Song Z-T, Zhang L-L, Han J-J, Zhou M, Liu J-X. 2021. Histone H3K4 methyltransferases SDG25 and ATX1 maintain heat-stress gene expression during recovery in Arabidopsis. The Plant journal: for cell and molecular biology **105**, 1326–1338.

Strenkert D, Schmollinger S, Gallaher SD, *et al.* 2019. Multiomics resolution of molecular events during a day in the life of *Chlamydomonas*. Proceedings of the National Academy of Sciences of the United States of America **116**, 2374–2383.

Takano W, Hisabori T, Wakabayashi K-I. 2021. Rapid estimation of cytosolic ATP concentration from the ciliary beating frequency in the green alga Chlamydomonas reinhardtii. The Journal of biological chemistry **296**, 100156.

Ullah A, Nadeem F, Nawaz A, Siddique KHM, Farooq M. 2022. Heat stress effects on the reproductive physiology and yield of wheat. Journal of agronomy and crop science **208**, 1–17.

Usadel B, Poree F, Nagel A, Lohse M, Czedik-Eysenberg A, Stitt M. 2009. A guide to using MapMan to visualize and compare Omics data in plants: a case study in the crop species, Maize. Plant, cell & environment **32**, 1211–1229.

Venn B, Mühlhaus T. 2022. CSBiology/OntologyEnrichment: Release 0.0.1 (0.0.1). Zenodo. https://doi.org/10.5281/zenodo.6340412.

Venn B, Weil L, Schneider K, Zimmer D, Mühlhaus T. 2022. fslaborg/FSharp.Stats. Zenodo. https://doi.org/10.5281/zenodo.6337056.

Vítová M, Bišová K, Hlavová M, Kawano S, Zachleder V, Cížková M. 2011. *Chlamydomonas reinhardtii*: duration of its cell cycle and phases at growth rates affected by temperature. Planta **234**, 599–608.

Voß B, Meinecke L, Kurz T, Al-Babili S, Beck CF, Hess WR. 2010. Hemin and Magnesium-Protoporphyrin IX Induce Global Changes in Gene Expression in Chlamydomonas reinhardtii. Plant physiology **155**, 892–905.

Vu LD, Gevaert K, De Smet I. 2019. Feeling the heat: searching for plant thermosensors. Trends in plant science **24**, 210–219.

Walker RP, Chen Z-H, Famiani F. 2021. Gluconeogenesis in Plants: A Key Interface between Organic Acid/Amino Acid/Lipid and Sugar Metabolism. Molecules **26**.

Wang L, Yang L, Wen X, Chen Z, Liang Q, Li J, Wang W. 2019. Rapid and high efficiency transformation of *Chlamydomonas reinhardtii* by square-wave electroporation. Bioscience reports **39**, BSR20181210.

Wulfert S, Schilasky S, Krueger S. 2020. Transcriptional and Biochemical Characterization of Cytosolic Pyruvate Kinases in Arabidopsis thaliana. Plants **9**.

Xiao L, Young EB, Grothjan JJ, Lyon S, Zhang H, He Z. 2015. Wastewater treatment and microbial communities in an integrated photo-bioelectrochemical system affected by different wastewater algal inocula. Algal Research **12**, 446–454.

Xie B, Bishop S, Stessman D, Wright D, Spalding MH, Halverson LJ. 2013. *Chlamydomonas reinhardtii* thermal tolerance enhancement mediated by a mutualistic interaction with vitamin B12-producing bacteria. The ISME journal **7**, 1544–1555.

Xu Z-S, Li Z-Y, Chen Y, Chen M, Li L-C, Ma Y-Z. 2012. Heat shock protein 90 in plants: molecular mechanisms and roles in stress responses. International journal of molecular sciences **13**, 15706–15723.

Yamori W, Shikanai T. 2016. Physiological functions of cyclic electron transport around Photosystem I in sustaining photosynthesis and plant growth. Annual review of plant biology **67**, 81–106.

Young EB, Reed L, Berges JA. 2022. Growth parameters and responses of green algae across a gradient of phototrophic, mixotrophic and heterotrophic conditions. PeerJ **10**, e13776.

Zachleder V, Ivanov I, Vítová M, Bišová K. 2019. Cell cycle arrest by supraoptimal temperature in the alga *Chlamydomonas reinhardtii*. Cells **8**, 1237.

Zhang N, Mattoon EM, McHargue W, *et al.* 2022*a*. Systems-wide analysis revealed shared and unique responses to moderate and acute high temperatures in the green alga Chlamydomonas reinhardtii. Communications biology **5**, 460.

Zhang N, Pazouki L, Nguyen H, *et al.* 2022*b*. Comparative phenotyping of two commonly used Chlamydomonas reinhardtii background strains: CC-1690 (21gr) and CC-5325 (The CLiP mutant library background). Plants **11**, 585.

Zhang X, Rerksiri W, Liu A, Zhou X, Xiong H, Xiang J, Chen X, Xiong X. 2013. Transcriptome profile reveals heat response mechanism at molecular and metabolic levels in rice flag leaf. Gene **530**, 185–192.

Zhang M, Zhang S. 2022. Mitogen-activated protein kinase cascades in plant signaling. Journal of integrative plant biology **64**, 301–341.

Zones JM, Blaby IK, Merchant SS, Umen JG. 2015. High-resolution profiling of a synchronized diurnal transcriptome from *Chlamydomonas reinhardtii* reveals continuous cell and metabolic differentiation. The Plant cell **27**, 2743–2769.

Figures

Fig. 1.

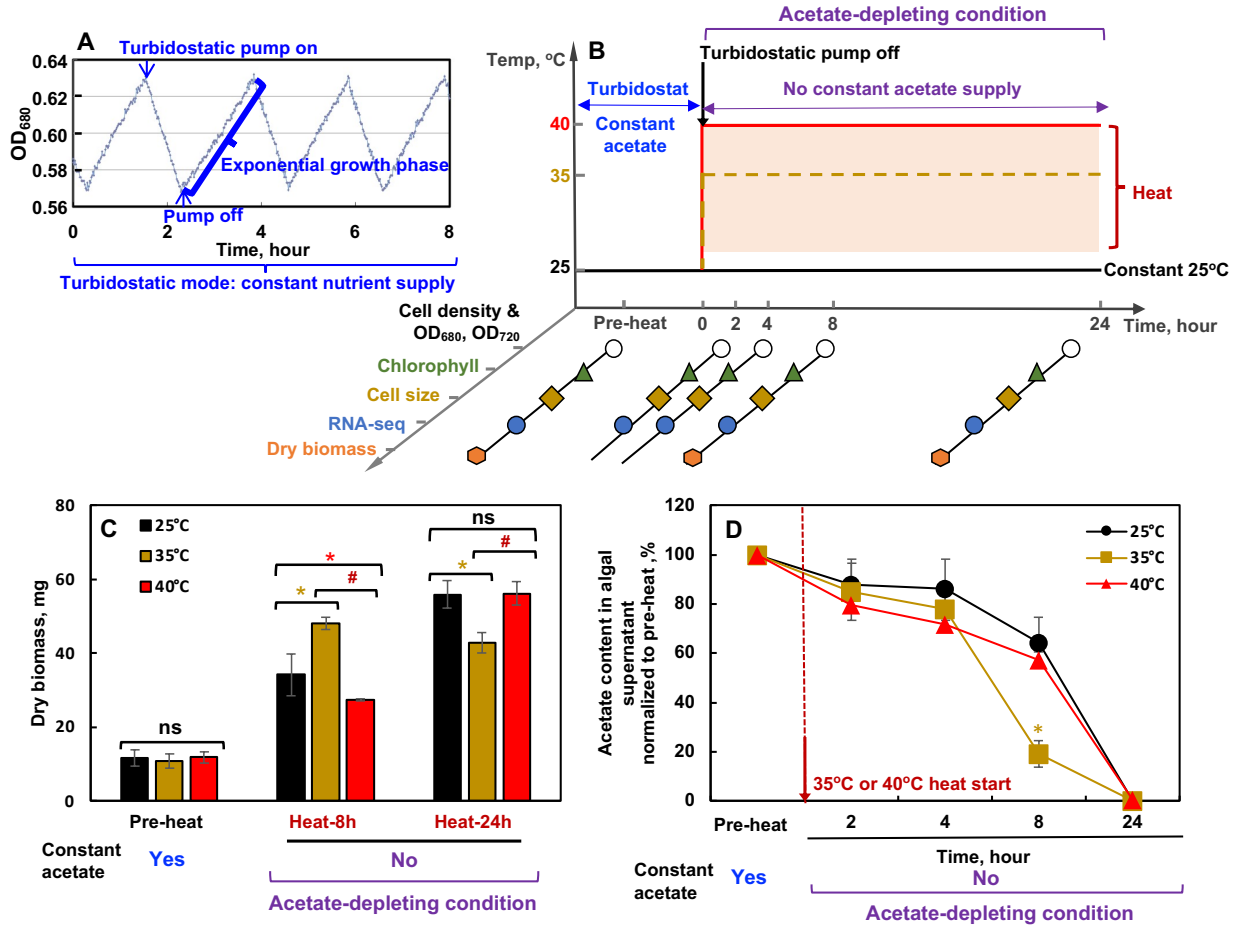

Fig. 1. Under the acetate-depleting condition, moderate high temperature of 35°C transiently increased but then decreased Chlamydomonas biomass accumulation. **(A)** Before heat treatments, Chlamydomonas cells (CC-1690, also called *21gr*, wild-type) were grown in photobioreactors (PBRs) in Tris-acetate-phosphate (TAP) medium (acetate as an organic carbon source) with a light intensity of 100 μmol photons m^{-2} s^{-1} and constant bubbling of air. Algal cultures were maintained turbidostatically with frequent medium dilution using a small range of OD_{680}, which monitors chlorophyll content. Figure cited and modified from a supplemental figure of our previous paper (Zhang *et al.*, 2022*a*). **(B)** Experimental outline and sampling time points for the acetate-depleting condition. **(C)** Under the acetate-depleting condition, algal dry biomass (in 90 mL cultures) increased with 8-h heat but decreased with 24-h heat of 35°C as compared to the constant 25°C. Mean ± SE, *n*=3-8 biological replicates. **(D)** Heat of 35°C accelerated acetate

consumption. Acetate content in algal supernatant was quantified using the Acetate Colorimetric Assay Kit. The red dashed line marks the start of heat or the corresponding time point at constant 25°C. **(C, D)** Statistical analyses were performed using two-tailed t-test assuming unequal variance; *, $p<0.05$, the colors of the asterisks match the heated condition as compared to 25°C at the same time points; #, $p<0.05$, for the comparisons between 35°C and 40°C at the same time points. Not significant, ns.

Fig. 2.

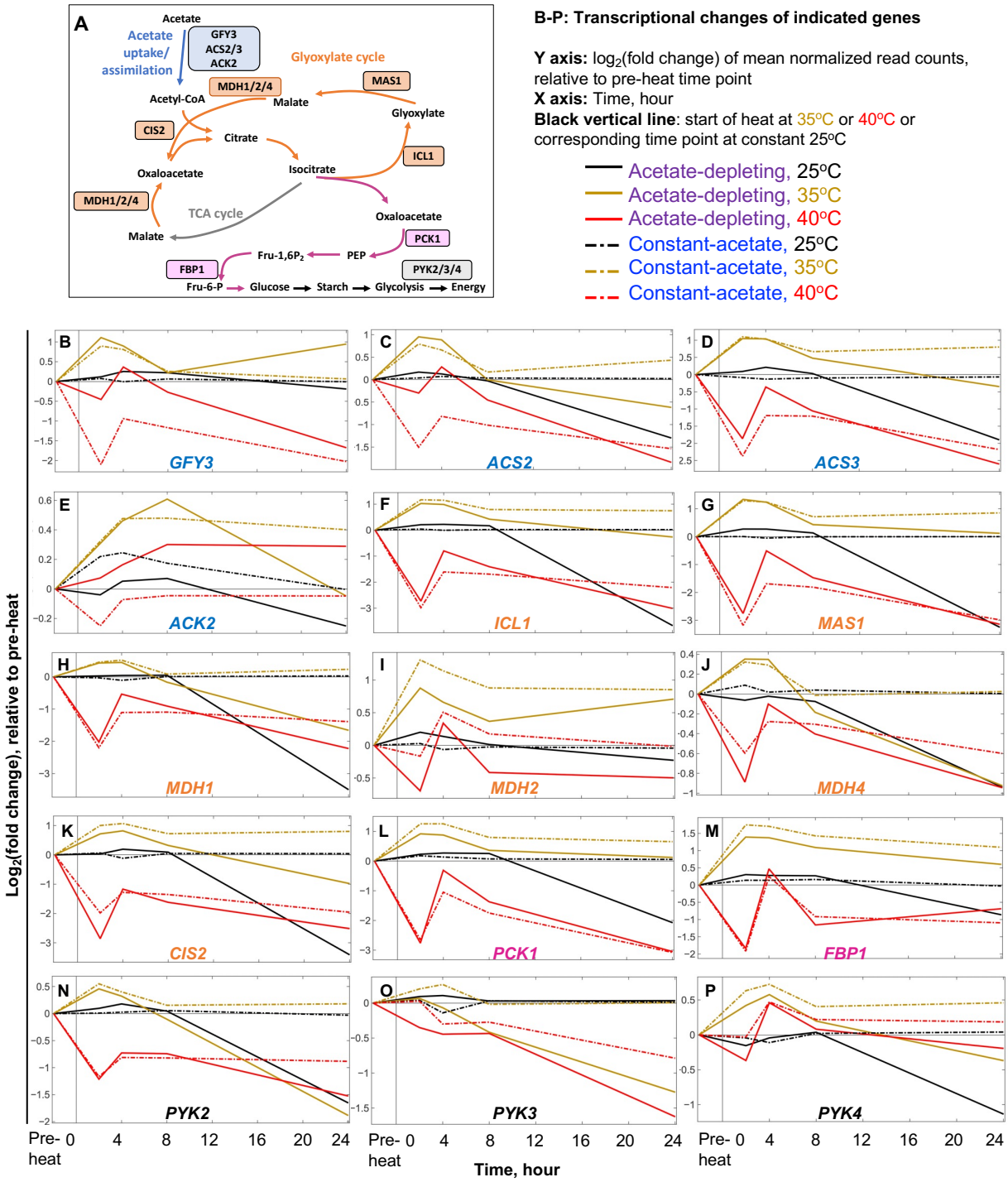

Fig. 2. Moderate high temperature of 35ºC up-regulated transcripts related to acetate uptake and assimilation, glyoxylate cycle, gluconeogenesis, and glycolysis pathways. (A) Simplified pathways of acetate metabolism in Chlamydomonas based on

these papers (Johnson and Alric 2013; Durante et al. 2019). Key enzymes are in boxes and were analyzed via RNA-seq in panels B-P. Acetate uptake/assimilation enzymes: GFY3, putative acetate transporter; ACS2/3, acetyl-CoA synthases; ACK2, acetate kinase. Glyoxylate cycle key enzymes: ICL1, isocitrate lyase; MAS1, malate synthase; CIS2, Citrate synthase; MDH1/2/4, NAD-dependent malate dehydrogenases. Gluconeogenesis key enzymes: PCK1, phosphoenolpyruvate carboxykinase; FBP1, fructose-1,6-bisphosphatase. Glycolysis key enzymes: PYK2/3/4, pyruvate kinase 2/3/4. See all gene IDs and annotations in Supplemental Table 1. PEP, phosphoenolpyruvate. Fru-6-P, fructose-6-phosphate. Fru-1,6-P_2, fructose-1,6-bisphosphate. **(B-P)** Transcriptional change of the indicated genes under six different conditions, presented as $\log_2$(fold change) of mean normalized read counts relative to the pre-heat time point. In each panel, each line represents the transcriptional time course of the indicated gene under one condition as indicated by the legend. The black vertical lines mark the start of heat or the corresponding time point at constant 25°C. Solid lines for the acetate-depleting condition and dashed lines for the constant-acetate condition. Black, brown, red lines for 25°C, 35°C, and 40°C temperature treatments, respectively. See Supplemental Dataset 1 for bigger pictures and more information.

Fig. 3.

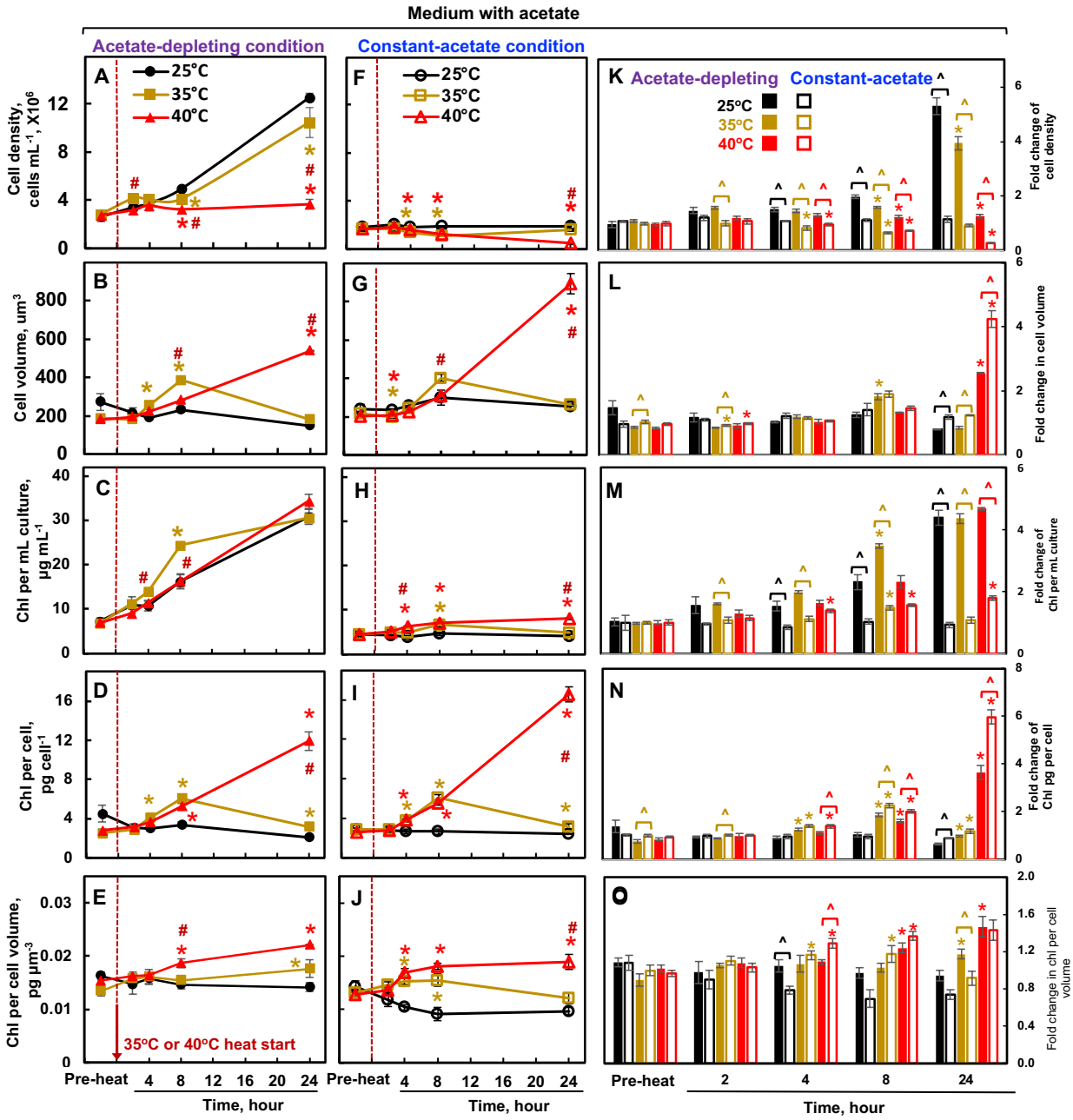

Fig. 3. Algal cells subjected to different temperature treatments under the acetate-depleting condition were compared at the physiological level with those under the constant-acetate condition. (A-E) Cell parameters from algal cultures under the acetate-depleting condition. The algal cultivation and heat treatments were the same as in Fig. 1B. **(F-J)** Cell parameters from algal cultures under the constant-acetate condition, with turbidostatic control, data plotted based on the results from Zhang *et al.*, 2022*a*. (**A-**

J) Two panels on the same row share the same y axis. The red dashed lines mark the start of heat or the corresponding time point at constant 25°C. **(K-O)** Fold change of the indicated cell parameters from algal cultures under the acetate-depleting condition (filled bars) and under the constant-acetate condition (empty bars). (**A-O**) Mean ± SE, n = 3-7 biological replicates. Statistical analyses were performed with two-tailed t-test assuming unequal variance; *, $p<0.05$, for the comparisons between 35°C or 40°C with 25°C at the same time point under the same acetate condition, the colors of the asterisks match the heat condition; #, $p<0.05$, for the comparisons between 35°C and 40°C at the same time point under the same acetate condition; ^, $p<0.05$, for the comparisons between the acetate-depleting and constant-acetate conditions at the same time point and under the same temperature. **(D, E, I, J)** Cell parameters at different time points during constant 25°C had little change, not significantly different from the pre-heat time points ($p>0.05$).

Fig. 4.

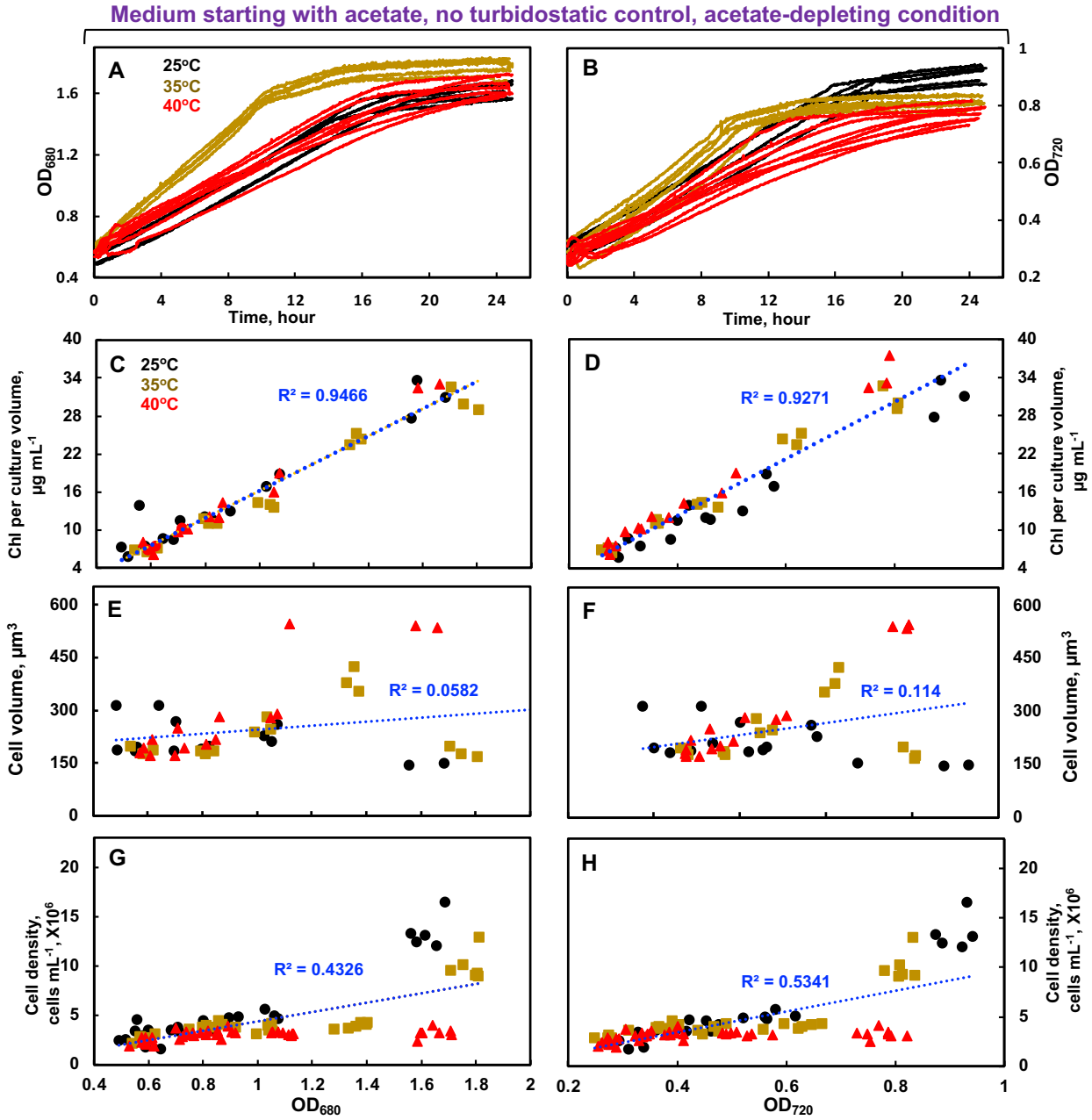

Fig. 4. Both OD_{680} and OD_{720} were linearly proportional to chlorophyll contents under different temperatures and can be used to monitor algal growth rates automatically. Black, brown, red lines and symbols represent 25°C, 35°C, and 40°C treatments, respectively. **(A, B)** OD_{680} and OD_{720} automatically monitored algal growth every one min in algal cultures grown in photobioreactors with different temperatures under the acetate-depleting conditions. The algal cultivation and heat treatments were the same as in Fig. 1B. Multiple lines with the same colors represent biological replicates

(n= 4-8) under the same condition. **(C-H)** OD_{680} and OD_{720} were linearly proportional to Chlorophyll (Chl) contents per mL cultures but not cell volume or cell density. Chl contents (**C, D**), cell volume (**E, F**), and cell densities (**G, H**) were plotted against OD_{680} or OD_{720} readings in algal cultures with different treatments. Dashed blue lines are linear trendlines of best fit and R-squared values are displayed.

Fig. 5.

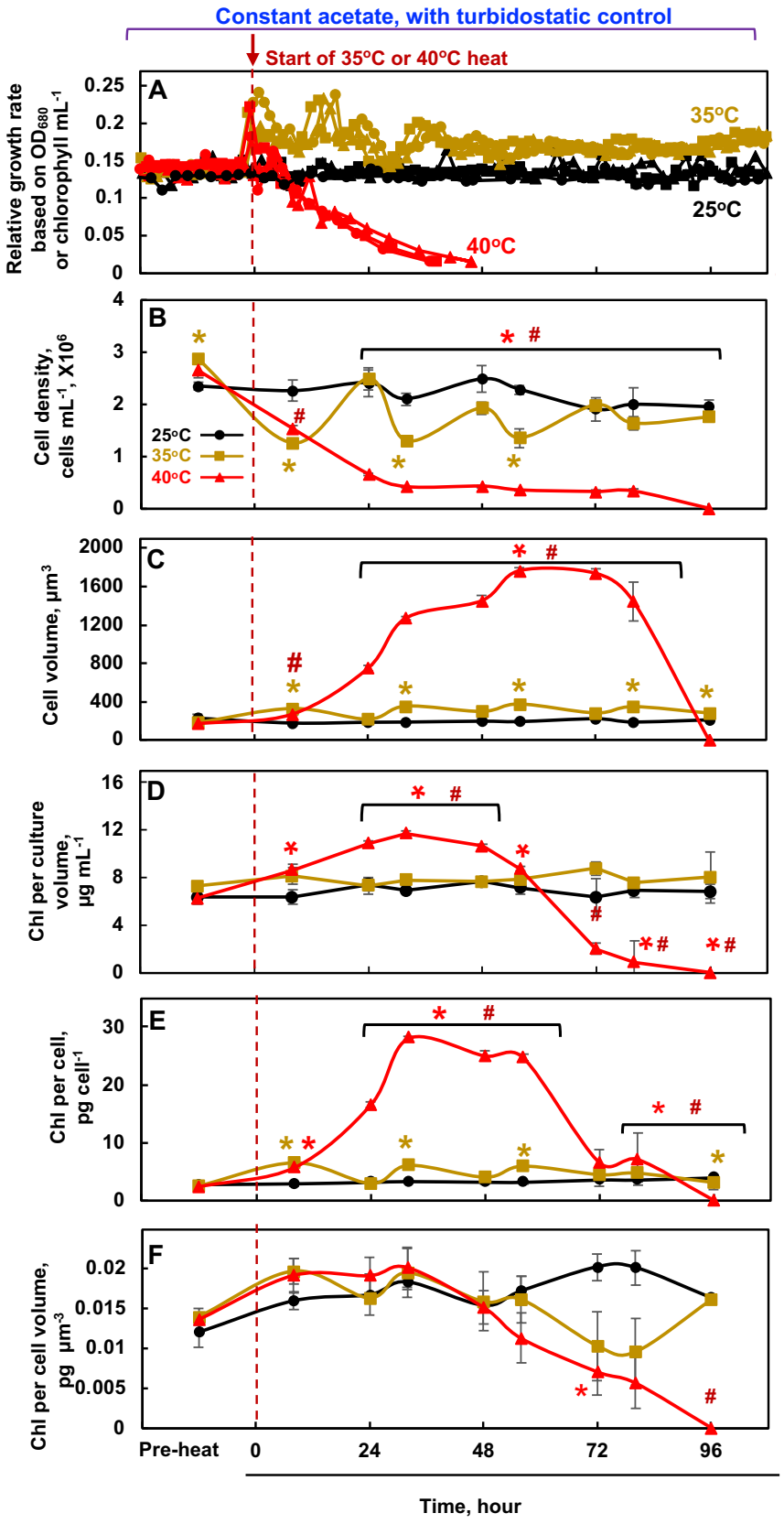
Constant acetate, with turbidostatic control
Start of 35°C or 40°C heat
A
Relative growth rate based on OD680 or chlorophyll mL-1
35°C
25°C
40°C
B
Cell density, cells mL-1, X10^6
25°C
35°C
40°C
C
Cell volume, µm3
D
Chl per culture volume, µg mL-1
E
Chl per cell, pg cell-1
F
Chl per cell volume, pg µm-3
Pre-heat
0
24
48
72
96
Time, hour

Fig. 5. Under the constant-acetate condition with turbidostatic control, moderate (35°C) and acute high temperatures (40°C) increased and reduced algal growth during 4-day heating, respectively. Black, brown, red lines and symbols represent 25°C, 35°C, and 40°C treatments, respectively. The red dashed lines mark the start of heat or the corresponding time point at constant 25°C. **(A)** Chlamydomonas cultures were grown in photobioreactors (PBRs) with turbidostatic control at different temperatures in acetate-containing medium. Algal cultures were first acclimated at 25°C for 4 days before the temperature was switched to 35°C or 40°C or stayed at 25°C for 4 days. Relative growth rates were calculated based on the cycling of OD_{680} caused by the turbidostatic control (see Fig. 1A and method for details). Each temperature treatment had 3 biological replicates in separate PBRs. **(B-F)** Cell parameters were quantified from algal cultures harvested at different time points with different treatments. Statistical analyses were performed with two-tailed t-test assuming unequal variance by comparing 35°C or 40°C with 25°C at the same time point. *, $p<0.05$, the colors of the asterisks match the heat condition; #, $p<0.05$, for the comparisons between 35°C and 40°C at the same time point. Chl, Chlorophyll.

Fig. 6

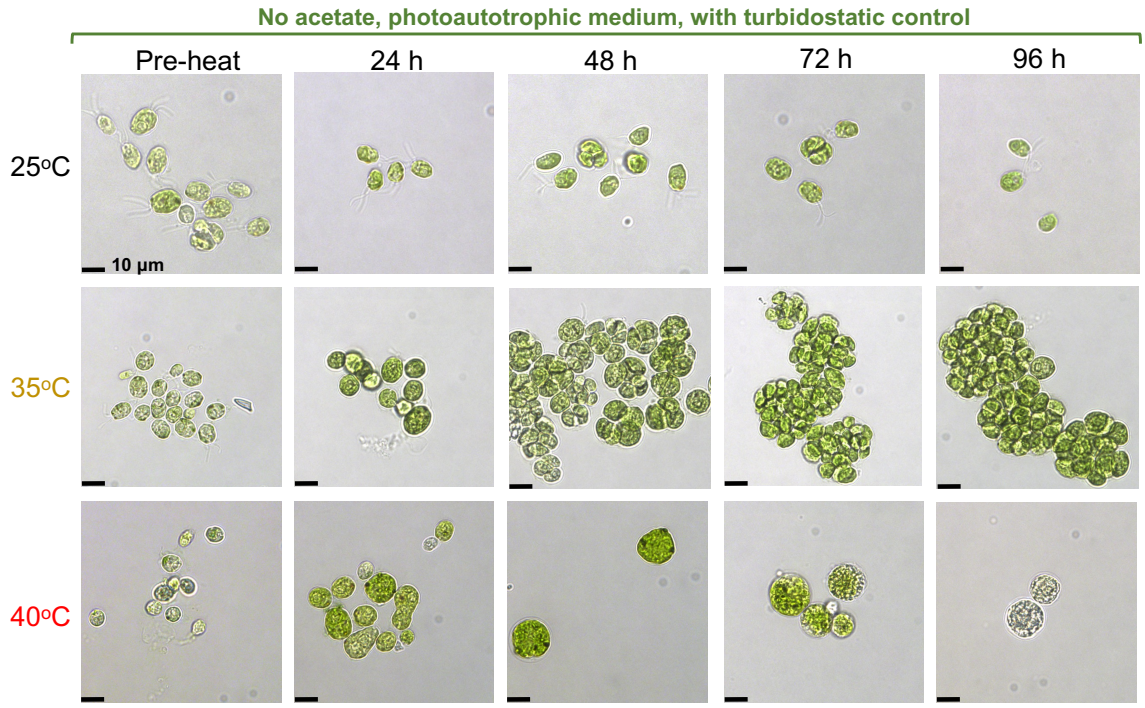

Fig. 6. Under the no-acetate condition (photoautotrophic medium) with turbidostatic control, 35°C-treated cells formed palmelloids and 40°C-treated cells were bleached after 4-day heat treatments. Light microscopic images of Chlamydomonas cells under different conditions. Chlamydomonas cultures were grown in photobioreactors with turbidostatic control at different temperatures in photoautotrophic medium without acetate. Algal cultures were first acclimated at 25°C for 4 days before the temperature was switched to 35°C or 40°C or stayed at 25°C for 4 days. Images shown are representative results from three biological replicates. Black scale bar on each panel represents 10 µm.

Fig. 7.

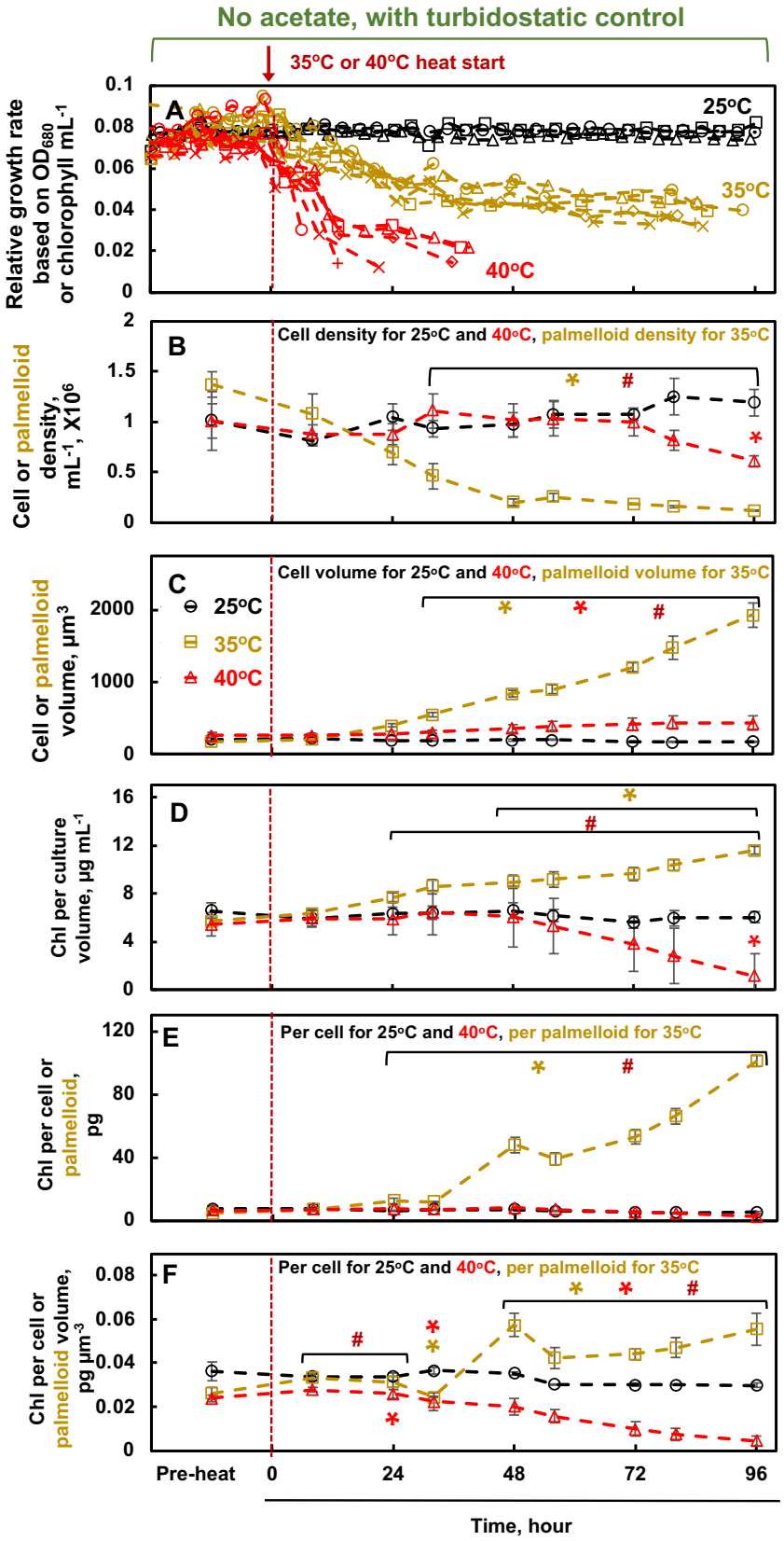
No acetate, with turbidostatic control
35°C or 40°C heat start
A
25°C
35°C
40°C
Relative growth rate based on OD680 or chlorophyll mL-1
B
Cell density for 25°C and 40°C, palmelloid density for 35°C
Cell or palmelloid density, mL-1, X10^6
C
Cell volume for 25°C and 40°C, palmelloid volume for 35°C
25°C
35°C
40°C
Cell or palmelloid volume, µm3
D
Chl per culture volume, µg mL-1
E
Per cell for 25°C and 40°C, per palmelloid for 35°C
Chl per cell or palmelloid, pg
F
Per cell for 25°C and 40°C, per palmelloid for 35°C
Chl per cell or palmelloid volume, pg µm-3
Pre-heat
0
24
48
72
96
Time, hour

Fig. 7. Under the no-acetate condition (photoautotrophic medium) with turbidostatic control, both moderate (35°C) and acute high temperatures (40°C) reduced algal growth during 4-day heating. Black, brown, red lines and symbols represent 25°C, 35°C, and 40°C treatments, respectively. The red dashed lines mark the start of heat or the corresponding time point at constant 25°C. **(A)** Chlamydomonas cultures were grown in photobioreactors (PBRs) with turbidostatic control at different temperatures in photoautotrophic medium without acetate. Algal cultures were first acclimated at 25°C for 4 days before the temperature was switched to 35°C or 40°C or stayed at 25°C for 4 days. Relative growth rates were calculated based on the cycling of OD_{680} caused by the turbidostatic control. Each temperature treatment had at least 3 biological replicates in separate PBRs. **(B-F)** Cell parameters were quantified from algal cultures harvested at different time points with different treatments. Because 35°C-treated cells under photoautotrophic condition formed palmelloids (see Fig 6), the term of "palmelloid" was used in place of "cell" for this condition only. Statistical analyses were performed with two-tailed t-test assuming unequal variance by comparing 35°C or 40°C with 25°C at the same time point. *, $p<0.05$, the colors of the asterisks match the heat condition; #, $p<0.05$, for the comparisons between 35°C and 40°C at the same time point. Chl, Chlorophyll.

Fig. 8

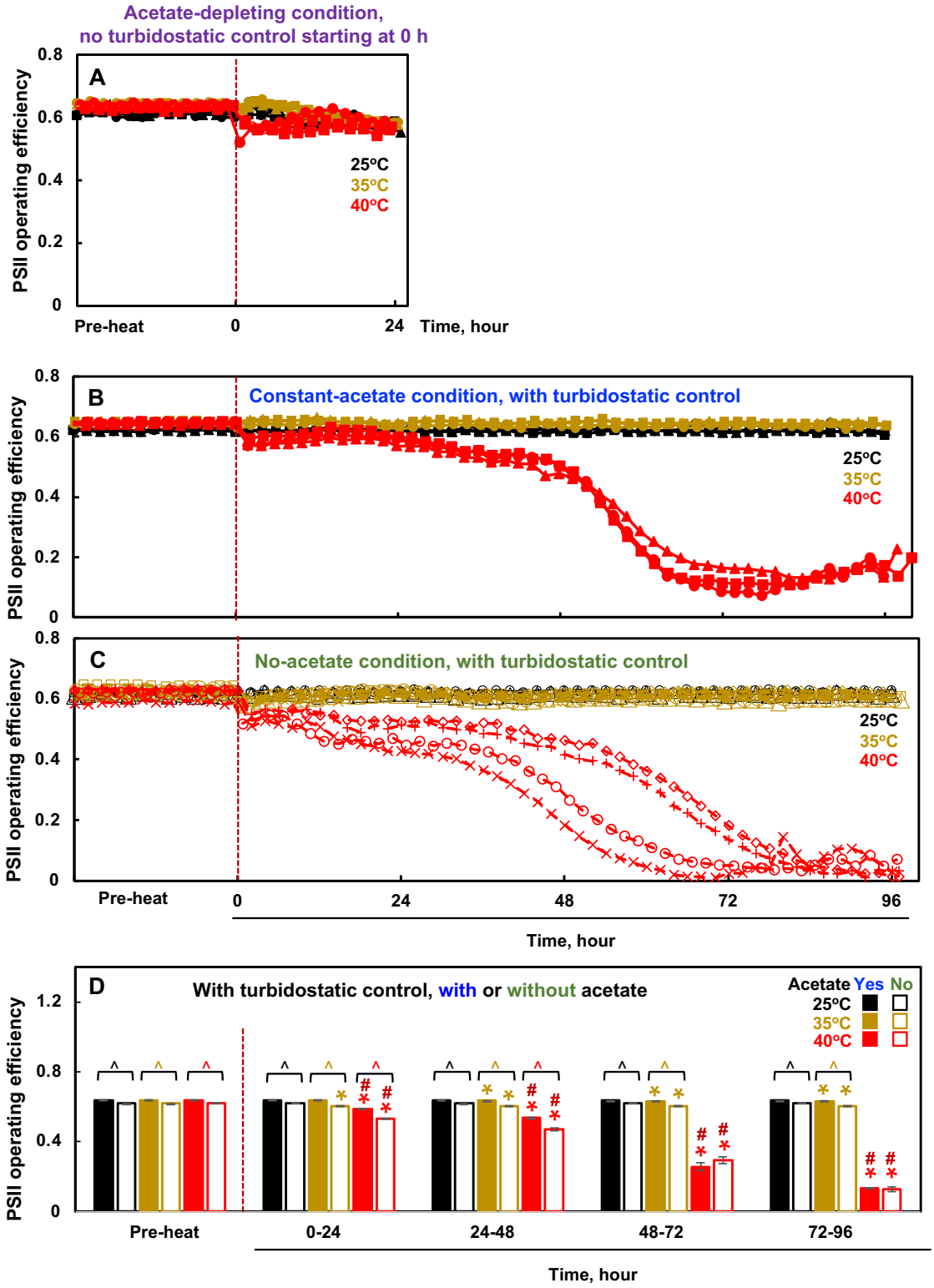
Acetate-depleting condition,
no turbidostatic control starting at 0 h
A
PSII operating efficiency
0.8
0.6
0.4
0.2
0
25°C
35°C
40°C
Pre-heat
0
24
Time, hour
B
Constant-acetate condition, with turbidostatic control
C
No-acetate condition, with turbidostatic control
48
72
96
Time, hour
D
With turbidostatic control, with or without acetate
Acetate Yes No
1.2
Pre-heat
0-24
24-48
48-72
72-96
Time, hour

Fig. 8. Under the turbidostatic control and no nutrient limitation, algal cultures had higher photosystem II (PSII) operating efficiency with acetate than without acetate during treatment of 25°C, 35°C, or 40°C, although the acetate effects diminished after 2-day heat of 40°C due to cell death. PSII operating efficiency was measured automatically in photobioreactors under different conditions. Black, brown, red lines and symbols represent 25°C, 35°C, and 40°C treatments, respectively. The red dashed lines mark the start of heat or the corresponding time point at constant 25°C. **(A)** Acetate-depleting condition at 25°C, 35°C, or 40°C for 24 h, in medium started with acetate but no turbidostatic control, thus no constant acetate supply. **(B)** Constant-acetate condition at 25°C, 35°C, or 40°C for 4 days, in medium with acetate and turbidostatic control, thus no nutrient limitation. **(C)** No-acetate condition at 25°C, 35°C, or 40°C for 4 days, in photoautotrophic medium without acetate but with turbidostatic control, thus no nutrient limitation. **(D)** The comparison of PSII operating efficiency in the constant-acetate (data from panel B, filled bars) and no-acetate (data from panel C, empty bars) conditions during the indicated periods at 25°C, 35°C, or 40°C for 4 days. Statistical analyses were performed with two-tailed t-test assuming unequal variance by comparing the indicated groups. *, $p<0.05$, comparing 35°C or 40°C with 25°C with the same medium type at the same time; #, $p<0.05$, for the comparisons between 35°C and 40°C with the same medium type at the same time; ^, $p<0.05$, for the comparisons between the same temperature treatment at the same time but with and without acetate. The colors of the significant marks match the heat condition, brown for 35°C and bright red color for 40°C related comparisons, and dark red for 35°C and 40°C comparisons.

Fig. 9.

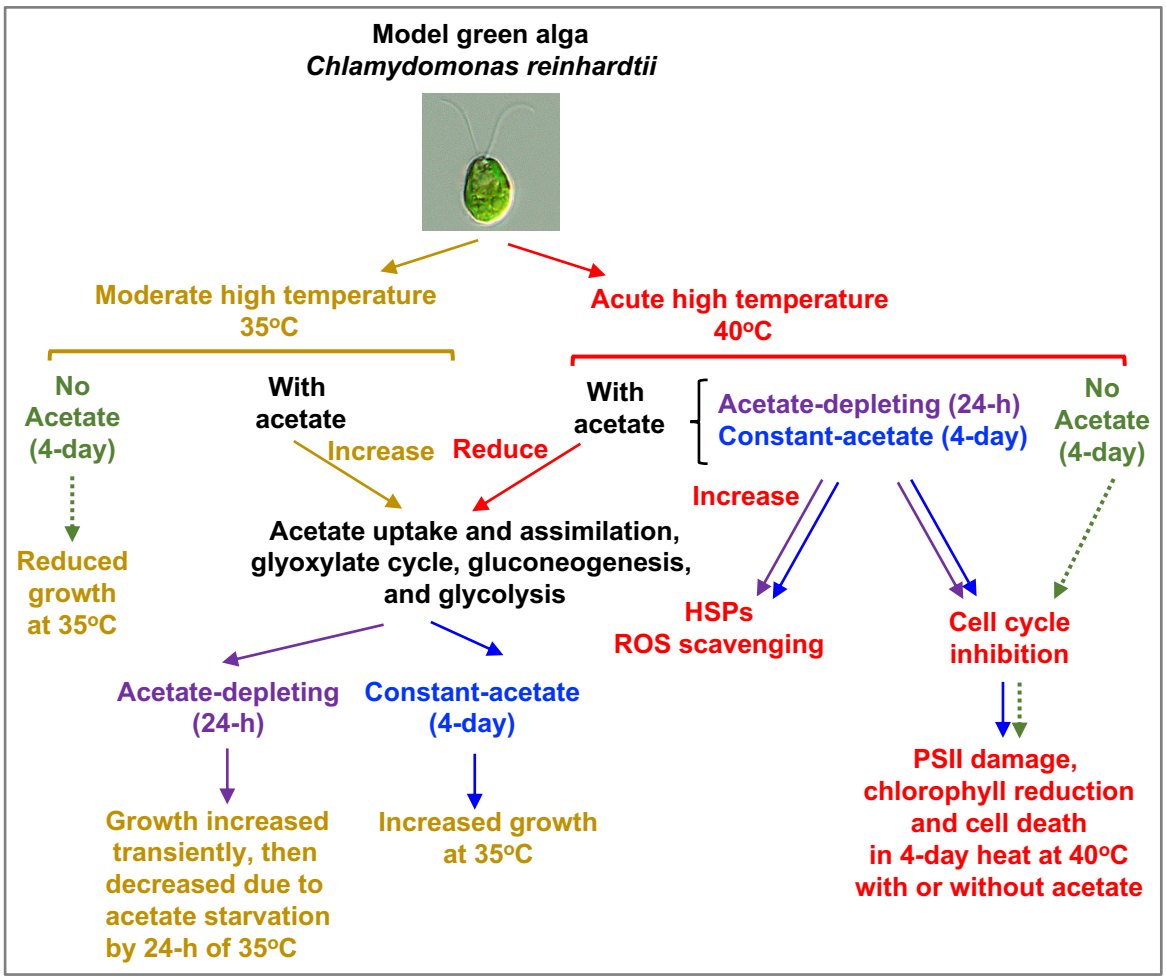

Fig. 9. Acetate availability affected Chlamydomonas heat tolerance under the moderate high temperature (35°C) but had much less effects under the acute high temperature (40°C). In medium containing the organic carbon source, acetate, heat of 35°C accelerated acetate metabolism by upregulating transcripts related to acetate uptake and assimilation, glyoxylate cycle, gluconeogenesis, and glycolysis pathways. With constant acetate supply, 35°C increased algal growth. Under the acetate-depleting condition, 35°C increased algal growth transiently followed by decreased growth and biomass accumulation due to acetate starvation. Without acetate supply in photoautotrophic medium, 35°C reduced algal growth rates. Under either constant-acetate or depleting-acetate condition, heat of 40°C down-regulated transcripts related to acetate metabolism, but up-regulated transcripts related to heat shock proteins (HSPs) and reactive oxygen species (ROS) scavenging. In medium with or without acetate, 40°C

decreased algal growth rates, inhibited cell division, damaged photosynthesis (e.g., photosystem II, PSII), reduced chlorophyll contents, and eventually led to cell death. Thus, Chlamydomonas cells could not survive continuous heat of 40°C for longer than 2 days, independent of acetate supply. Brown and red labels and lines represent the effects of 35°C and 40°C, respectively. Purple, blue, and green labels and lines represent the acetate-depleting, constant-acetate, and no-acetate conditions, respectively.

Supplemental Fig. 1.

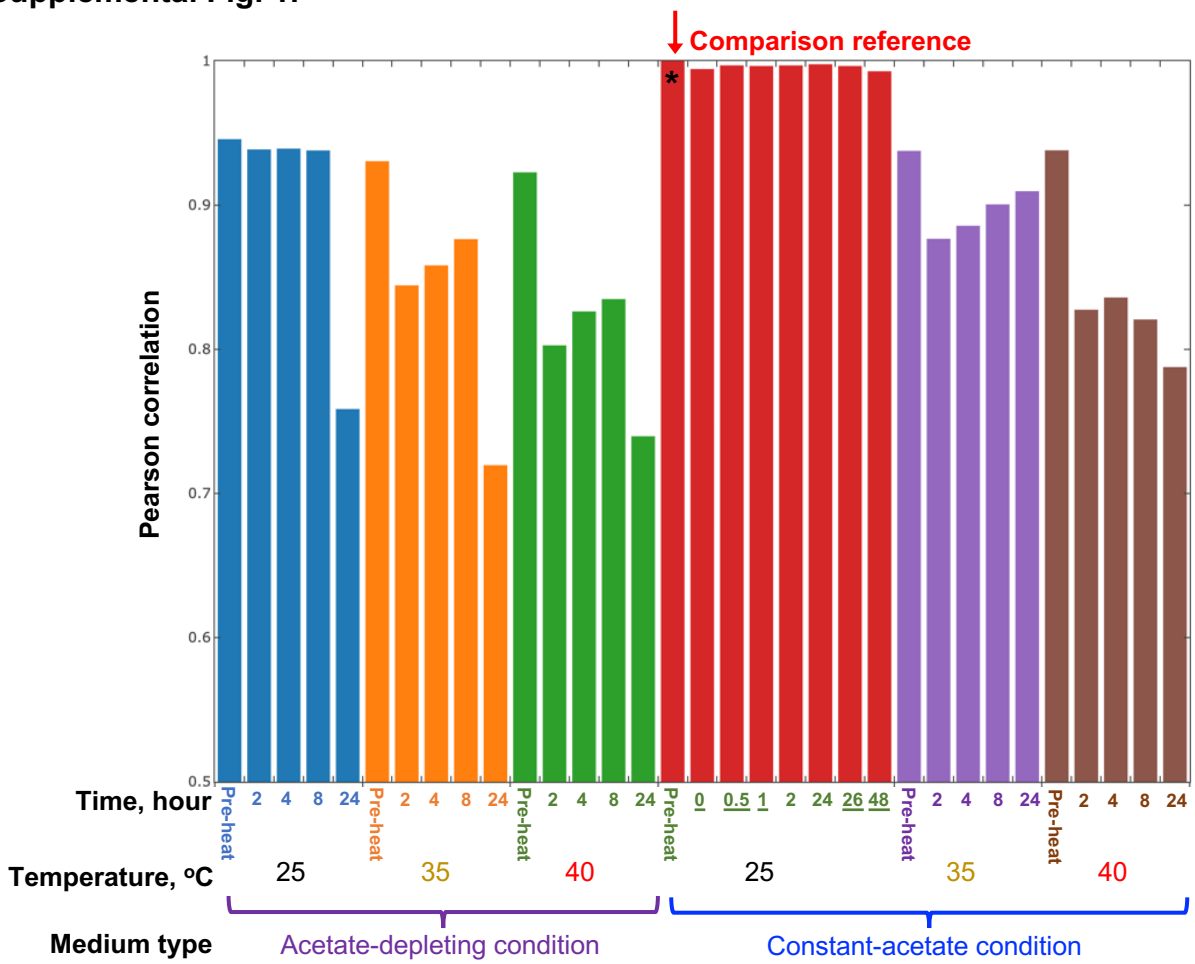

Supplemental Fig. 1. RNA-seq data from algal samples harvested from photobioreactors (PBRs) under the constant-acetate-25°C with turbidostatic control were highly correlated with each other. The Pearson correlations were generated by comparing all RNA-seq samples to the first sample (marked by *) of the constant-acetate-25°C condition. Under constant acetate, 25°C, and light (constant-acetate-25°C) with turbidostatic control in PBRs, the algal growth rates and cell physiologies stay constant (Fig. 5). We had RNA-seq data for 8 time points under the constant-acetate-25°C condition, and these samples were highly correlated with each other (with Pearson correlation ≥ 0.993). The 0 h of the constant-acetate-25°C condition corresponds to the time when PBRs reach expected high temperatures during heat treatments, which takes about 30 min from 25°C to 35°C or 40°C. All pre-heat samples were harvested from PBRs under the same constant-acetate-25°C condition with turbidostatic control and these RNA-seq samples had Pearson correlation > 0.95.

Because the cell status and transcriptome stay steady under the constant-acetate-25°C, we used the five extra time points under the constant-acetate-25°C condition (with underlines) to impute the 2 h and 4 h time points under the constant-acetate-25°C condition. See method for details.

Supplemental Fig. 2.

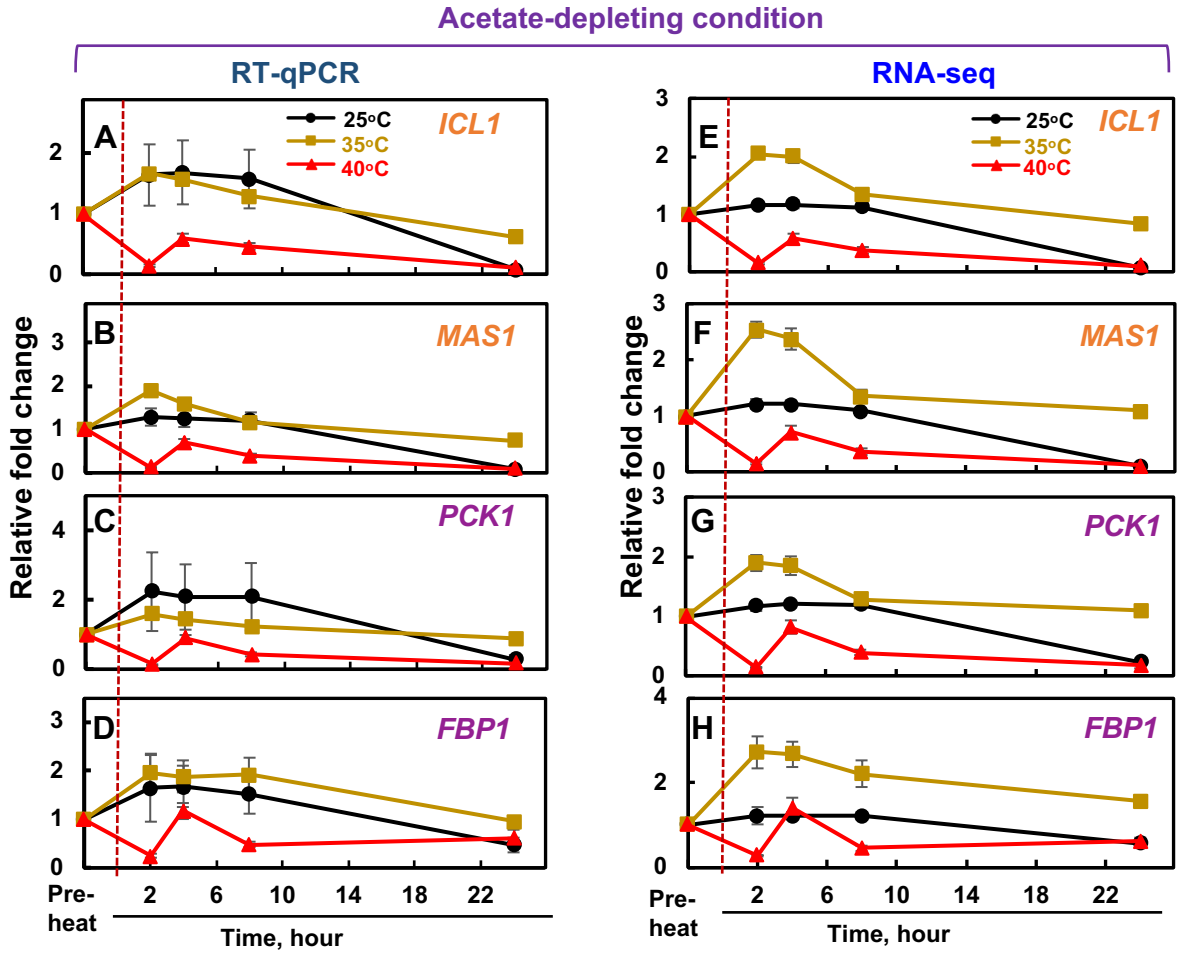

Supplemental Fig. 2. RT-qPCR analysis was consistent with RNA-seq results. Fold changes of four selected transcripts involved in the glyoxylate cycle (*ICL1* and *MAS1*) and gluconeogenesis cycle (*PCK1* and *FBP1*) as in Fig. 2A were calculated based on RT-qPCR (**A-D**) or RNA-seq (**E-H**) results. The red dashed lines mark the start of heat or the corresponding time point at constant 25°C. For RT-qPCR results, the relative fold changes were calculated by normalizing the transcript expression to the reference genes *CBLP*, *EIF1A* and the pre-heat level. For RNA-seq results, the relative fold changes were calculated based on normalized RNA-seq read counts relative to the pre-heat level. Values are mean ± SE, n = 3 biological replicates. Glyoxylate cycle key enzymes: ICL1, isocitrate lyase; MAS1, malate synthase. Gluconeogenesis key enzymes: PCK1, phosphoenolpyruvate carboxykinase; FBP1, fructose-1,6-bisphosphatase (See all gene IDs and RT-qPCR primers in Supplemental Table 1).

Supplemental Fig. 3

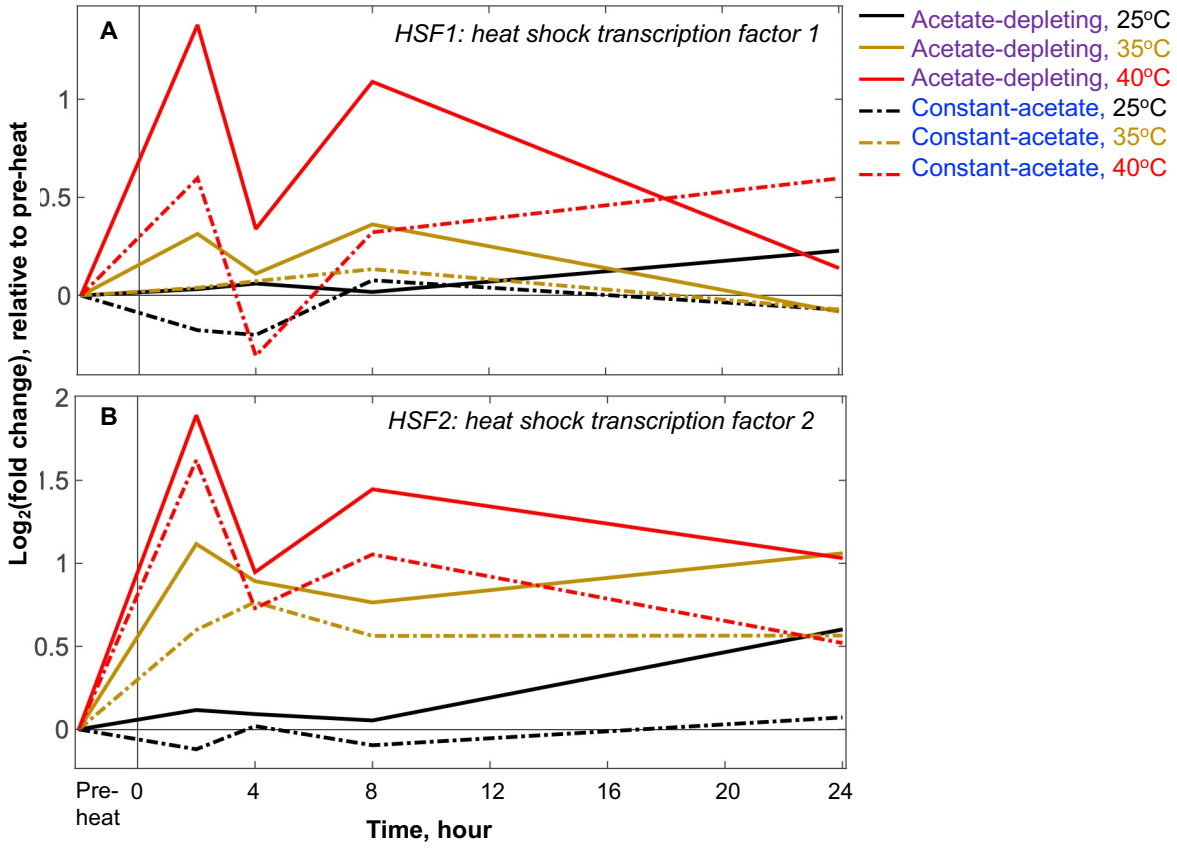

Supplemental Fig. 3 continued

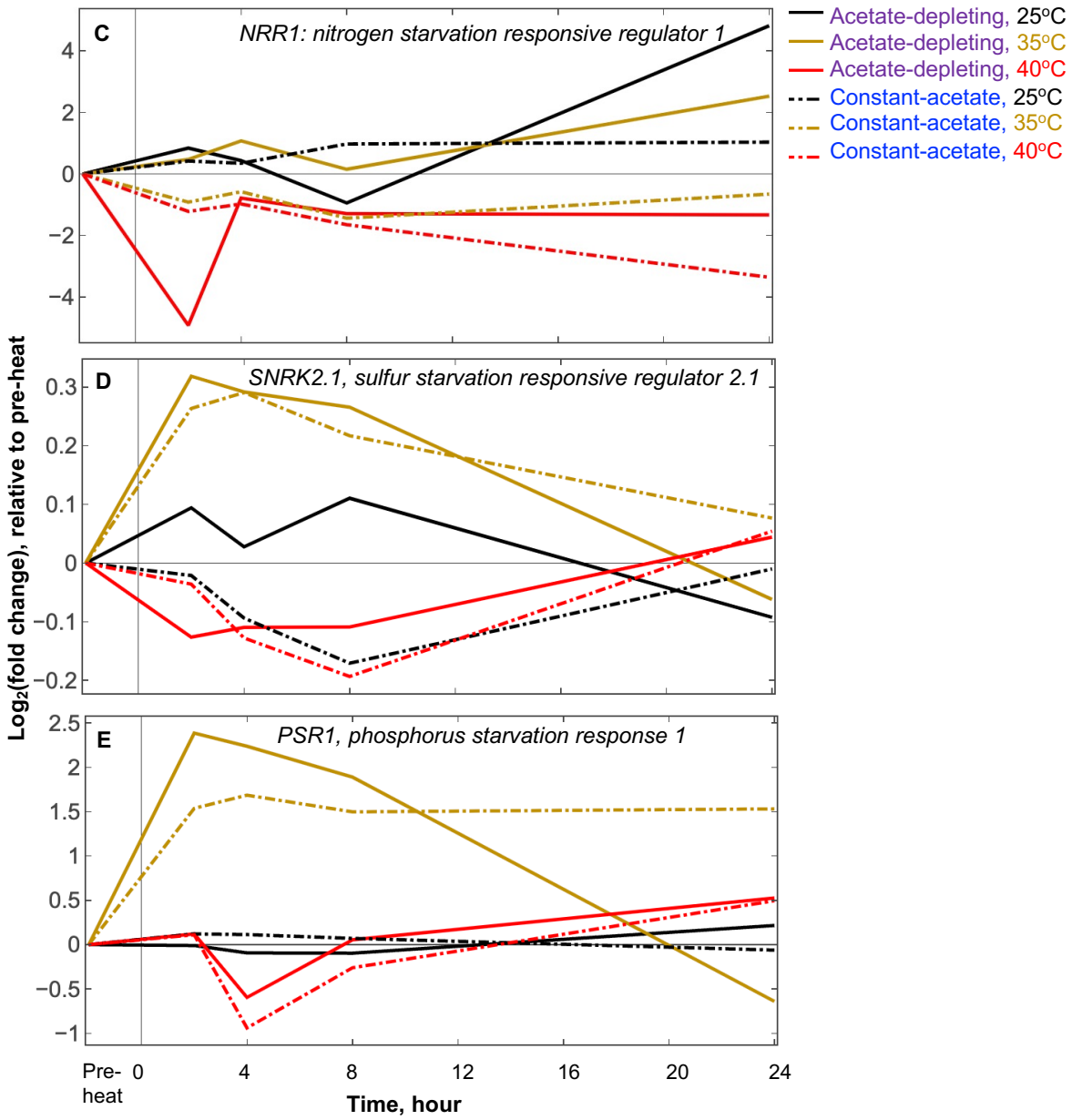

Supplemental Fig. 3 continued

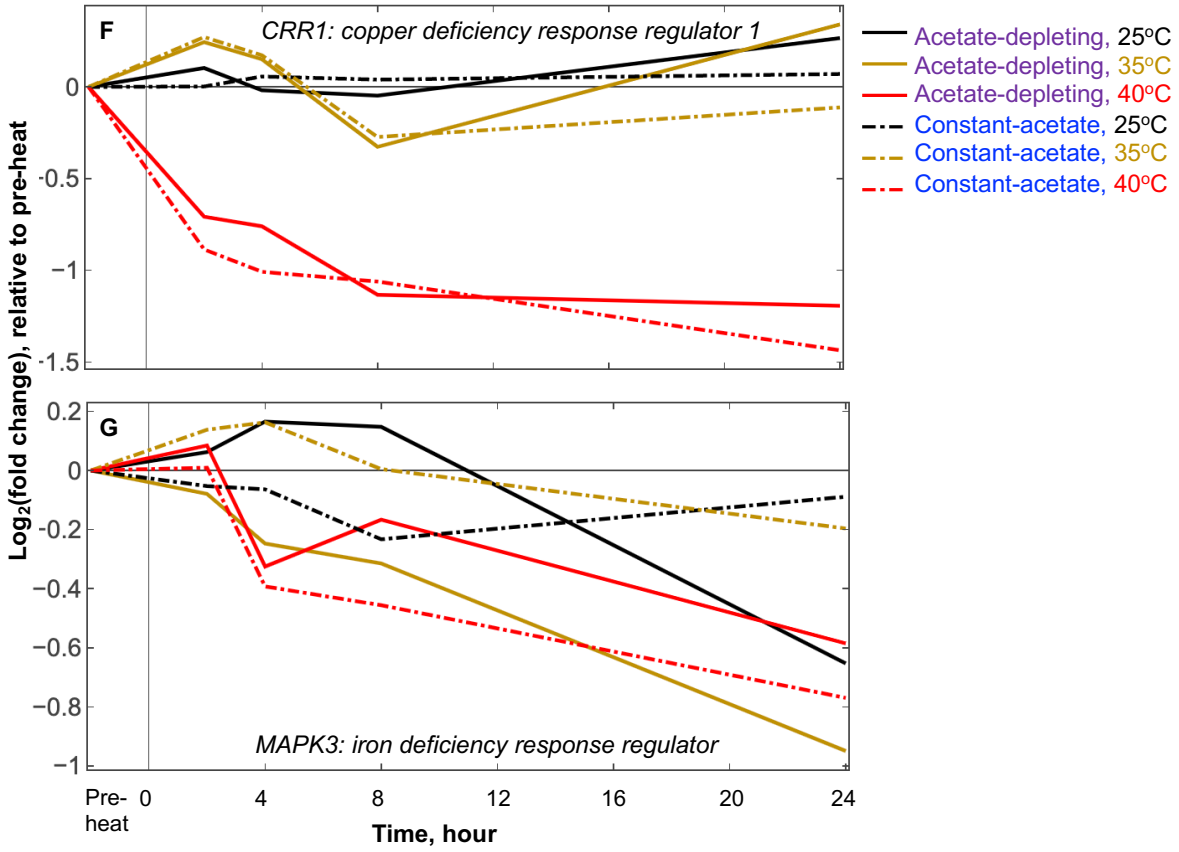

Supplemental Fig. 3 continued

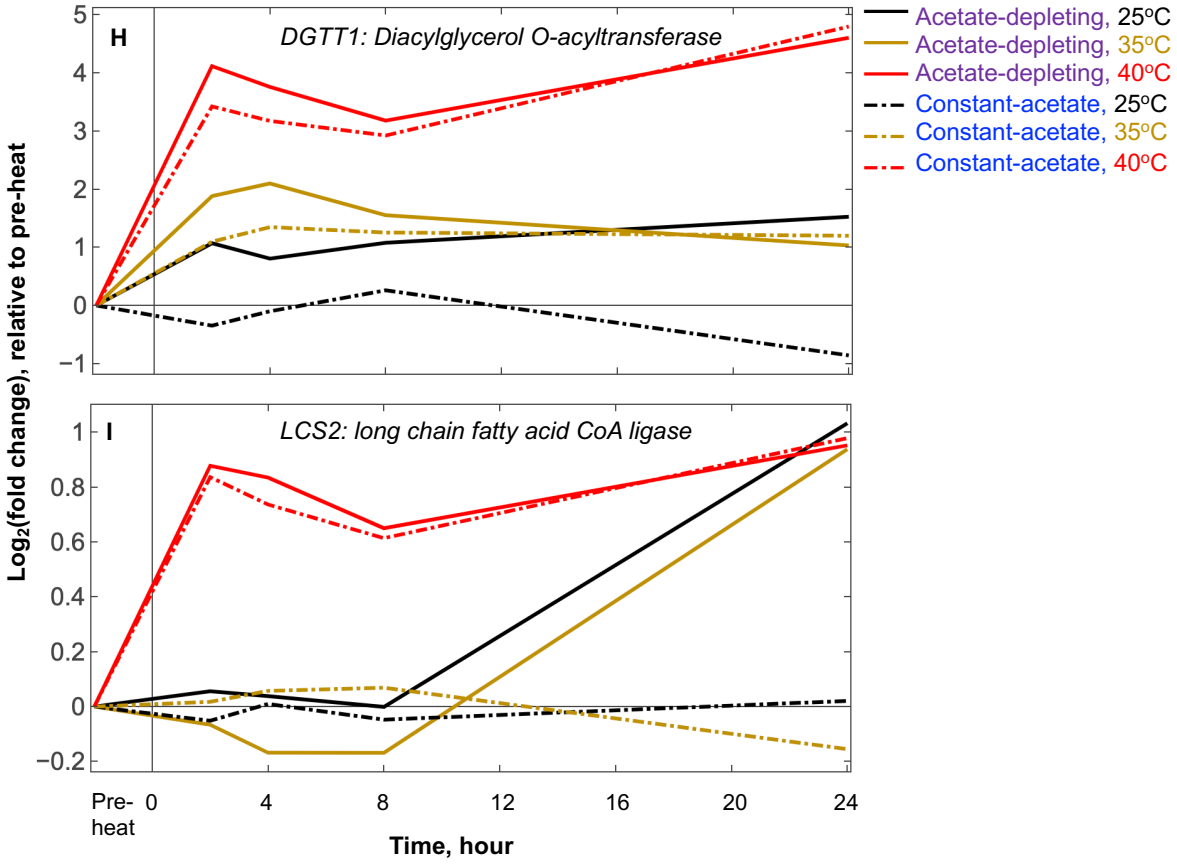

Supplemental Fig. 3. Log_2(fold change) of the indicated transcript relative to pre-heat under different conditions. Log_2(fold change) were determined on the mean normalized transcript abundance, relative to the pre-heat time point. Each line represents one condition as indicated by the legend. The black vertical lines mark the start of heat or the corresponding time point at constant 25ºC. Solid lines for the acetate-depleting condition and dashed lines for the constant-acetate condition. Black, brown, red lines for 25ºC, 35ºC, and 40ºC temperature treatments, respectively. See all gene IDs in Supplemental Table 1 and Supplemental Dataset 1 for bigger pictures and more information.

Supplemental Fig. 4.

A. Transcripts related to HSP60s (HSP, heat shock protein)

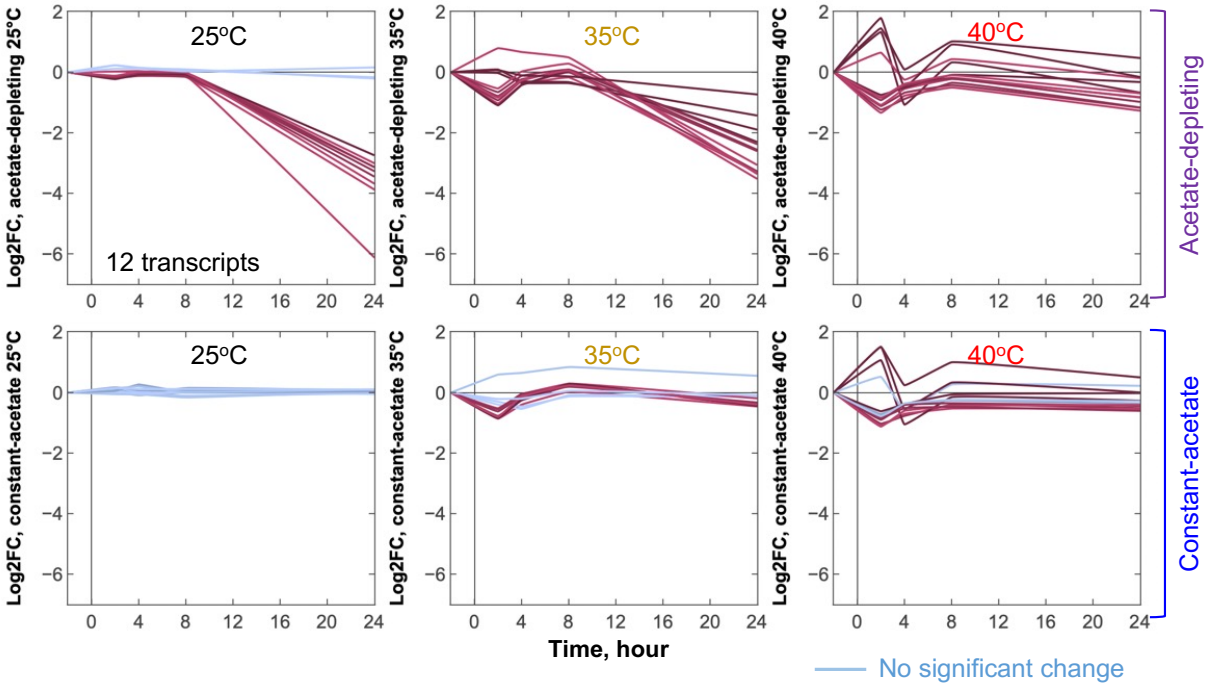

No significant change
Global significant change

B. Transcripts related to HSP70s

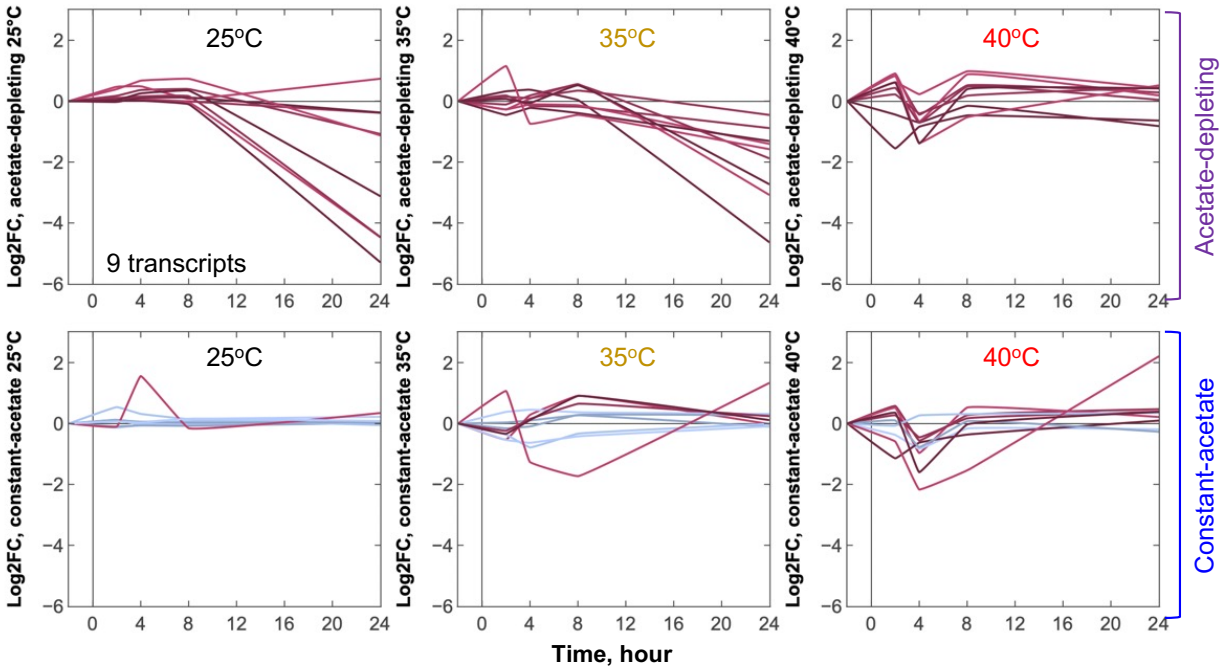

Supplemental Fig. 4. Log_2(fold change, FC) of mean normalized read counts of groups of transcripts based on MapMan function annotation or manual curation. Plots are Log_2FC of transcripts related to the indicated function groups under six different treatments, as compared to the pre-heat time points. RNA-seq data with normalized read counts were used for this analysis. Black vertical lines mark the start of heat treatments or the corresponding time point at constant 25°C. Each line represents one unique transcript in the indicated function group. ANOVA test was applied to the time course (five time points) of one transcript for each condition. If a transcript differed significantly during the time course (or underwent a global significant change) of one condition, it is colored purple (ANOVA significant); blue lines had no significant changes during the time course. Different intensities of purple and blue colors were used to distinguish different transcripts. The total number of transcripts plotted in each function group is marked on the top left panel. See interactive figures with gene IDs and annotations in Supplemental Dataset 2. **See more panels of Supplemental Fig. 4 below.**

Supplemental Fig. 4. continued

C. Transcripts related to HSP90s

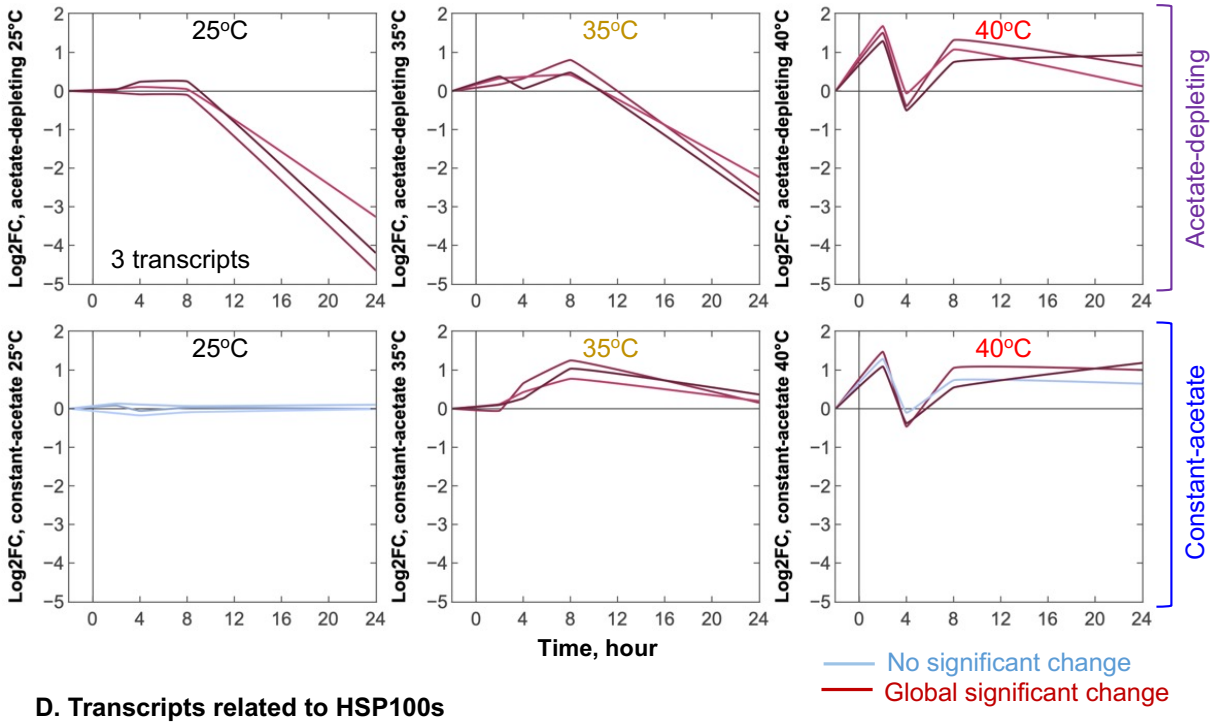

D. Transcripts related to HSP100s

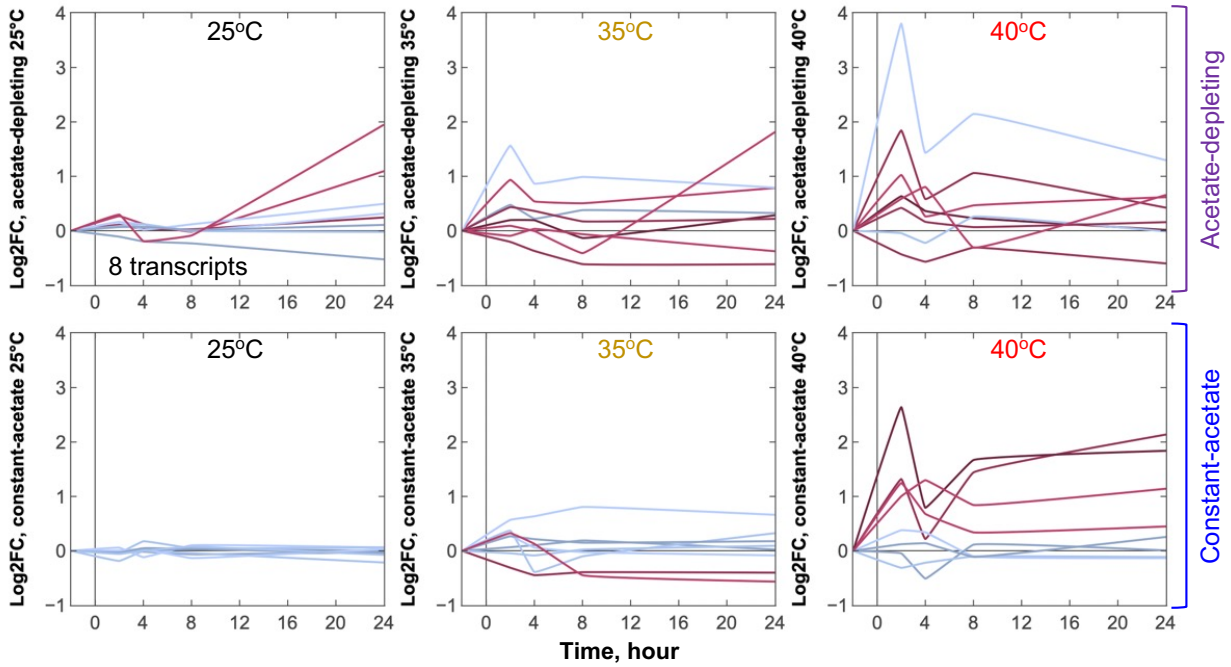

Supplemental Fig. 4. continued

E. Transcripts related to small HSPs

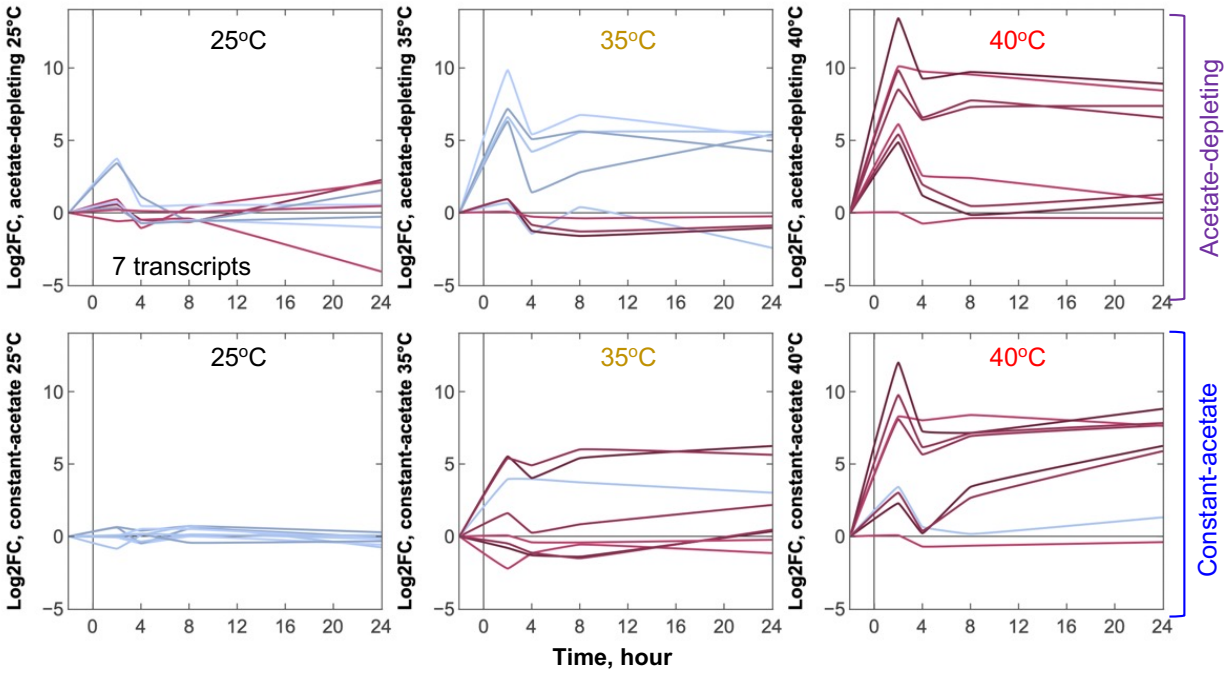

F. Transcripts related to LHCII

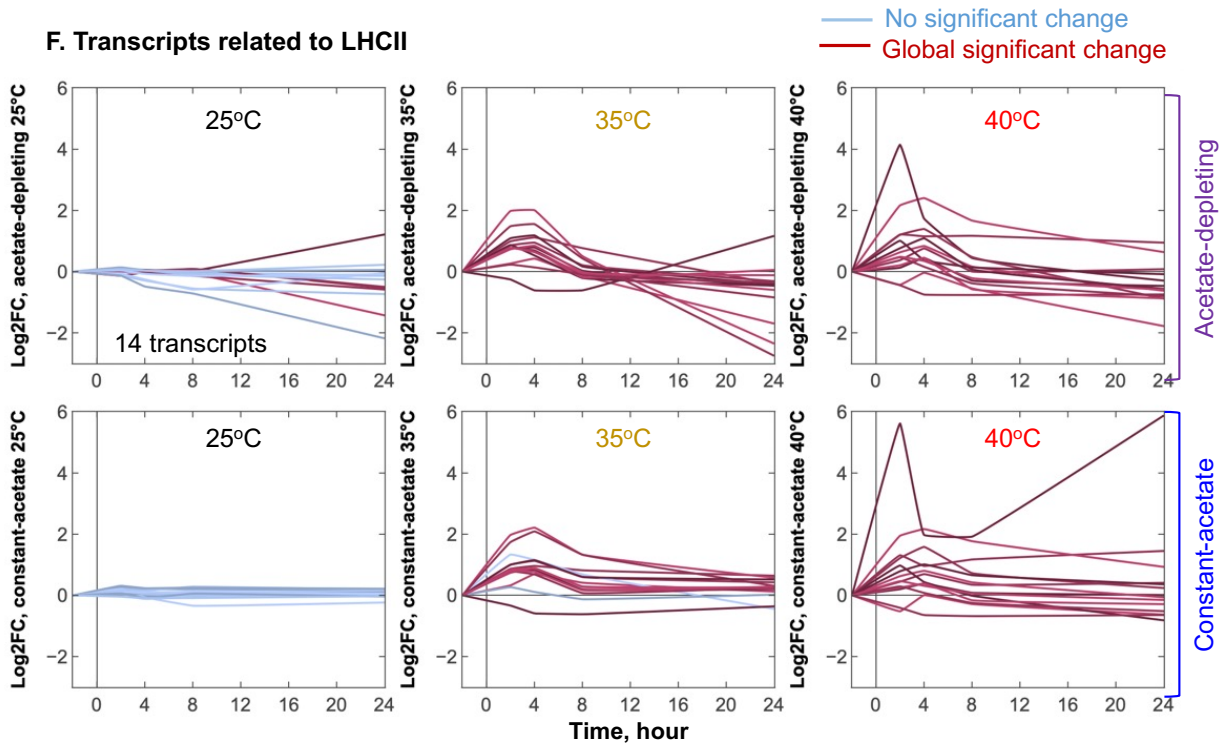

Supplemental Fig. 4. continued

G. Transcripts related to PSII biogenesis

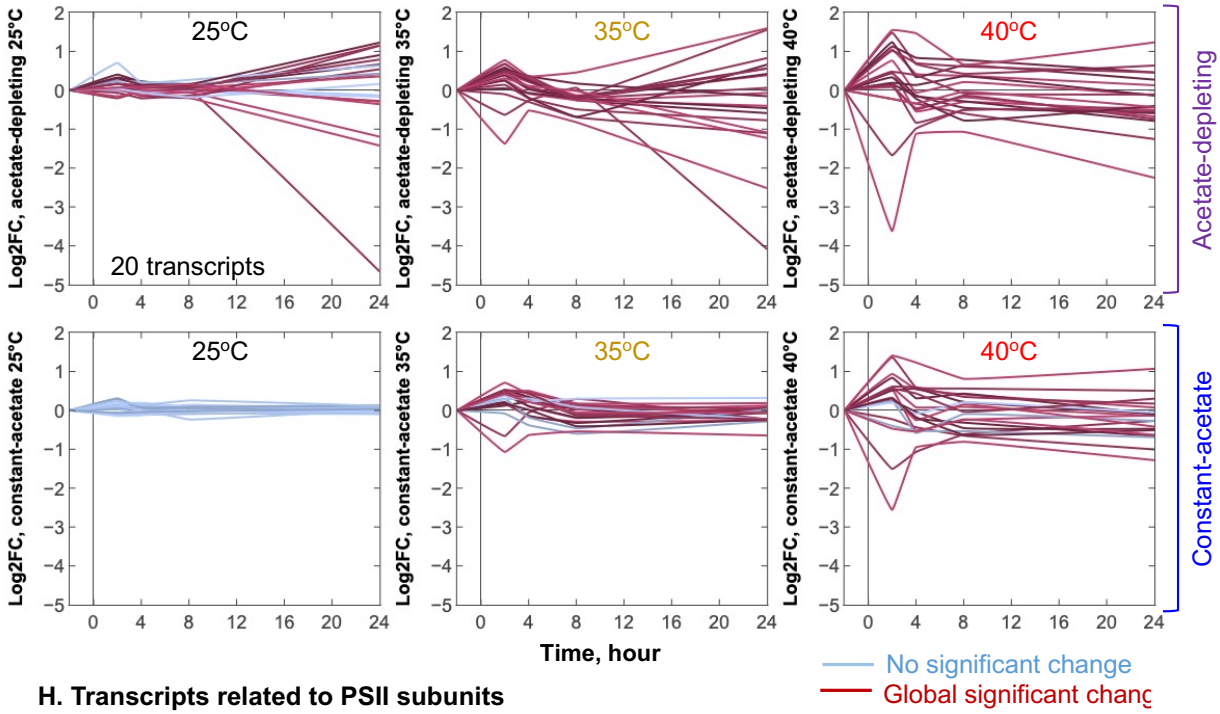

H. Transcripts related to PSII subunits

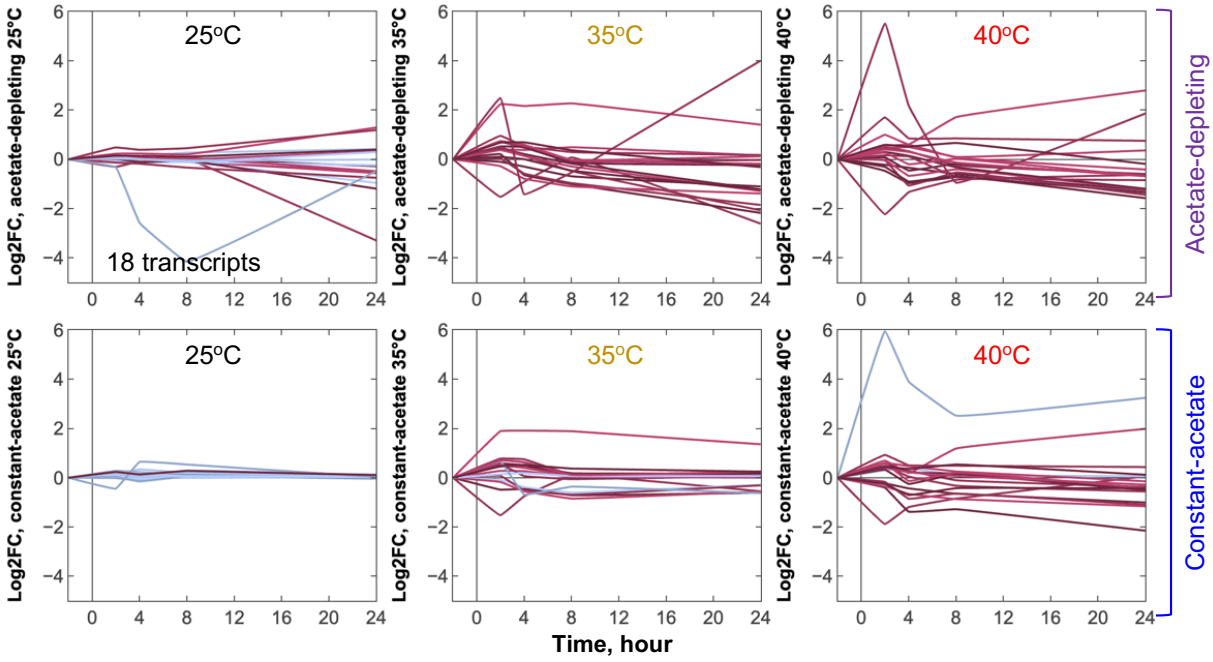

Supplemental Fig. 4. continued

I. Transcripts related to LHCI

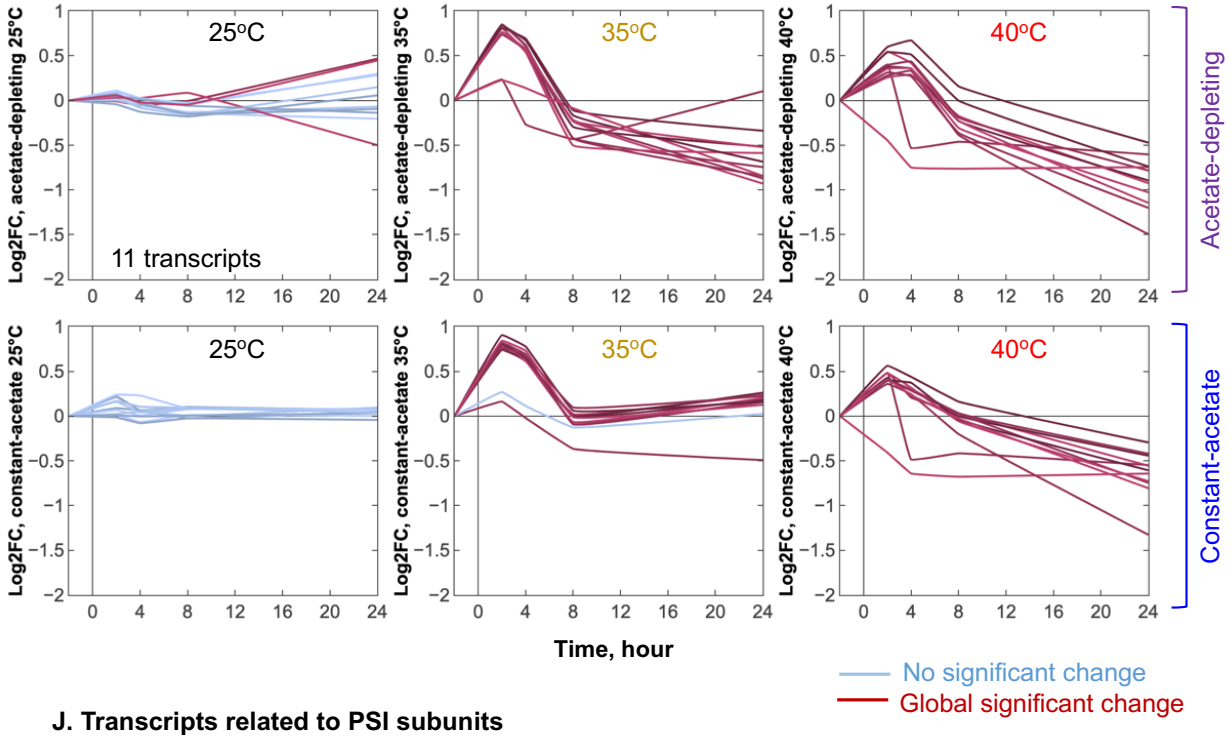

J. Transcripts related to PSI subunits

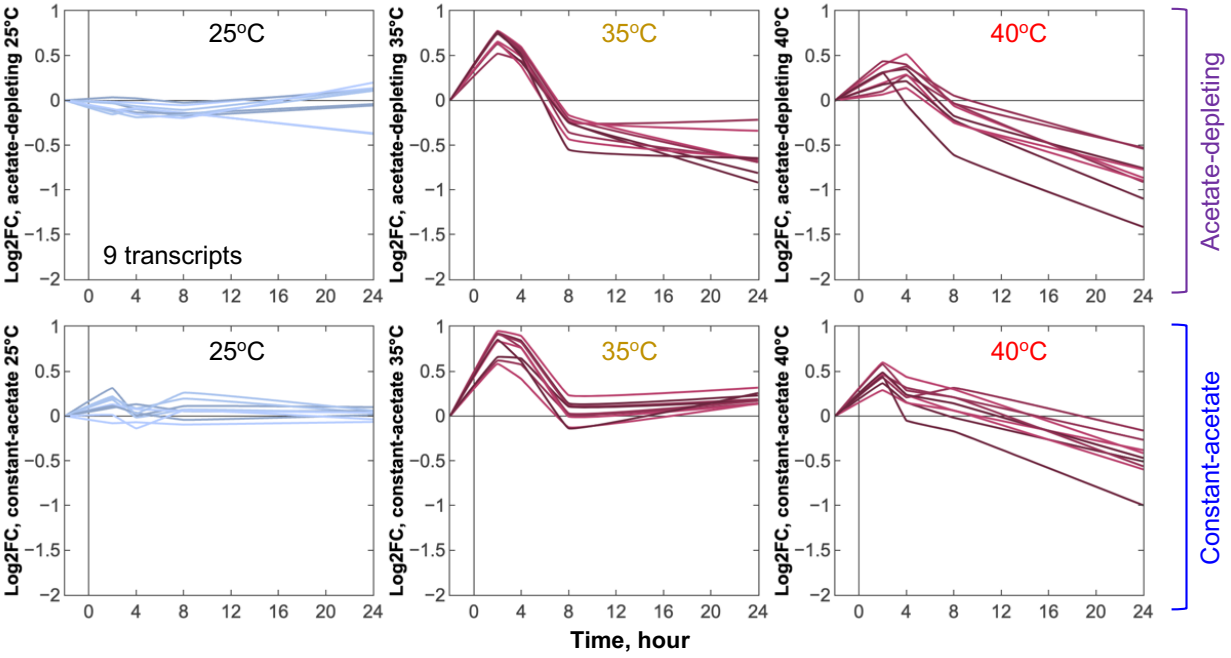

Supplemental Fig. 4. continued

K. Transcripts related to Cytochrome b_6f subunits

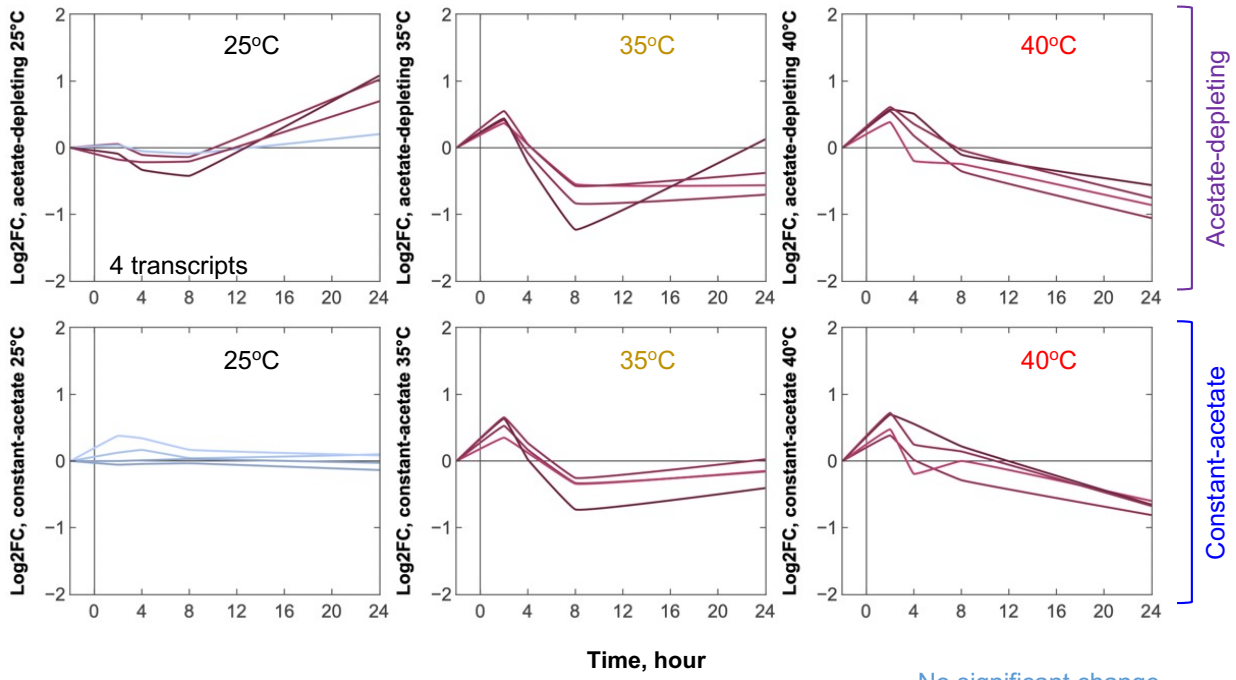

L. Transcripts related to ATP synthase subunits

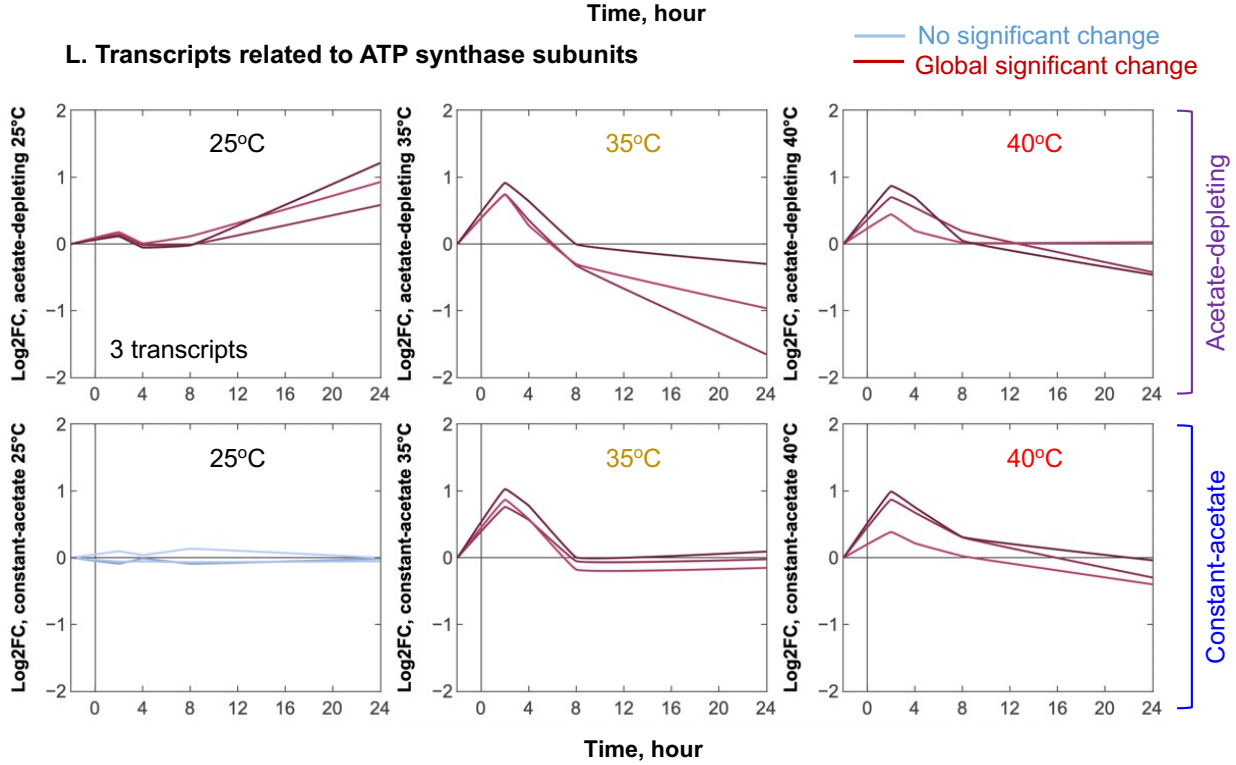

Supplemental Fig. 4. continued

M. Transcripts related to Calvin-Benson cycle

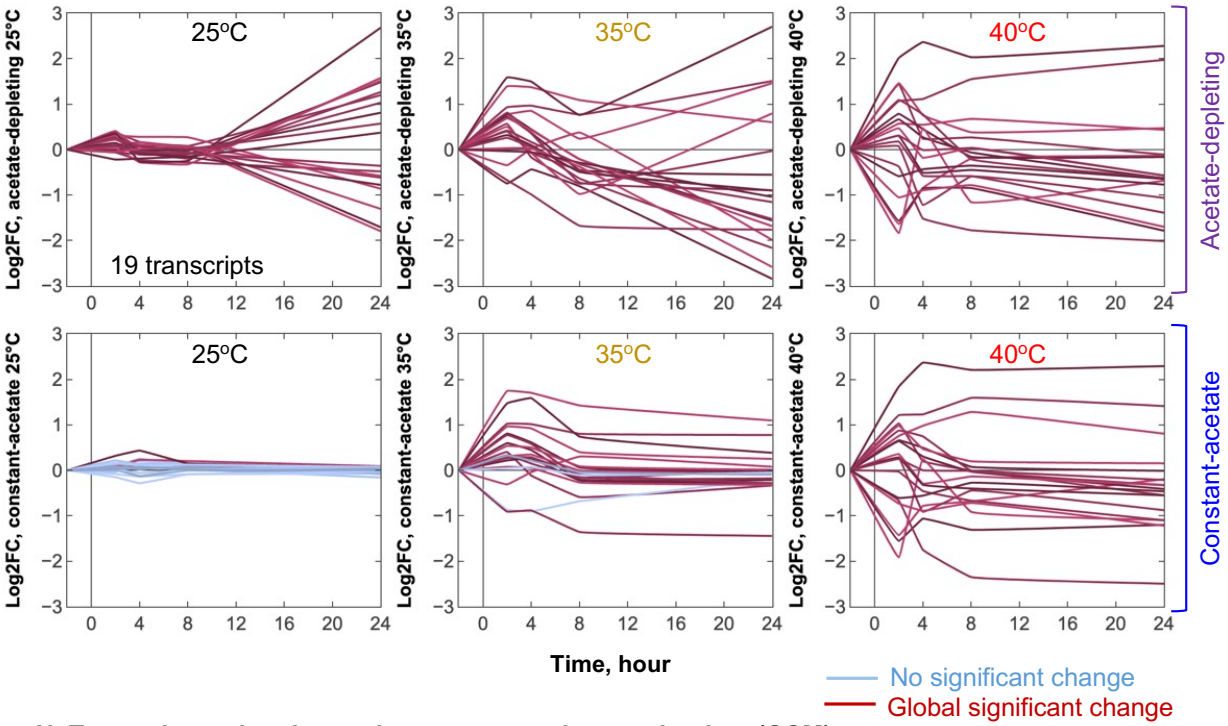

N. Transcripts related to carbon concentrating mechanism (CCM)

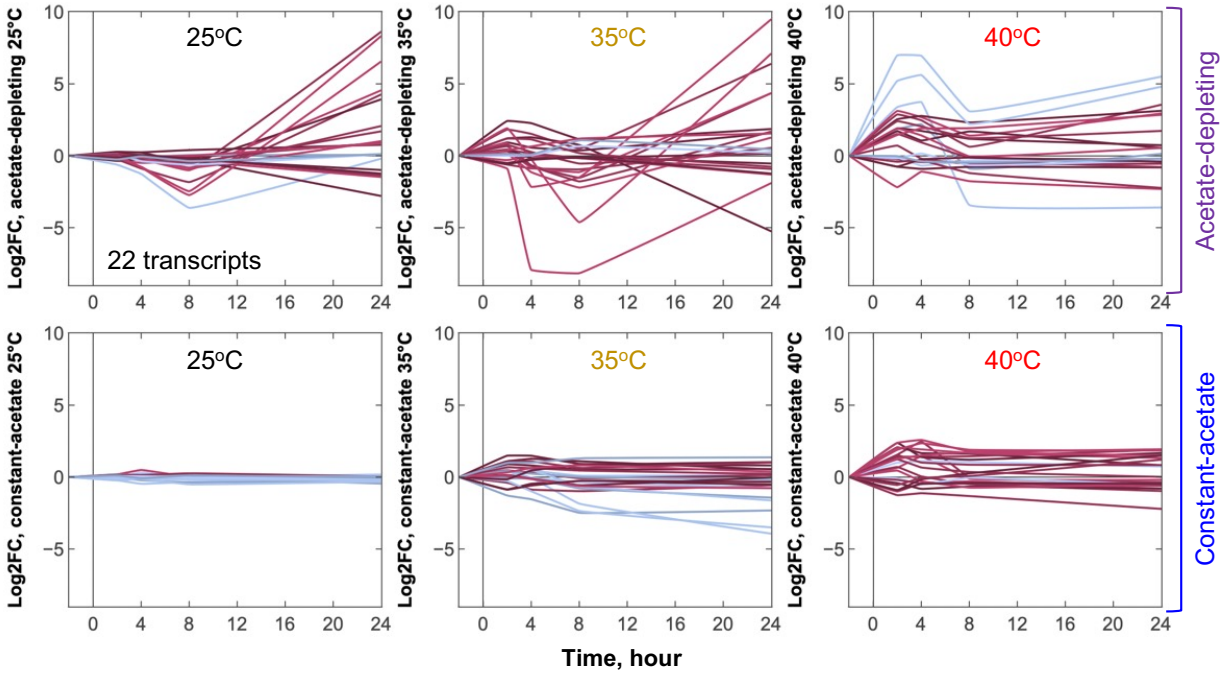

Supplemental Fig. 4. continued

O. Transcripts related to photoprotection

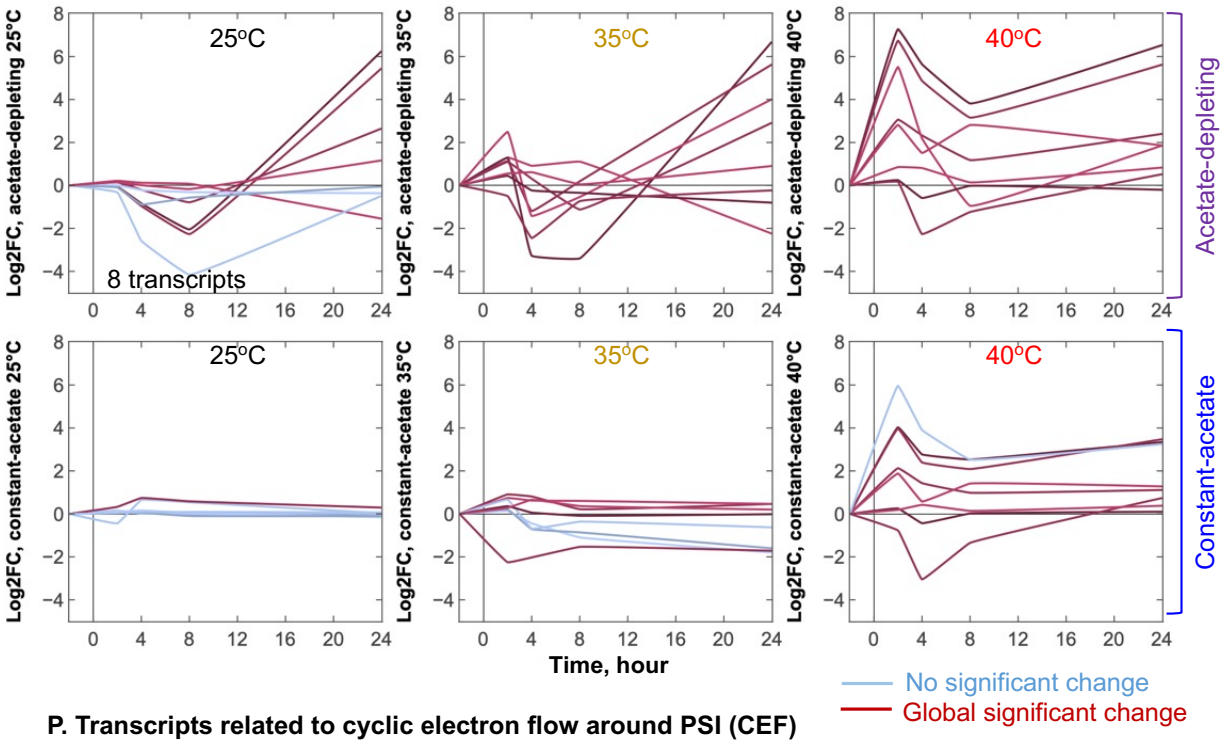

P. Transcripts related to cyclic electron flow around PSI (CEF)

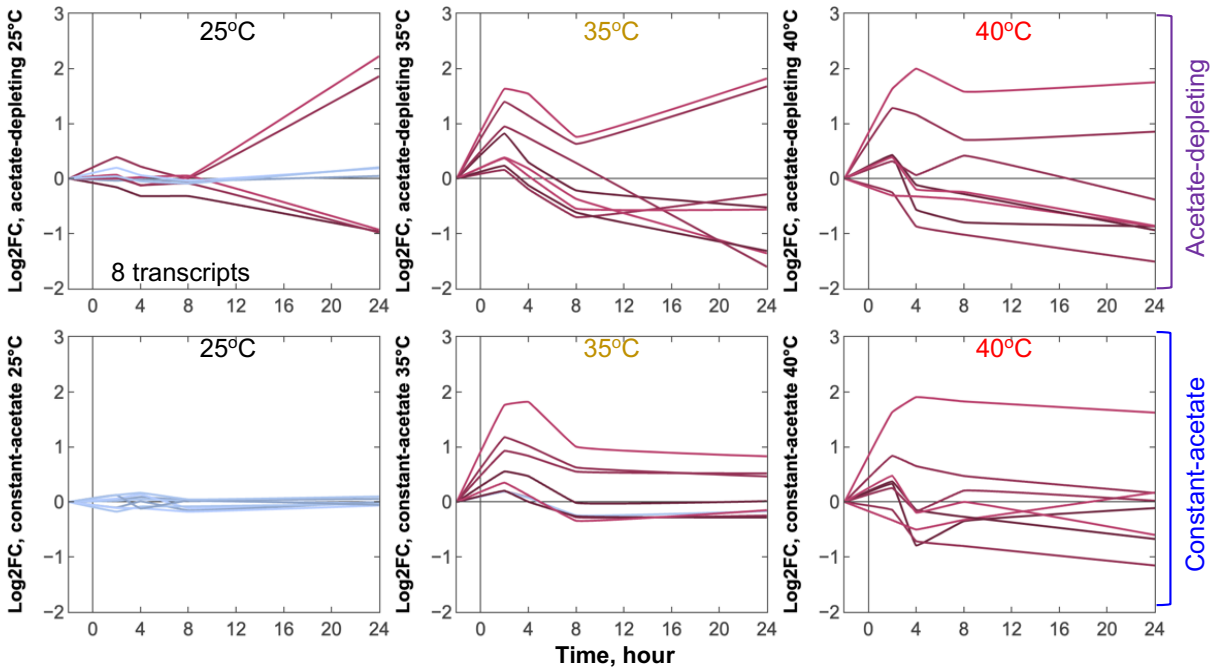

Supplemental Fig. 4. continued

Q. Transcripts related to chlorophyll biosynthesis

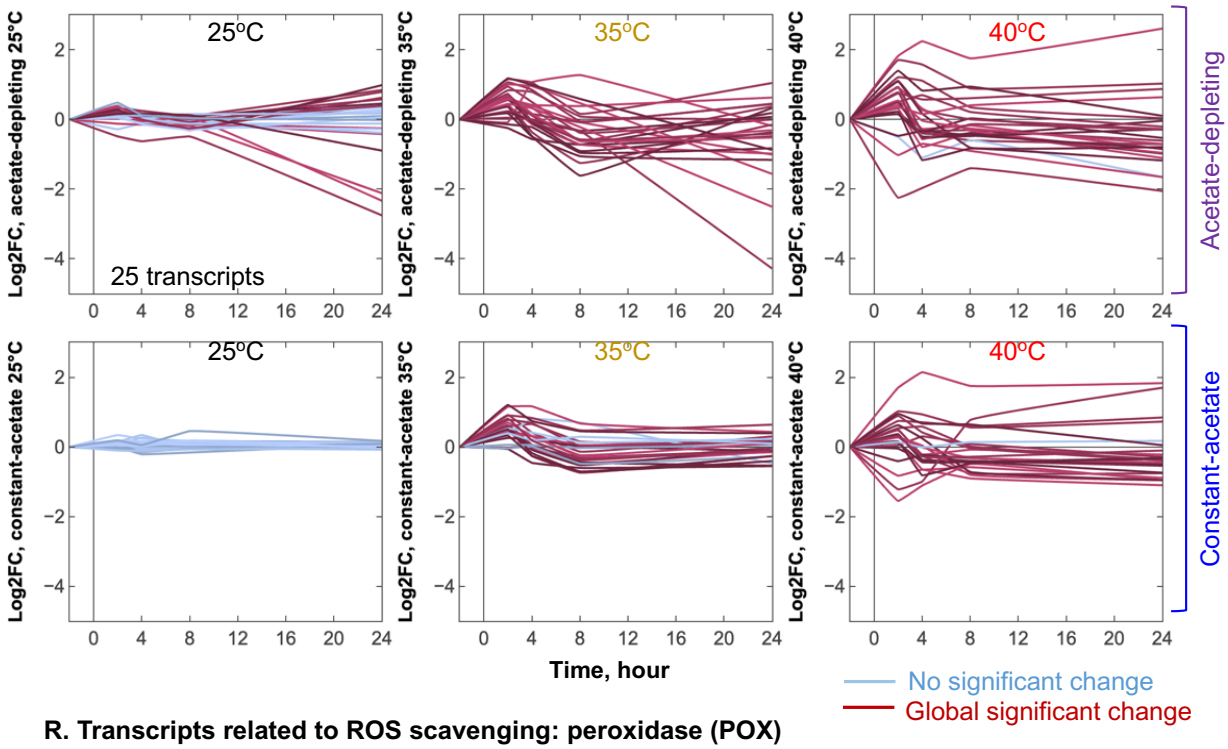

R. Transcripts related to ROS scavenging: peroxidase (POX)

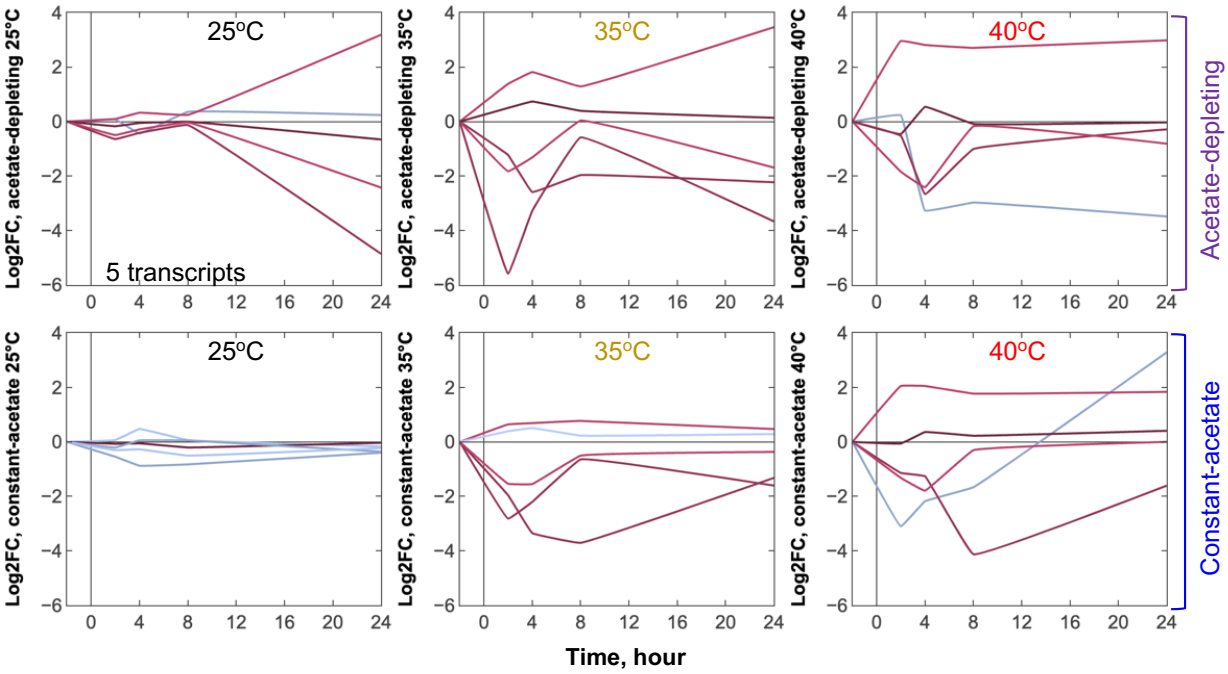

Supplemental Fig. 4. continued

S. Transcripts related to ROS scavenging: ascorbate peroxidase (APX)

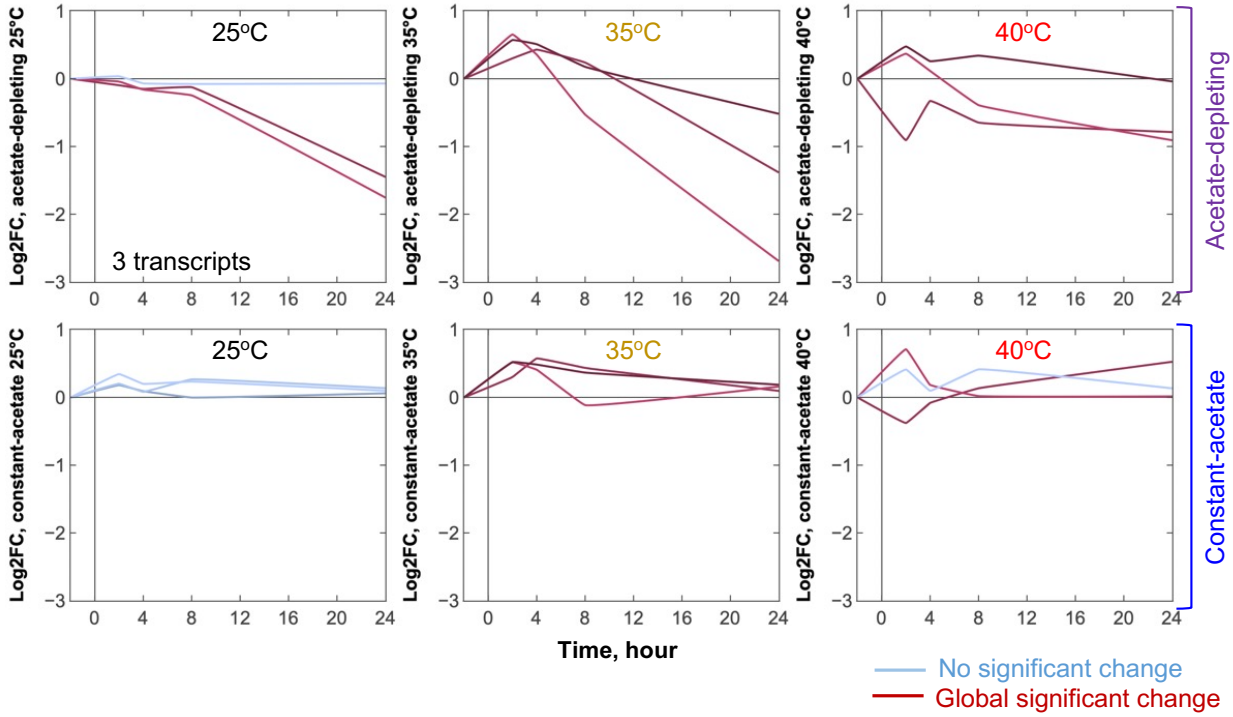

T. Transcripts related to ROS scavenging: catalase (CAT)

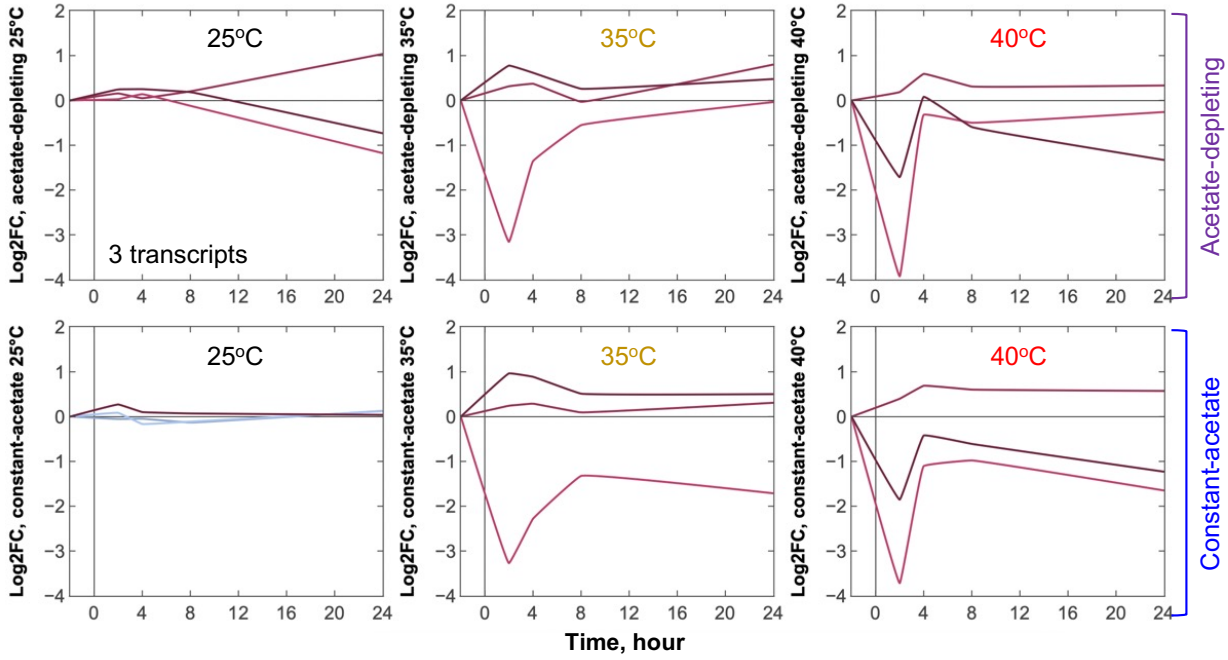

Supplemental Fig. 4. continued

U. Transcripts related to ROS scavenging: glutathione reductase (GR)

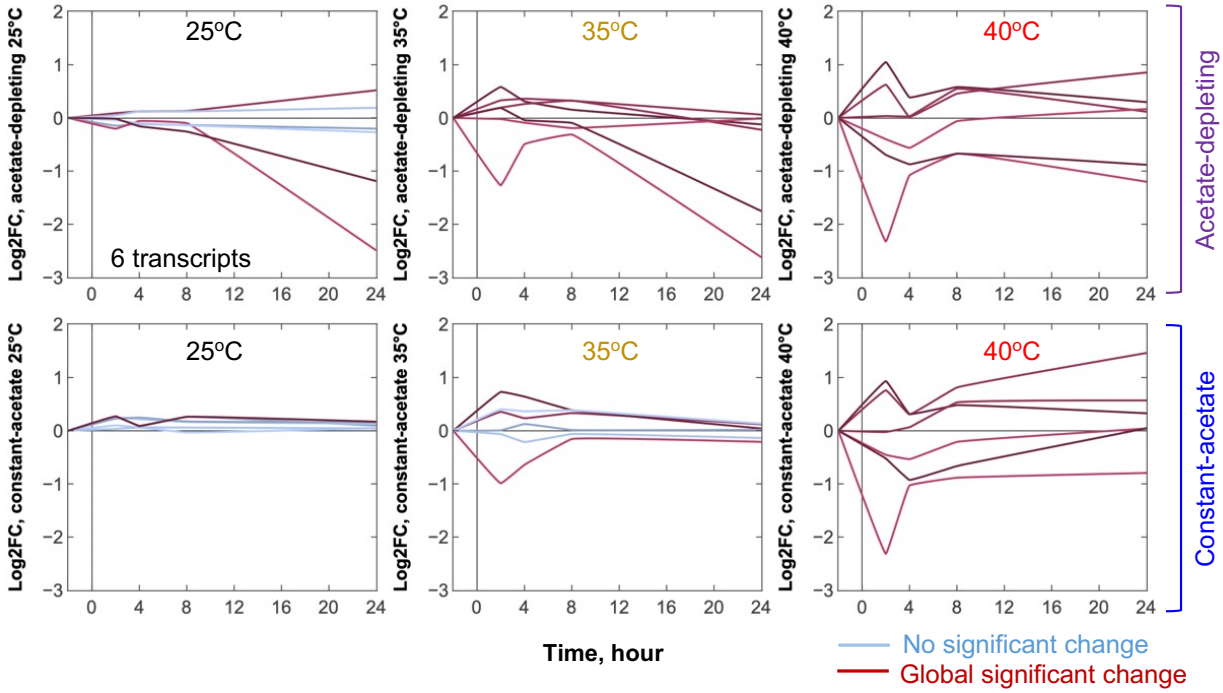

V. Transcripts related to ROS scavenging: glutathione S-transferase (GST)

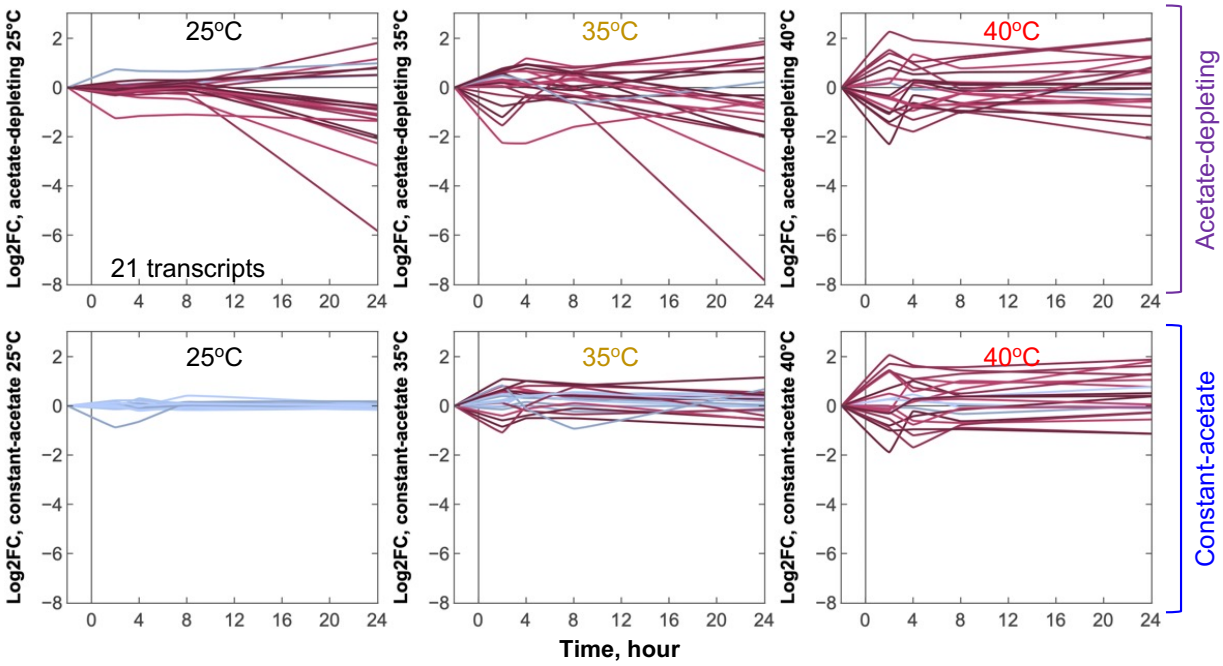

Supplemental Fig. 4. Continued

W. Transcripts related to cell cycle

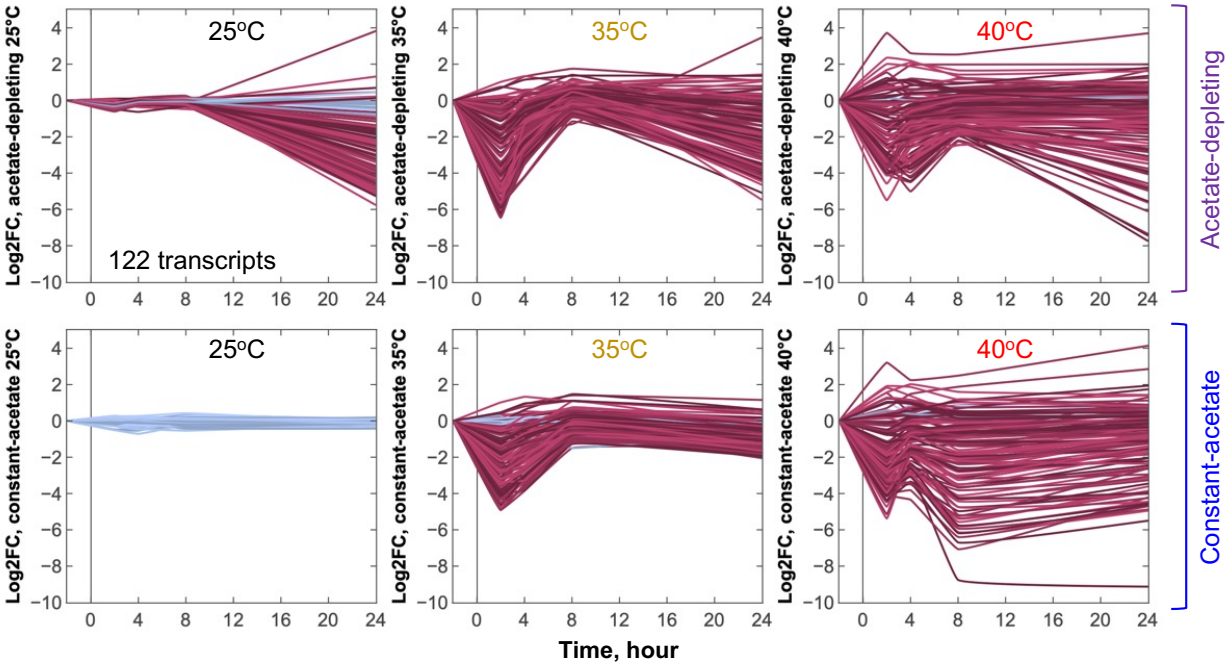

No significant change
Global significant change

X. Transcripts related to cell wall

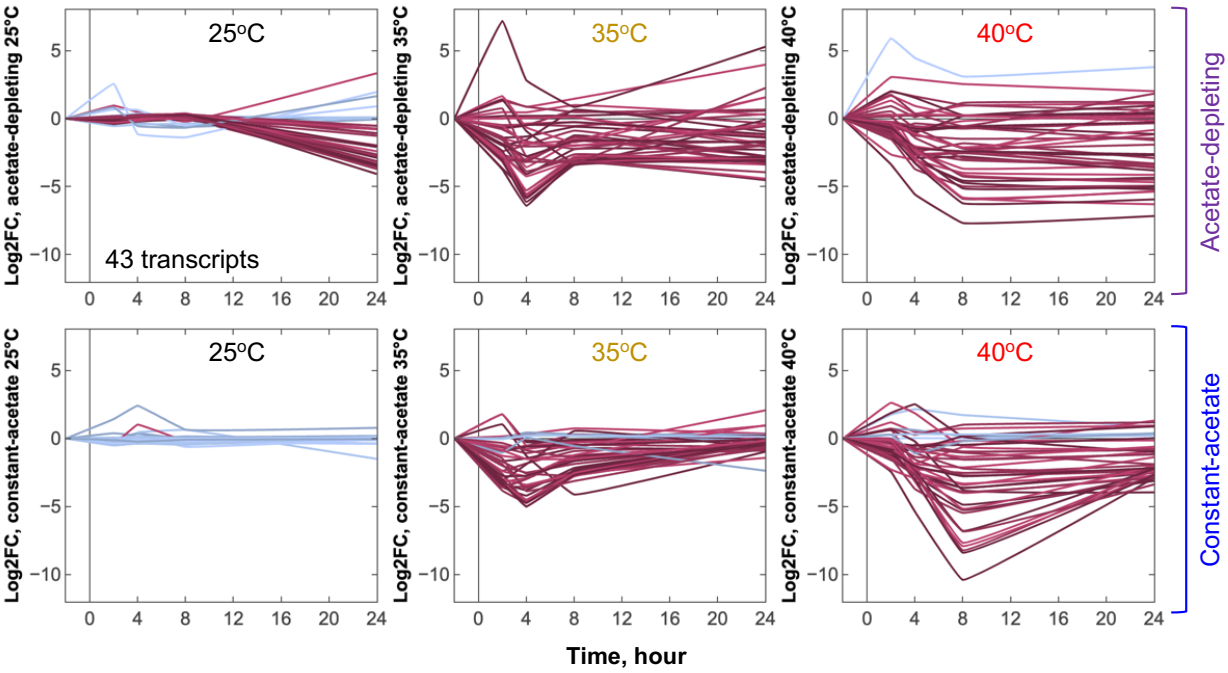

Supplemental Fig. 4. Continued

Y. Transcripts related to protein synthesis, ribosomal protein, prokaryotic

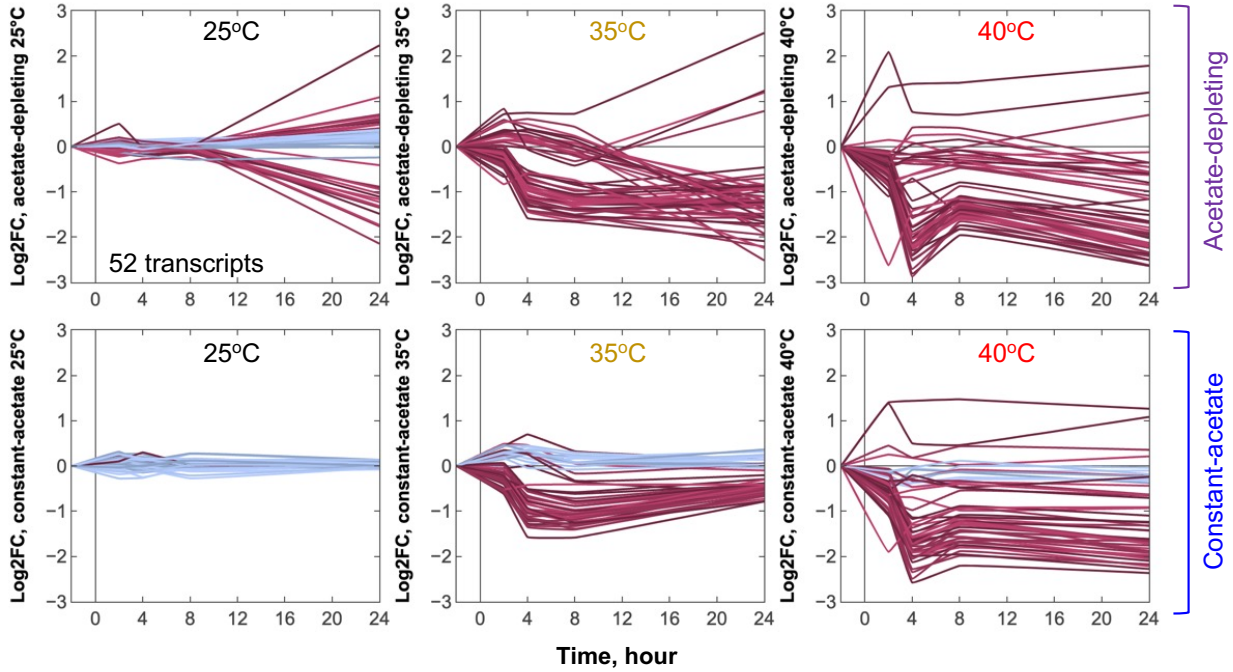

Z. Transcripts related to protein synthesis, ribosomal protein, chloroplast

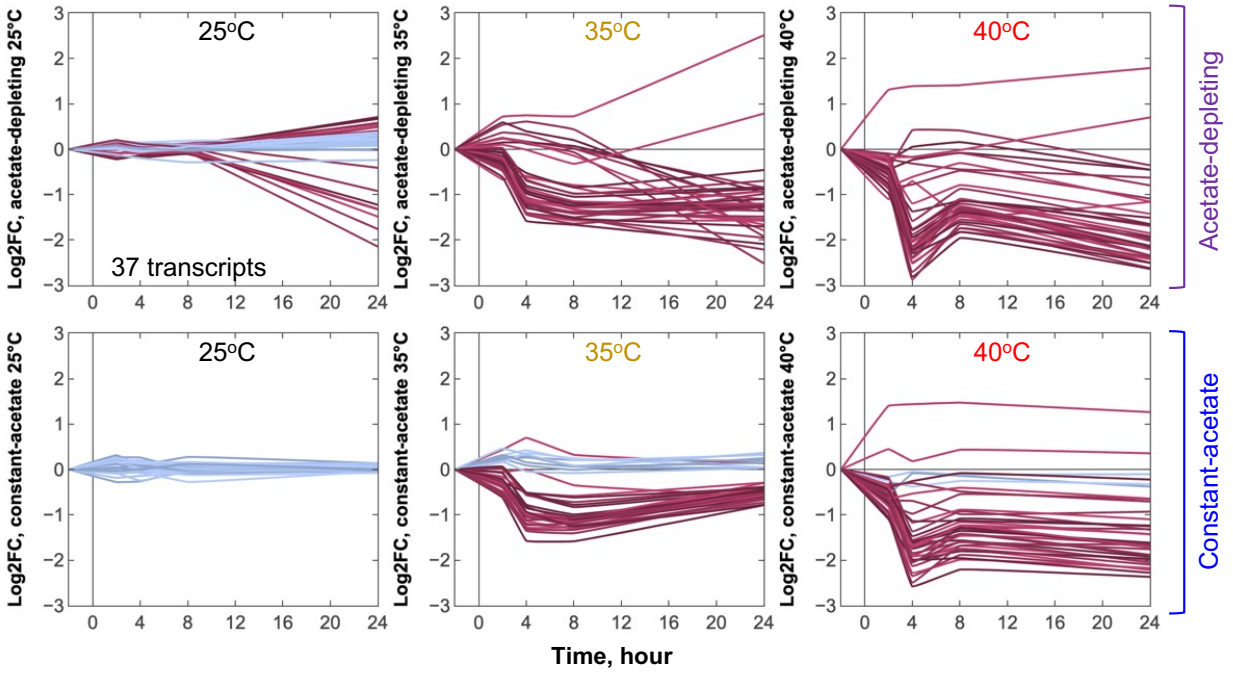

Supplemental Fig. 4. Continued

AA. Transcripts related to mitochondrial electron transport / ATP synthesis (F1-ATPase)

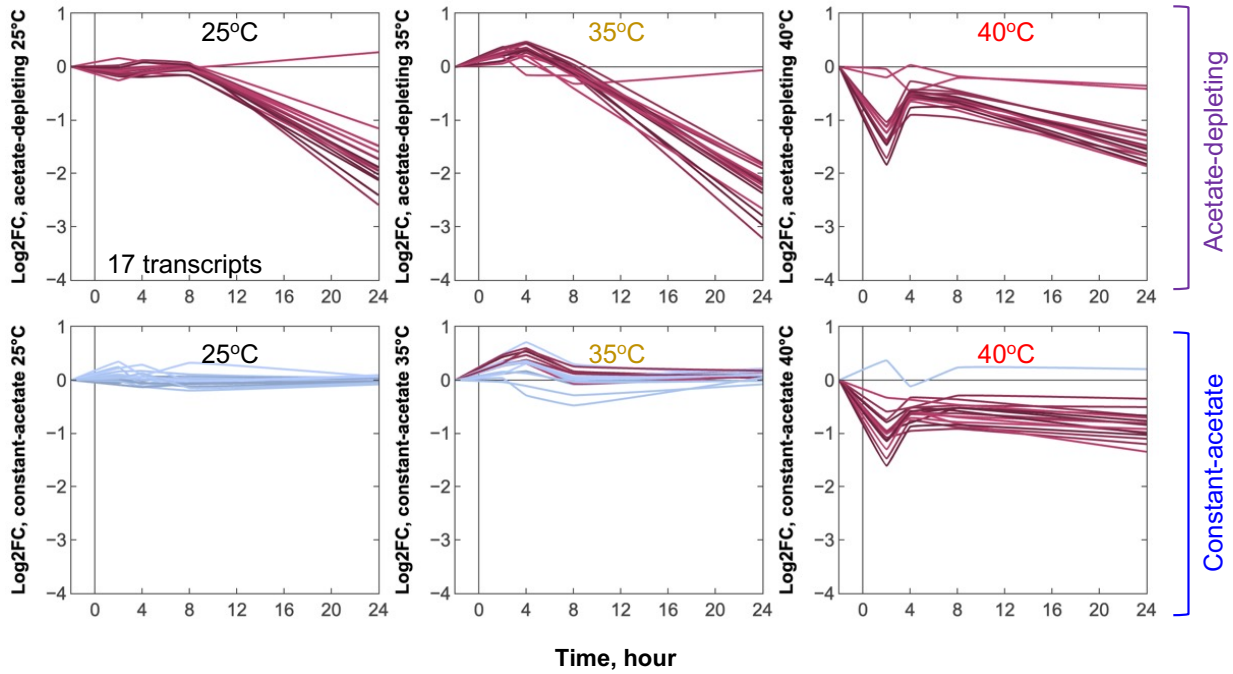

AB. Transcripts related to mitochondrial electron transport / ATP synthesis

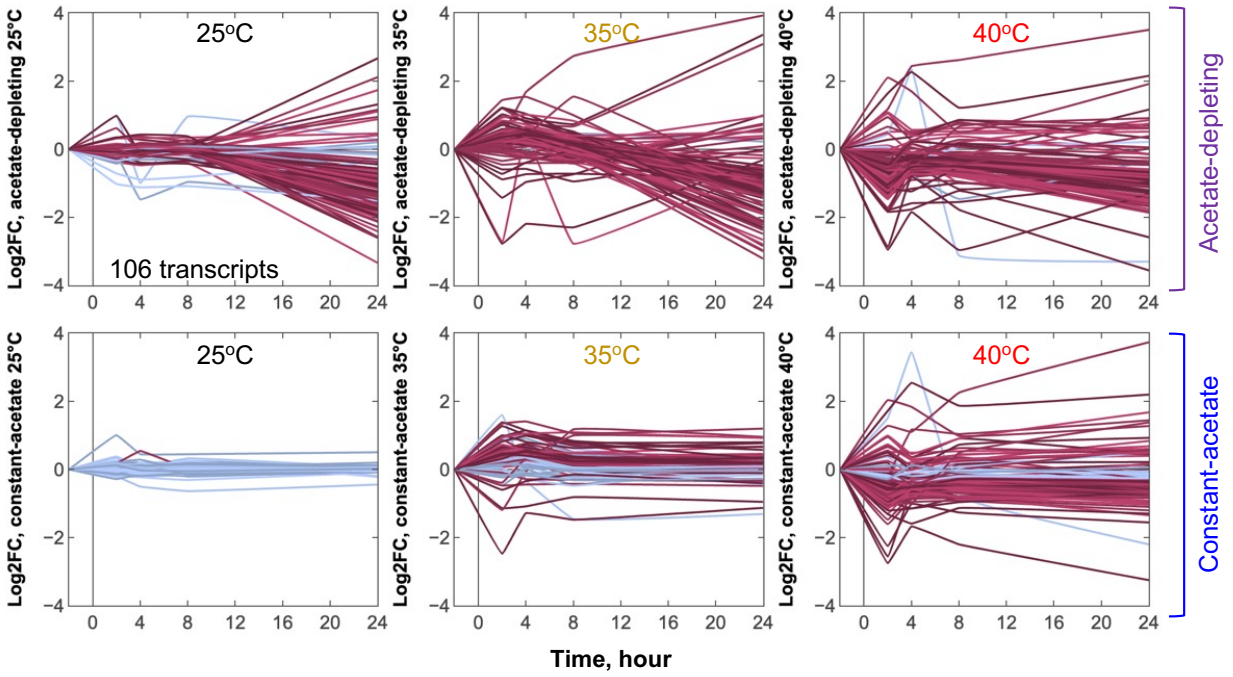

Supplemental Fig. 4. Continued

AC. Transcripts related to RNA

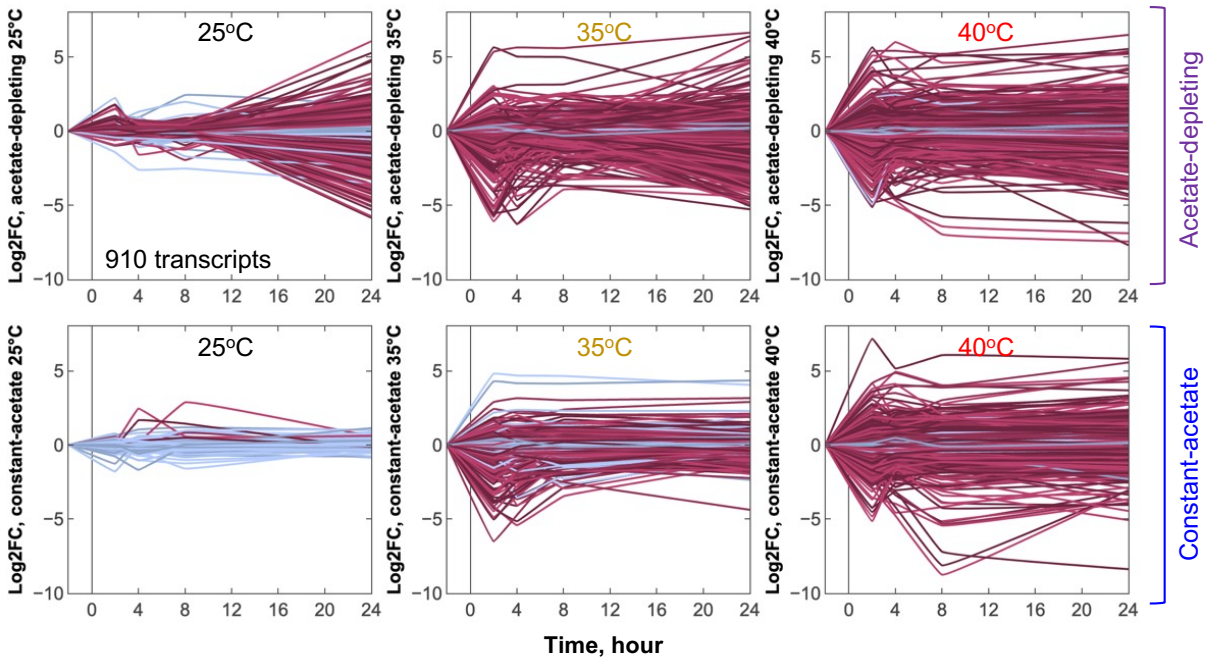

AD. Transcripts related to RNA processing

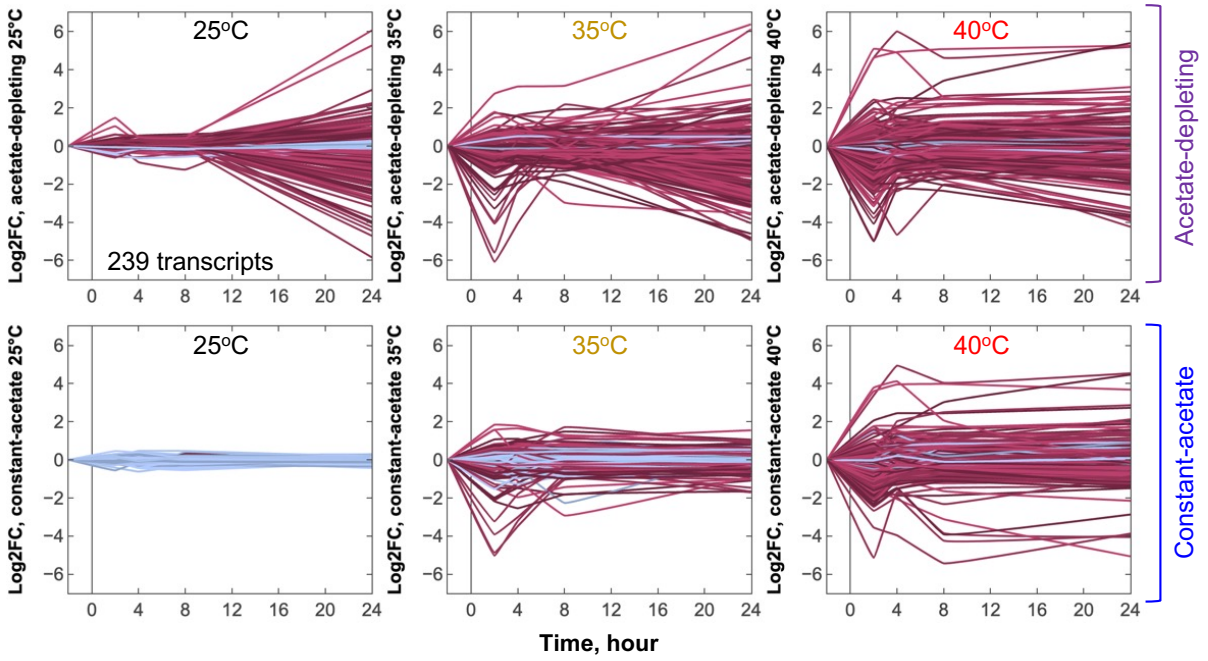

Supplemental Fig. 4. Continued

AE. Transcripts related to transport. phosphate

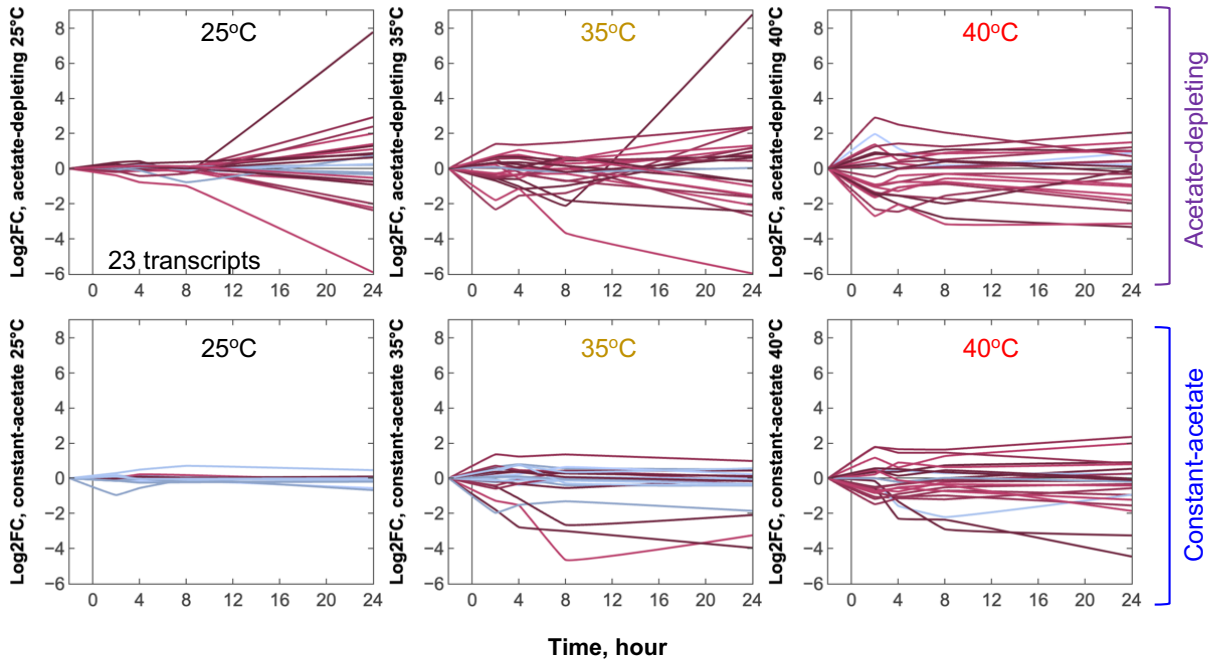

AF. Transcripts related to signaling. mitogen-activated protein kinase (MAP kinase)

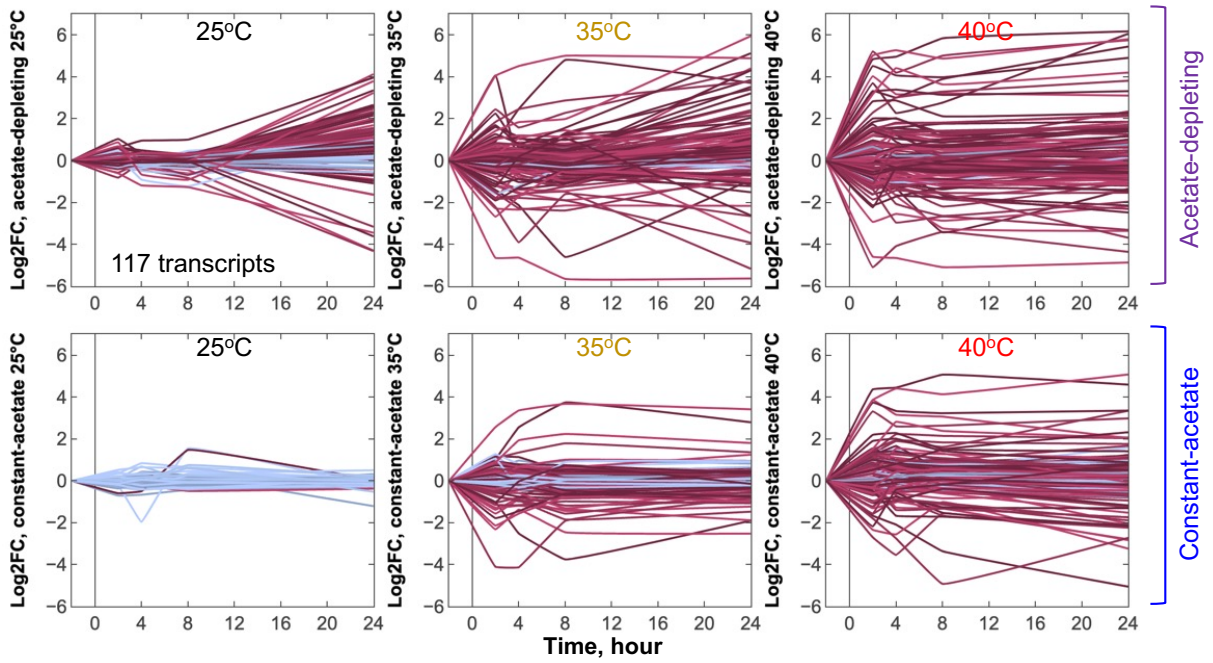

Supplemental Fig. 4. Continued

AG. Transcripts related to cell motility. eukaryotes. axonemal dyneins

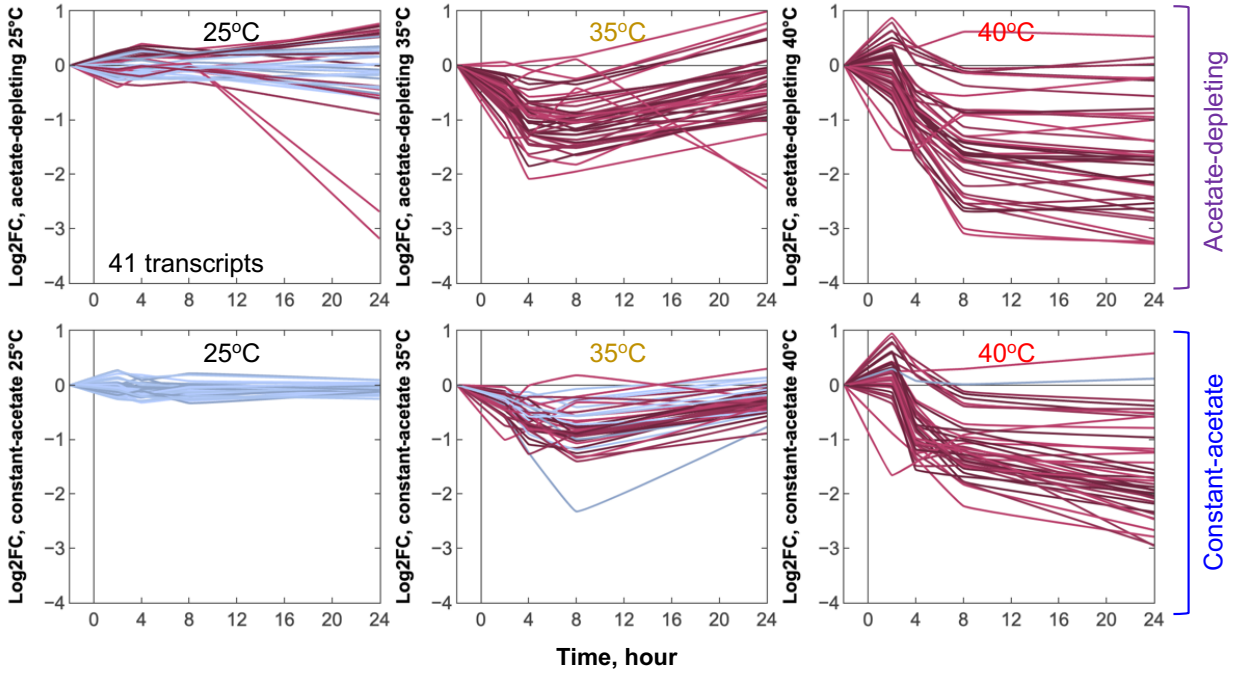

AH. Transcripts related to cell motility

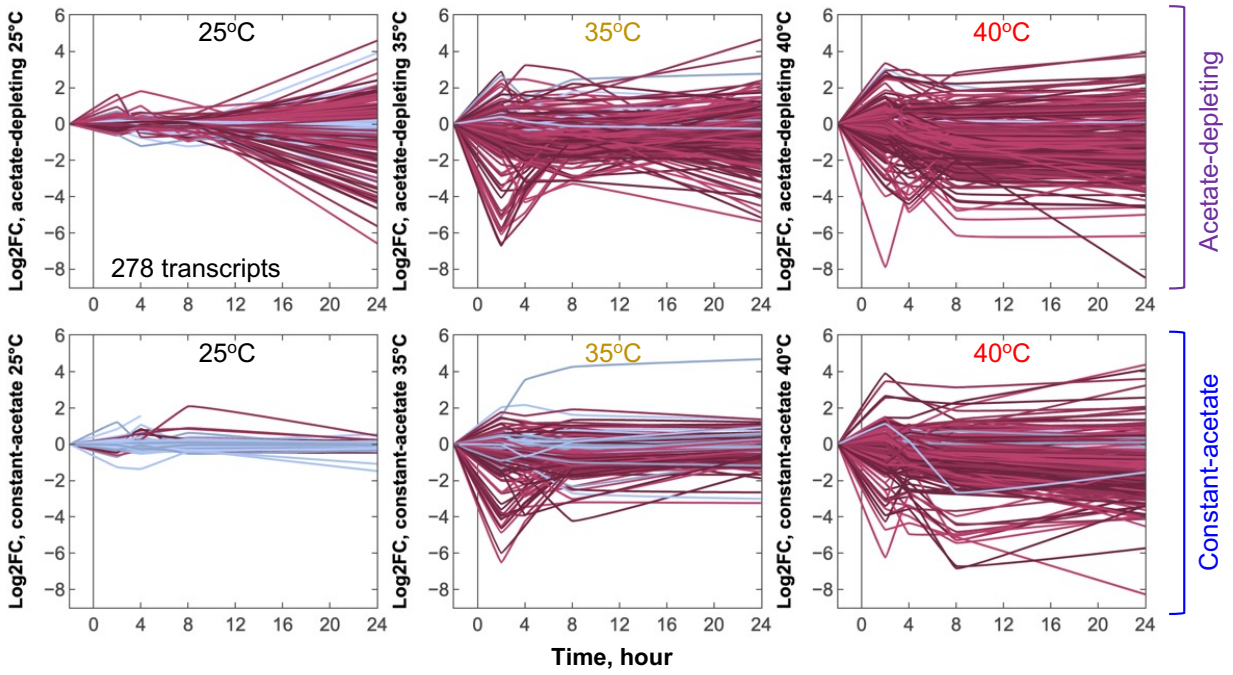

Supplemental Fig. 4. Log_2(fold change, FC) of mean normalized read counts of groups of transcripts based on MapMan function annotation or manual curation. Plots are Log_2FC of transcripts related to the indicated function groups under six different treatments, as compared to the pre-heat time points. RNA-seq data with normalized read counts were used for this analysis. Black vertical lines mark the start of heat treatments or the corresponding time point at constant 25°C. Each line represents one unique transcript in the indicated function group. ANOVA test was applied to the time course (five time points) of one transcript for each condition. If a transcript differed significantly during the time course (or underwent a global significant change) of one condition, it is colored purple (ANOVA significant); blue lines had no significant changes during the time course. Different intensities of purple and blue colors were used to distinguish different transcripts. The total number of transcripts plotted in each function group is marked on the top left panel. See interactive figures with gene IDs and annotations in Supplemental Dataset 2.

Supplemental Fig. 5A

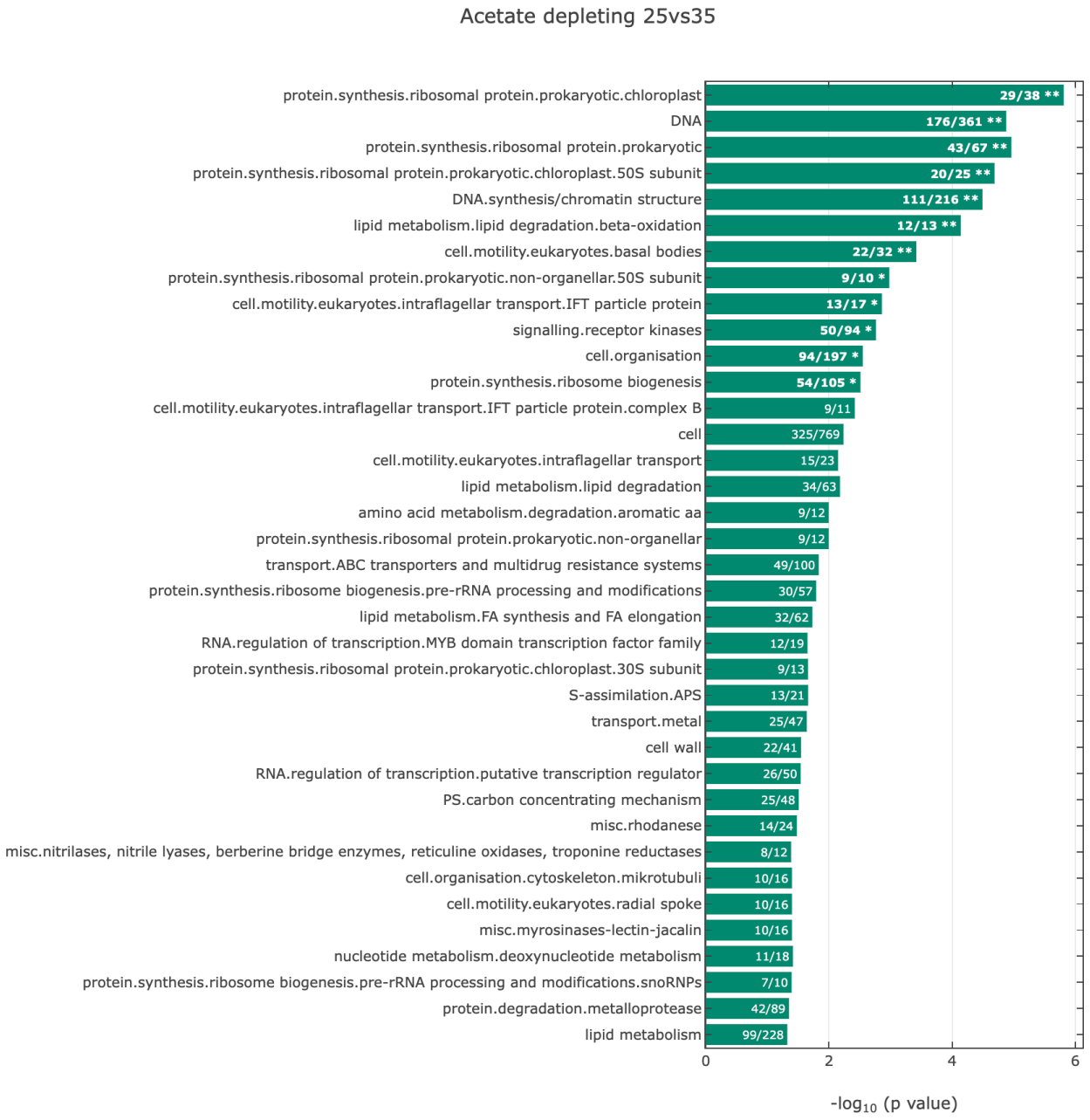

Supplemental Fig. 5B

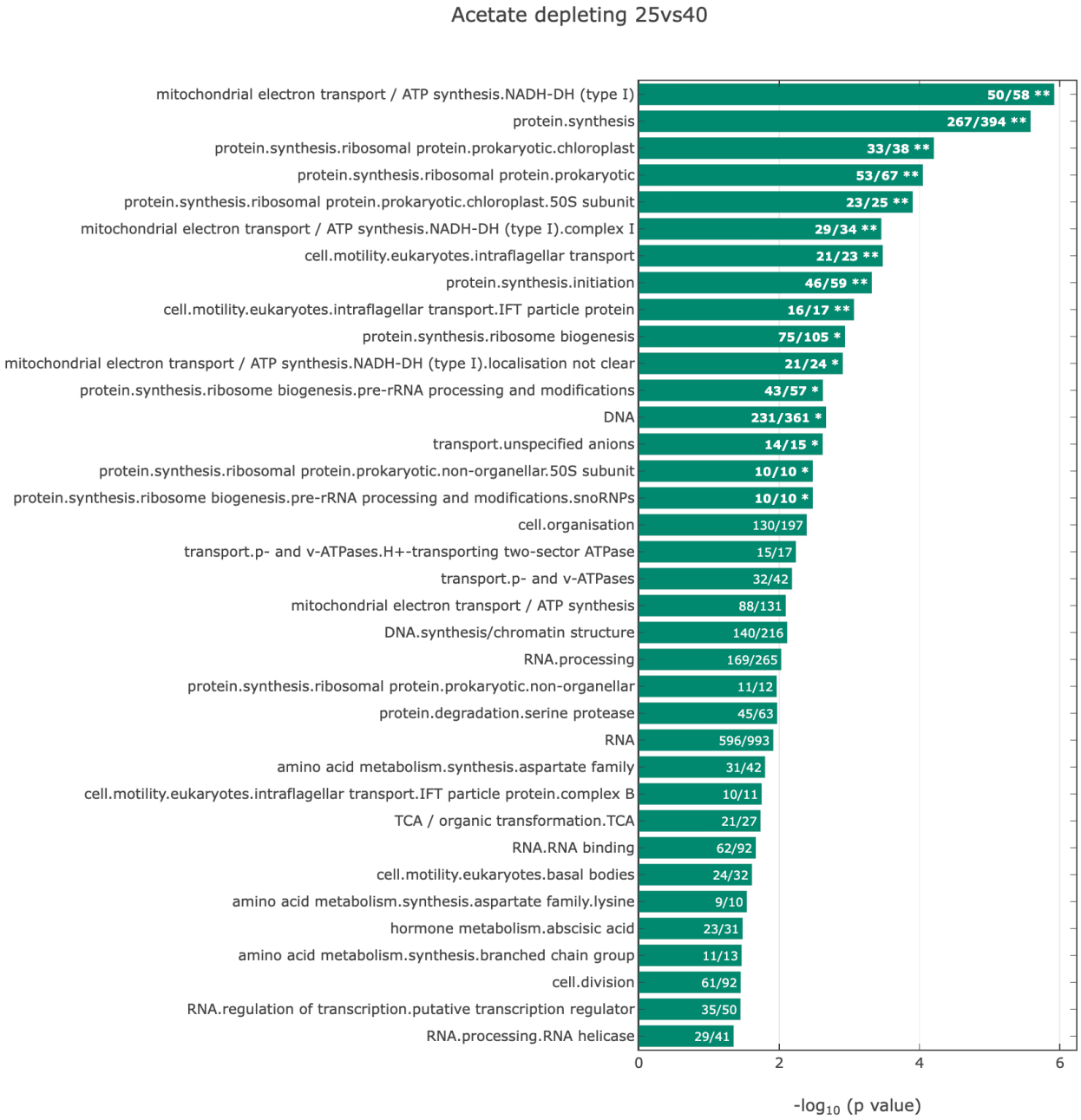

Supplemental Fig. 5C

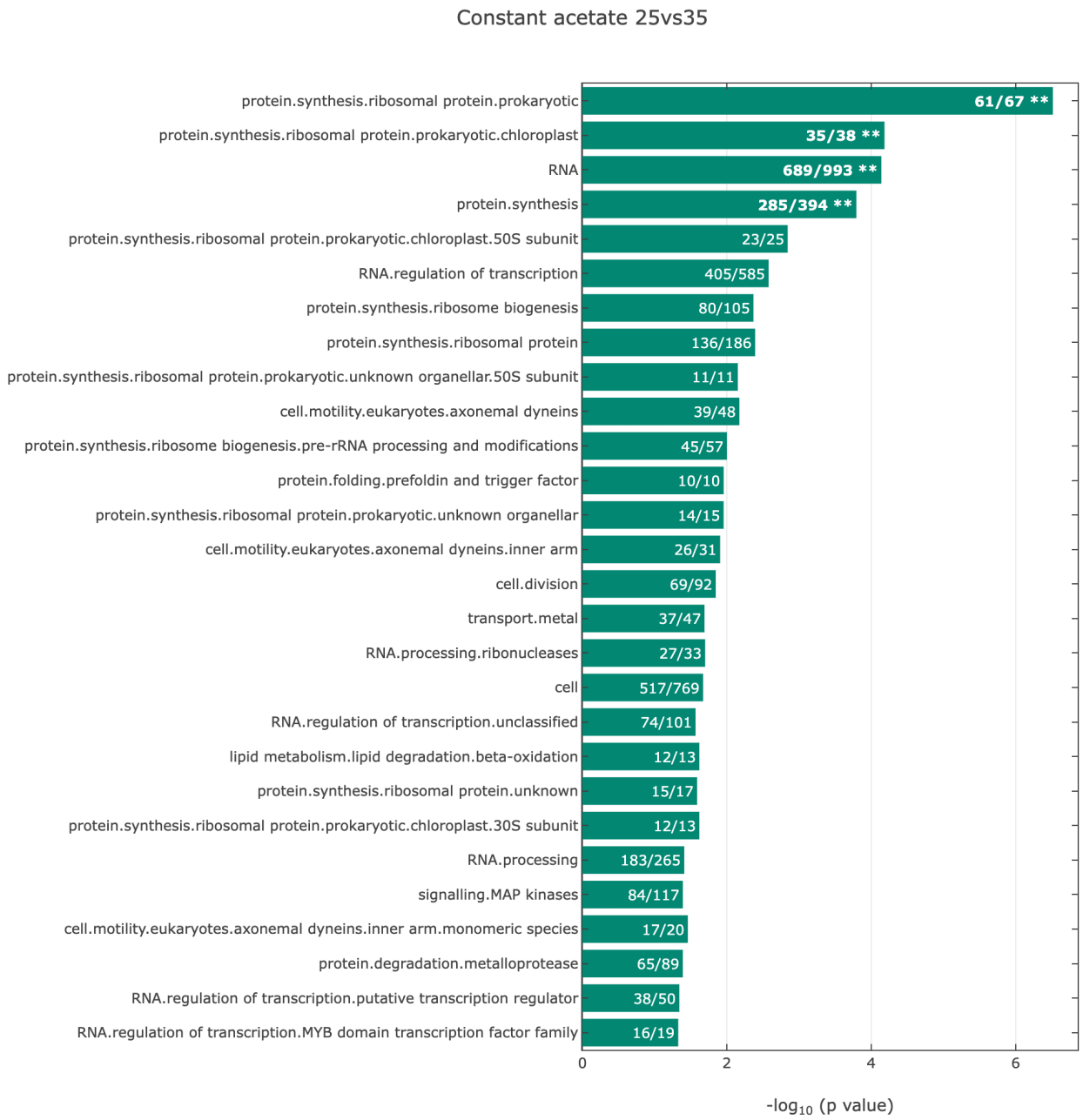

Supplemental Fig. 5D

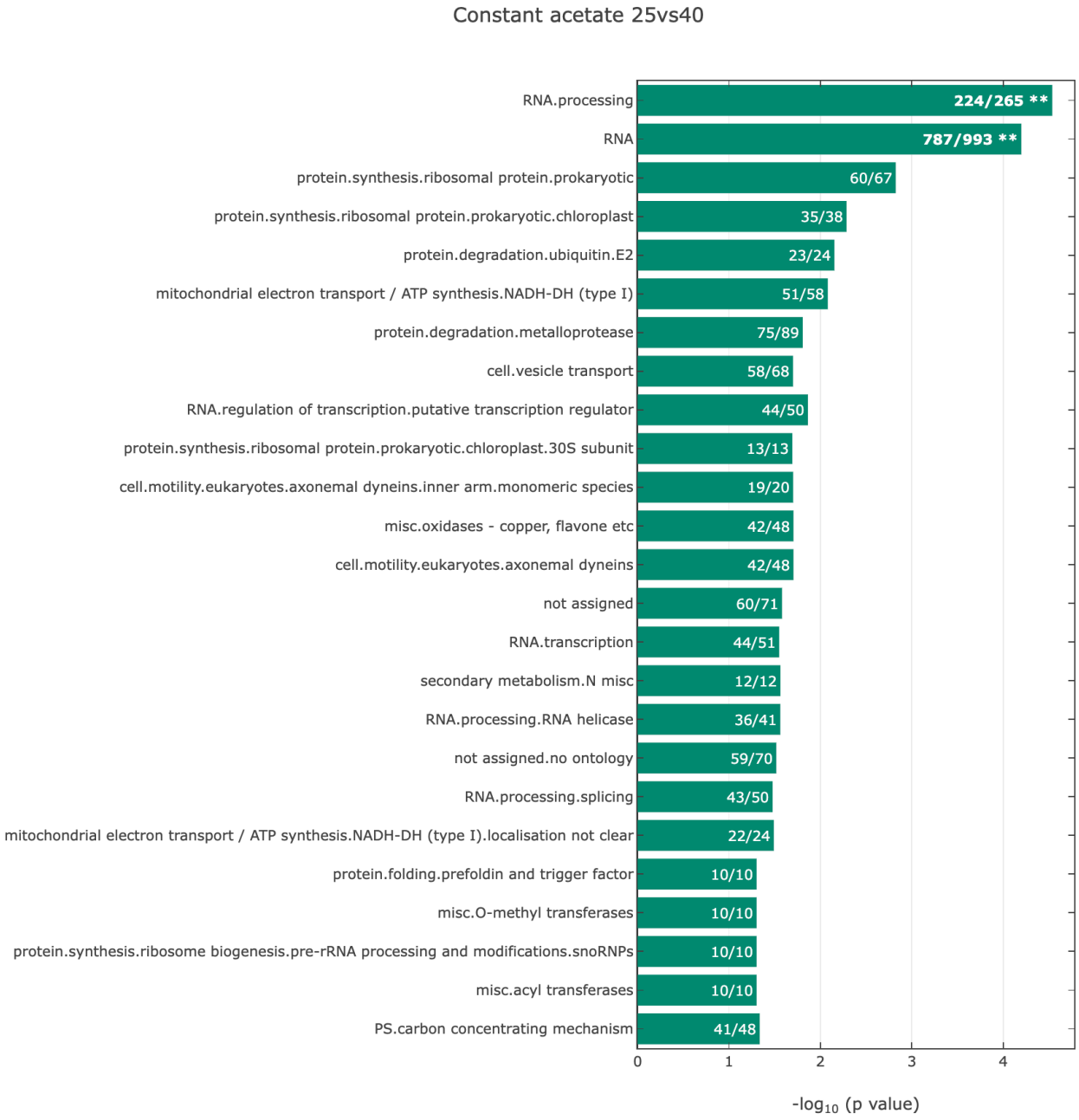

Supplemental Fig. 5E

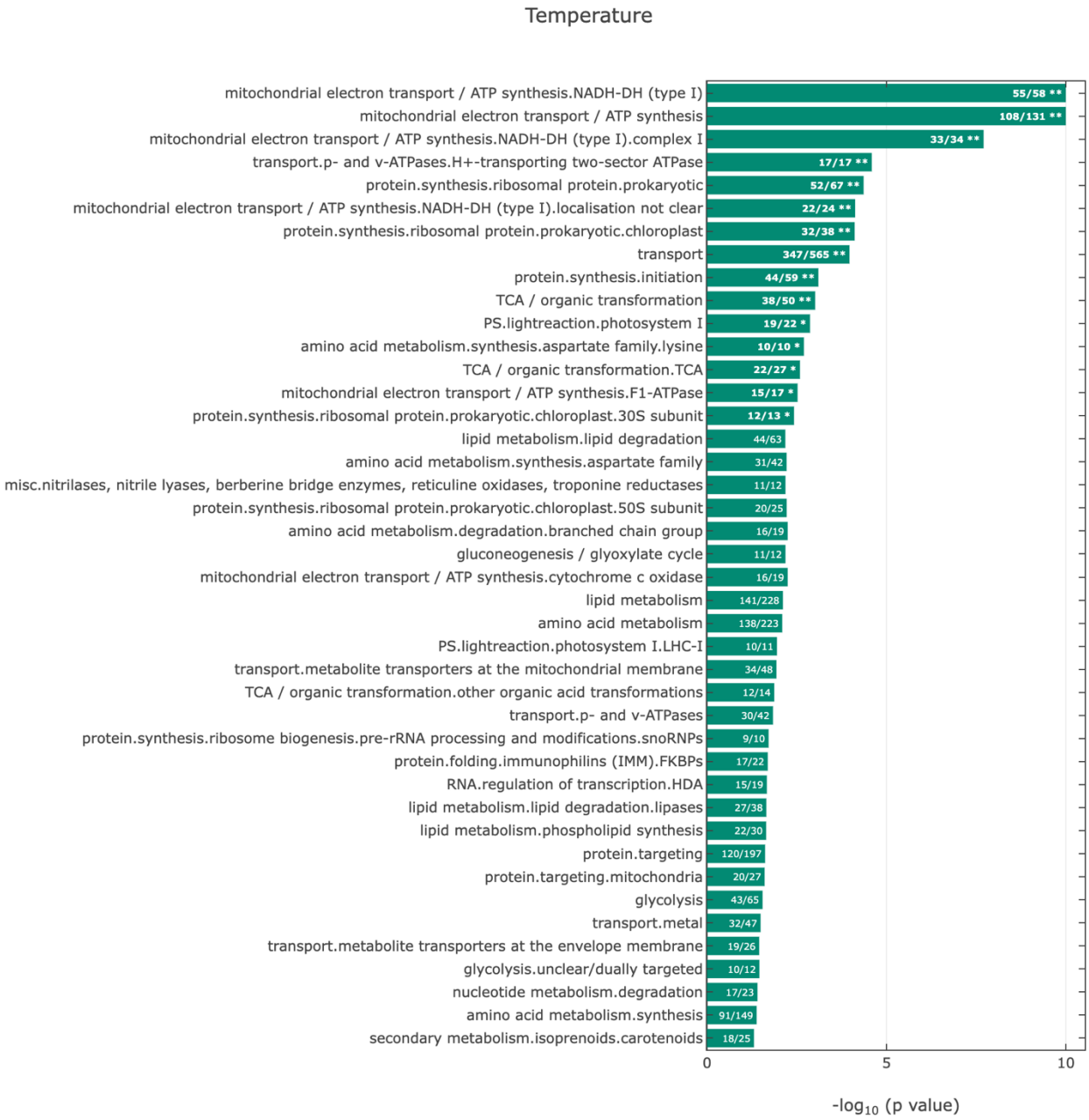

Supplemental Fig. 5F

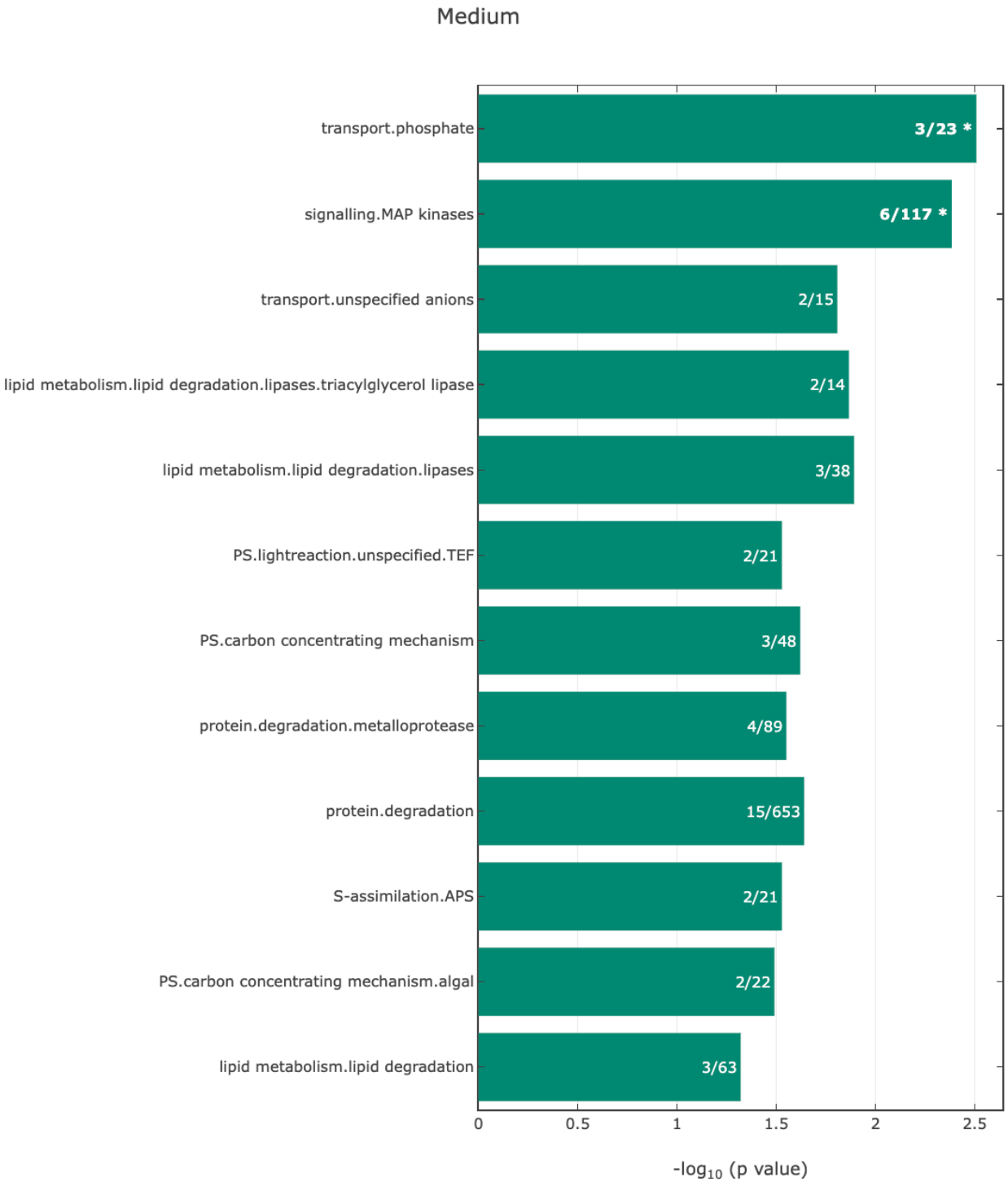

Supplemental Fig. 5G

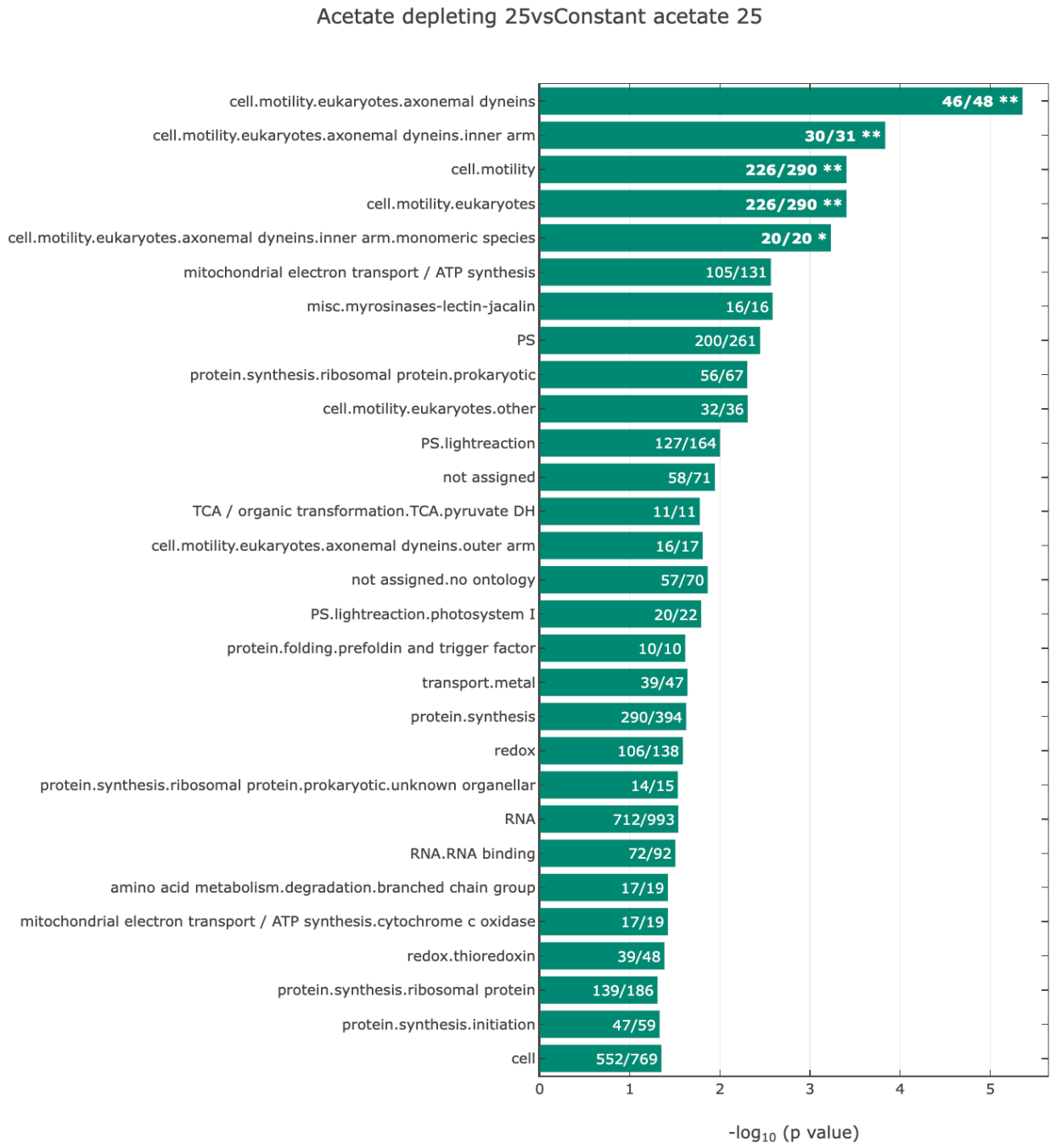

Supplemental Fig. 5. MapMan ontology enrichment revealed differentially regulated biological processes under different conditions. Ontology enrichment was performed for transcripts with significantly differential expression in the indicated comparisons using the extended MapMan ontology. The p values were calculated using a hypergeometric test. All functional sets with a p value less than 0.05 and more than 10 annotated transcripts

are shown. The ratio at the end of each bar indicates the number of significant transcripts between the two compared conditions vs detected transcripts in our RNA-seq data contained in the respective function bin. Multiple testing correction was performed by Benjamini & Hochberg FDR, * FDR < 0.1, ** FDR < 0.05. The bars are sorted based on the FDR p values, from top to bottom, from the small to big FDR values. **(A)** acetate-depleting 25°C vs acetate-depleting 35°C; **(B)** acetate-depleting 25°C vs acetate-depleting 40°C; **(C)** constant-acetate 25°C vs constant-acetate 35°C; **(D)** constant-acetate 25°C vs constant-acetate 40°C; **(E)** temperature effect: (constant-acetate 35°C and acetate-depleting 35°C) vs (constant-acetate 40°C and acetate-depleting 40°C); **(F)** medium effect: (constant-acetate 35°C and constant-acetate 40°C) vs (acetate-depleting 35°C and acetate-depleting 40°C); **(G)** acetate-depleting 25°C vs constant-acetate 25°C. See interactive figures and detailed enrichment analysis in Supplemental Dataset 3.

Supplemental Fig. 6

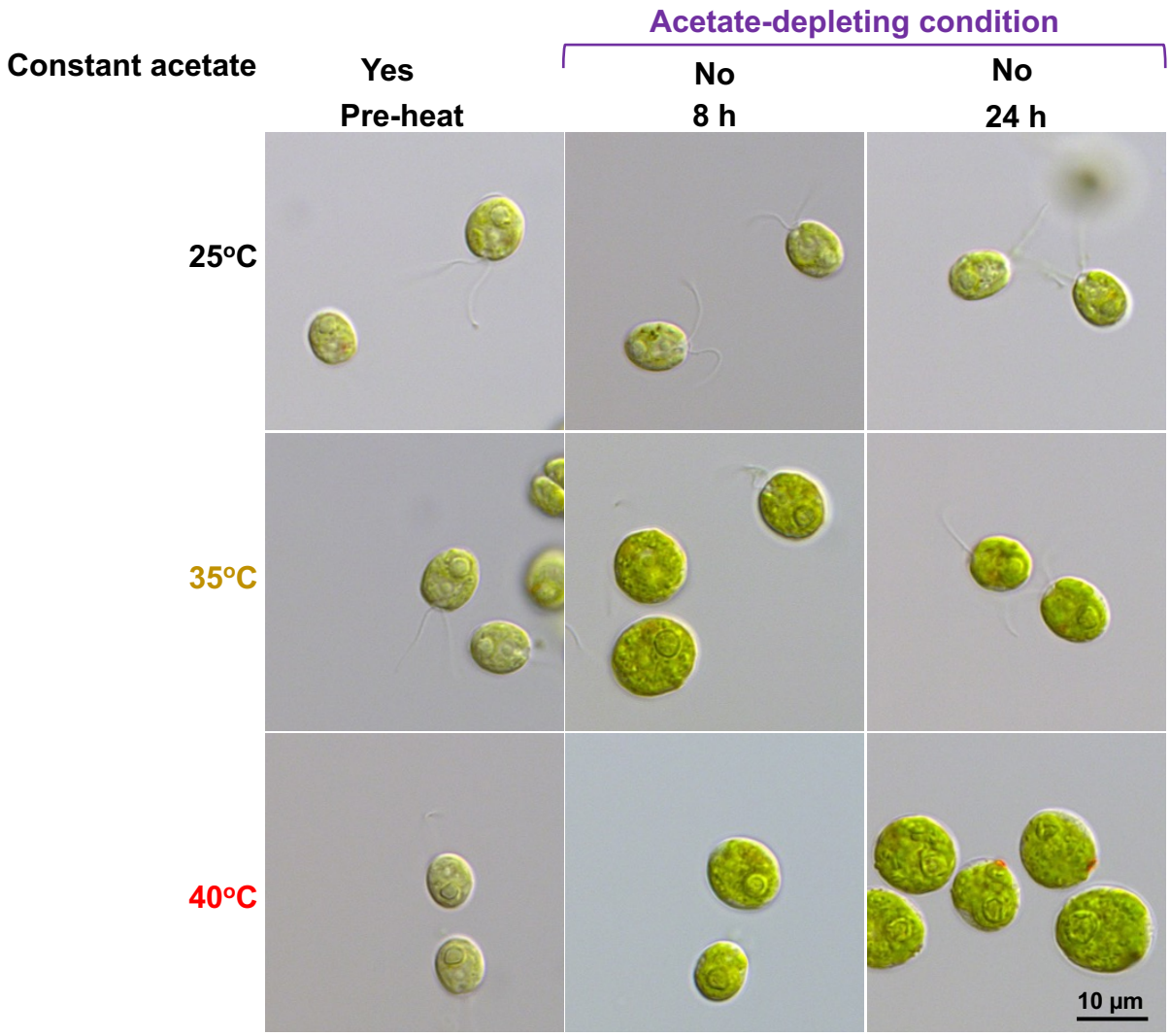

Supplemental Fig. 6. Chlamydomonas cells had different morphologies at different temperatures under the acetate-depleting condition. Light microscopic images of Chlamydomonas cells under the acetate-depleting condition. Images shown are representative results from at least three biological replicates. The algal cultivation and heat treatments were the same as in Fig. 1B.